

# POLITECNICO DI TORINO

Master of science in Mechatronic Engineering

Master Degree Thesis

## **Designing and Implementing a Modular Mechatronics Infrastructure for Autonomous Robotic Planetary Exploration**



**Academic Supervisor**

Prof. Marcello CHIABERGE

**Candidate**

André FONSECA PRINCE

**Advisor**

Dipl.-Inform. Univ. Bernhard VODERMAYER

MARCH 2020

“Exploration is in our nature. We began as wanderers, and we are wanderers still. We have lingered long enough on the shores of the cosmic ocean. We are ready at last to set sail for the stars.”

(Carl Sagan - Cosmos)

# Acknowledgments

This Master Thesis is a result of eight months working at the Robotics and Mechatronics Institute (RMI) at the German Aerospace Center (DLR) in Oberpfaffenhofen, Germany. I would like to thank my Thesis Advisor Bernhard Vodermayr for the productive discussions, the knowledge exchange, and the support during this entire journey. Also, I would like to thank Dr. Armin Wedler for the great opportunity of being part of the ARCHES team, which has fulfilled my dream of working in space robotics projects. Many thanks to Benedikt Pleintinger for the help with electronics and the great conversations in the Electronics Lab, to Alexander Kolb for the support in mechanics, to Dr. Emanuel Staudinger for the positive meetings to make the RCLOFA payload box possible, to Dr. Enrico Dietz, Dr. Susanne Schroder and Sven Frohman for making me understand the LIBS spectrometer concepts, to Peter Lehner and Sabolc Jut for the uncountable tests we have performed with the LRU-2 robotic arm, and to everyone in the RMI who has contributed in some way to this work directly or indirectly.

I would like to thank all my colleagues, professors and staff in the Politecnico di Torino, who made this journey very pleasant and enjoyable. Many thanks to my Academic Supervisor, Prof. Marcello Chiaberge, for the support during the thesis and for the inspiring lessons of Electronics Systems for Mechatronics and Electronics Fundamentals and Applications. Also, I would like to thank my colleagues and friends Dario, Giovanni, Daniel, Sara, Andrea, Giada, Sebasthian, and Abdallah for their friendship, talks, laughs and support during our activities inside and outside the Politecnico.

I also would like to thank the International Space University (ISU) for sparking my interest into Space and helping me to see that the space career has so many possibilities. Thanks to all my friends from the Space Studies Program (SSP) 2018 and to the Team Project (TP) Lunar Night Survival for keeping me inspired about our Universe exploration every day. Many thanks to my friend Cian O'Regan for reading this work and for giving me edit suggestions.

Finally, I would like to thank my family and friends for always supporting me and encouraging me to pursue my dreams. To my parents Ailton and Claudia for their unconditional love and support during my entire life. To my siblings Rafa e Bela for being always by my side even with the distance which put us apart. To my beloved wife Luisa for her love, support, patience and understanding during this moment of transition in our lives. Thanks for embracing this adventure with me every single day!

André

March 2020.

This work has received funding from the Helmholtz Association and Project ARCHES (contract number ZT-0033).

# Abstract

Traditionally, the robotic vehicles to be sent to other celestial bodies carry with them all the instruments and tools necessary for the mission. With this approach these units are built as unique. They are heavy, complex, costly and do not present any interchangeable parts that could be replaced in the event of permanent failure. However, for future missions, agencies, institutes and commercial companies have been developing robotics systems based on the concept of modular robotics. This new strategy becomes critical for planetary exploration because it can reduce load, costs and development time.

ARCHES, the German Aerospace Center (DLR) multi-robot system project, is in line with this modern design methodology. Robotic cooperation and modularity are the core of its structure. These characteristics are present in the collaboration between the two rovers and the unmanned aerial vehicle (UAV) during navigation tasks, or when the Lightweight Rover Unit (LRU) interacts to changeable manipulator tools and payload boxes through its robotic arm and its standardized electromechanical interface. Examples of these dockable modules include scientific packages, power supply systems, communication and data acquisition architectures, soil sample storage units, and specific purpose end-effectors.

The focus of this work is in the design and implementation of a mechatronics infrastructure (MI) which encompasses the docking interface, the payload modules, and the power and data management electronics board in the interior of each box. These three elements are essential for the extension of the capabilities of the rover and the enhancement of the robotics systems according to the tasks to be performed in the field. This will ensure that robots can cooperate with each other either in scientific missions or in the construction and maintenance of large structures such as habitats, power grids and mining facilities.

The MI's hardware and software development applied to this thesis was the Model-Based Engineering (MBE) approach. This methodology was implemented with the purpose of standardizing the several interfaces and reducing the fault occurrence likelihood during the integration process. However, unlike in industry, it was adapted to the research center's experimental nature with the introduction of some agile and low-cost methods between the MBE's stages.

Finally, it is important to highlight that modularity and standardization were considered at all levels of the infrastructure. From the robotics systems to the internal architecture of each payload module, these two concepts can provide versatility and reliability to the cooperative robotic network. This will improve how robots solve problems and perform complex tasks in planetary exploration missions.

**Keywords: modular robotics, mechatronics infrastructure, model-based engineering, planetary exploration.**

## Sommario

È consuetudine che i veicoli robotici da inviare ad altri corpi celesti portino con sé tutti gli strumenti robotici e scientifici necessari per la missione ma, così facendo, si è obbligati a realizzare le unità come uniche. Sono pesanti, complesse, costose e non presentano parti intercambiabili che potrebbero essere sostituite in caso di guasto permanente. Tuttavia, per future missioni, agenzie, istituti e società aziendali hanno sviluppato sistemi robotici basati sul concetto di robotica modulare. Questa nuova strategia diventa fondamentale per l'esplorazione planetaria perché può ridurre carico, costi e tempi di sviluppo.

ARCHES, il progetto del sistema multi-robot dell'Agenzia Aerospaziale Tedesca (DLR), è in linea con questo nuovo metodo di progettazione. La cooperazione robotica e la modularità sono al centro del progetto del sistema multi-robot. Queste caratteristiche sono presenti nella collaborazione tra due rover e un aeromobile senza pilota (Unmanned Aerial Vehicle, UAV) durante le attività di navigazione o quando l'unità Lightweight Rover Unit (LRU) interagisce con gli strumenti del manipolatore e con le scatole di payload attraverso il braccio robotico e l'interfaccia elettromeccanica standardizzata. Esempi di questi moduli agganciabili comprendono pacchetti scientifici, sistemi di alimentazione, architetture di comunicazione e acquisizione dati, unità di immagazzinamento dei campioni di suolo e specifici dispositivi di estremità.

L'obiettivo principale di questo lavoro è la progettazione e l'implementazione di un'infrastruttura mecatronica (MI) che comprenda l'interfaccia di attracco, i moduli di payload e la scheda elettronica di gestione dei dati e dell'alimentazione all'interno di ogni scatola. Questi tre elementi sono essenziali per l'estensione delle capacità del rover e il miglioramento dei sistemi robotici in base alle attività da svolgere sul campo. Ciò garantirà che i robot possano cooperare tra loro in missioni scientifiche o nella costruzione e manutenzione di grandi strutture come habitat, reti elettriche e strutture minerarie.

Lo sviluppo hardware e software dell'MI utilizzato in questa tesi si è focalizzato su una tipologia di progettazione basata sul modello, detta anche Model-Based Engineering (MBE). Questa metodologia è stata implementata per standardizzare le diverse interfacce e ridurre la probabilità di riscontrare errori durante il processo di integrazione. Tuttavia, a differenza dell'industria, è stato adattato alla natura sperimentale del centro di ricerca introducendo una metodologia agile e a basso costo tra le fasi del MBE.

In conclusione, è importante sottolineare che la modularità e la standardizzazione sono state prese in considerazione a tutti i livelli dell'infrastruttura. Dai sistemi robotici all'architettura interna di ciascun modulo di payload, questi due concetti possono fornire versatilità e affidabilità alla rete robotica cooperativa. Ciò migliorerà il modo in cui i robot risolvono i problemi e svolgono compiti complessi nelle missioni di esplorazione planetaria.

**Parole chiave:** robotica modulare, infrastruttura mecatronica, model-based engineering, esplorazione planetaria.

# Table of Contents

Acknowledgments .....	i
Abstract .....	ii
Sommario .....	iii
Table of Contents .....	iv
List of Figures .....	viii
List of Tables .....	xi
List of Acronyms .....	xii
1 Introduction .....	1
1.1 Motivation .....	1
1.2 Problem Statement .....	2
1.3 Objectives .....	3
1.4 Hardware and Software Development .....	3
1.5 Thesis Outline .....	4
2 Background .....	5
2.1 Modular Robotics .....	5
2.1.1 CEBOT .....	5
2.1.2 ATRON .....	6
2.1.3 ATHLETE .....	7
2.1.4 SCARAB .....	7
2.1.5 DFKI RIMRES .....	8
2.1.6 Modularity Qualitative Assessment .....	9
2.2 Small Satellites .....	14
2.2.1 Mars Cube One (MarCO) .....	14
2.2.2 ArgoMoon .....	15
2.2.3 Flying Laptop from University of Stuttgart .....	15
2.3 Model-Based Engineering .....	17
2.3.1 Waterfall .....	17
2.3.2 V-Shaped .....	18
2.3.3 Spiral .....	18
2.4 Docking Interfaces .....	19
2.4.1 Hook .....	20

2.4.2	Clamp .....	20
2.4.3	Carabiner .....	21
2.4.4	Roto-Lock.....	21
2.5	Power System.....	22
2.5.1	Primary and Secondary Power Sources .....	23
2.5.2	Power Management, Control and Distribution .....	24
2.5.3	Power Budget .....	33
2.6	Data Communication Buses .....	34
2.6.1	I2C .....	34
2.6.2	SPI .....	35
2.6.3	UART .....	36
2.6.4	CAN .....	37
2.6.5	USB.....	38
2.6.6	ETHERNET.....	39
2.6.7	Wi-Fi.....	39
2.6.8	Bluetooth.....	39
2.7	Scientific Instruments .....	40
2.7.1	Chemistry and Camera (ChemCam).....	40
2.7.2	Robotic Sample Acquisition.....	41
2.7.3	Radio Telescope.....	42
3	ARCHES and Thesis Requirements .....	45
3.1	ARCHES .....	45
3.1.1	ARCHES Mission Scenario.....	46
3.1.2	ARCHES Goals .....	47
3.1.3	Light Weight Rover Unit (LRU).....	47
3.1.4	Electromechanical Docking Interface .....	47
3.1.5	Payload Modules Constraints.....	48
3.2	Thesis Requirements .....	49
4	Mechatronics Infrastructure Design .....	50
4.1	Mechatronics Infrastructure Outline.....	50
4.2	Payload Box Infrastructure Management System (PBIMS) Board .....	50
4.2.1	Power Control and Distribution Unit (PCDU) .....	53
4.2.2	Microcontroller Unit (MCU) .....	59
4.2.3	Actuator .....	61
4.2.4	Communication Buses.....	61
4.2.5	Integrated Sensors.....	64

4.2.6	External Analog to Digital Converters (ADCs).....	66
4.3	Software Architecture .....	68
4.4	Payload Modules and Tools .....	70
4.4.1	Radio Communication and Low Frequency Array (RCLOFA) Payload Box .....	71
4.4.2	LIBS Spectrometer Payload Box.....	73
4.4.3	Power Supply (PS) Payload Box .....	75
4.4.4	Sample Payload Box.....	76
4.4.5	Wi-Fi Repeater Box .....	77
4.4.6	KIT Hand Tool.....	78
4.4.7	Shovel and Segregation Tool .....	79
4.5	Electromechanical Docking Interface .....	80
4.5.1	Electrical Interface Connector (EIC) .....	80
4.5.2	Passive Female Mechanical Interface (PFMI) .....	82
4.5.3	Passive Male Mechanical Interface (PMMI) .....	83
4.5.4	Active Female Interface (AFI) .....	83
5	Testing and Evaluation .....	84
5.1	Hardware Testing .....	84
5.1.1	Docking interfaces .....	84
5.1.2	PBIMS .....	85
5.1.3	Payload Modules .....	90
5.2	Software Testing.....	91
5.2.1	Power Buses and Switches Activation Test .....	91
5.2.2	Communication Network Test.....	93
5.3	System Integration and Testing.....	96
5.3.1	Electrical and Mechanical Interface Test between Payload Modules .....	96
5.3.2	Electrical and Mechanical Interface Test between Robotic End-Effector and Payload Modules	99
5.3.3	PBIMS with Scientific Instruments.....	102
5.3.4	PBIMS with Power Sources .....	105
5.4	Experimental Results .....	107
6	Discussion and Lessons Learned .....	108
6.1	Discussion of Results .....	108
6.2	Lessons Learned .....	111
7	Conclusion and Future Work .....	112
7.1	Conclusion.....	112
7.2	Future Work .....	113

References.....	115
Appendices .....	123
Appendix A – PBIMS Layout .....	123
Appendix B – Modularity Qualitative Assessment.....	125

# List of Figures

Figure 1: Four different CEBOT prototypes. The cells can be connected and separated with the use of a docking interface [7].	6
Figure 2: ATRON modules in different configurations: snake, cluster-walk and car [9].	6
Figure 3- ATHLETE vehicle [10].	7
Figure 4- Scarab rover and RESOLVE modules [11].	8
Figure 5 -The DFKI RIMRES system encompasses the four-wheeled Sherpa rover, the legged scout CREX and immobile payload units. [12].	9
Figure 6 - Marco CubeSat [22].	14
Figure 7 - ArgoMoon [23].	15
Figure 8 - CDPI adapted diagram [25].	16
Figure 9 - Waterfall Model [30].	17
Figure 10 - V-Shaped model [34].	18
Figure 11 - Spiral Model [31].	19
Figure 12 – (a) Docking mechanism with hooks [42]; (b) ATRON hook docking mechanism [15].	20
Figure 13 – (a) Clamping Docking Mechanism [42]; (b) Grapple mechanism showing three clamps and three connectors in the ERA [43].	21
Figure 14 – Carabiner Docking Mechanism [42].	21
Figure 15 – (a) Roto-Lock Docking Mechanism [42]; (b) iBoss modular satellite [44]	22
Figure 16 - Diagram of Spacecraft Electrical Power System [46].	23
Figure 17 - Diagram of BMS [47].	25
Figure 18 - Prioritized Power Path Control example with three power sources [48].	26
Figure 19 - Switching voltage between V1, V2 and V3.	27
Figure 20 - Power MOSFET switch to control DC motor [49].	28
Figure 21 - (a) Buck Converter Circuit. (b) Flow Switch ON (c) Flow Switch OFF (d) Waveforms [50].	29
Figure 22 - (a) Boost Converter Circuit. (b) Flow Switch ON (c) Flow Switch OFF (d) Waveforms [50].	30
Figure 23 - PWM signal in 25%, 50% and 90% duty cycle [52].	31
Figure 24 - PWM generator circuit [51].	32
Figure 25 - Generalized I2C connection diagram [54].	34
Figure 26 - Communication sequence [53].	35
Figure 27- SPI in Daisy Chain connection [55].	36
Figure 28 - UART Diagram [57].	37
Figure 29 - CAN Bus state [58].	37
Figure 30 - Arbitration between three nodes [58].	38
Figure 31 - Bus and Star configurations [60].	39
Figure 32 - Example of type of data collected by the ChemCam instrument on the Mars Curiosity rover (NASA/JPL-Caltech/LANL).[64].	40
Figure 33 - Schematic of NASA MSL Curiosity Drill and Drill bit (NASA JPL) [65].	41
Figure 34 - Viking lander soil sampler (NASA JPL) [66].	42
Figure 35- Radio telescope diagram [68].	42
Figure 36 - a. Aerial photography of Superterp, the heart of LOFAR core; b. Schematic illustrating the signal connections at station level [75].	43
Figure 37 - OLFAR network [77].	44
Figure 38 - ARCHES robotics platforms [79].	45
Figure 39 - Docking Sequence [83].	48
Figure 40 - The three main elements of the Mechatronics Infrastructure. (a) Docking interface with electrical connector; (b) PBIMS board; (c) Payload Box.	50
Figure 41 - PBIMS Diagram	51
Figure 42 - PADS electronic schematics of the PPC	53
Figure 43 - Demonstration of the accurate switching of power sources. Vout (green line), V1 (blue line), V2 (red line) and V3 (violet line). OV/UV window between 23-28 V $\pm$ 5%.	54

Figure 44 - Maximum current through the FET.....	55
Figure 45 - DC1717 A oscilloscope measurements.....	56
Figure 46 - PADS electronic schematics of the Buck converter.....	57
Figure 47 - PADS electronic schematics of the Boost converter.....	57
Figure 48 – No-load condition step-down conversion from 24V to 5V. Measurements performed with oscilloscope.....	58
Figure 49 - Load condition step-down conversion from 24V to 5V. Measurements performed with oscilloscope.....	59
Figure 50 - Schematics of the MCU.....	60
Figure 51 - ARM Keil MCB1700 evaluation board [88]. ....	60
Figure 52 - Servo motor mechanism.....	61
Figure 53 - UART circuit.....	62
Figure 54 - USB circuit.....	62
Figure 55 - Ethernet circuit.....	63
Figure 56 - Bluetooth circuit.....	63
Figure 57 – Wi-Fi circuit.....	64
Figure 58 - BNO055 circuit schematics.....	65
Figure 59 - BME280 circuit schematics.....	66
Figure 60 - VL6180X circuit schematics.....	66
Figure 61 – External ADC converter circuit schematics.....	67
Figure 62 - Software Architecture Diagram.....	68
Figure 63 – Functional Block Diagram for the Basic Software.....	69
Figure 64 - RCLOFA payload module 3D-Model.....	71
Figure 65 - RCLOFA scientific system diagram.....	72
Figure 66 - Standard Payload Box Structural Analysis. (a) Loads from 20 to 60 N applied in specific parts of the box; (b) Stresses in MPa after simulation. ....	73
Figure 67 - LIBS payload module 3D-model.....	74
Figure 68 - LIBS scientific system diagram.....	74
Figure 69 - PS payload box 3D-model.....	75
Figure 70 - Sample Payload Box 3D-Model.....	76
Figure 71 – Wi-Fi Repeater system diagram.....	77
Figure 72 – Wi-Fi Repeater Payload Box 3D-Model. ....	78
Figure 73 - KIT Hand tool 3D-Model.....	79
Figure 74 – (a) Shovel; (b) Segregation Tool 3D-Model. ....	80
Figure 75 - Electrical Interface Connector (EIC) 3-D Model.....	81
Figure 76 - Structure Analysis Male Electrical Interface Connector with CREO simulate.....	81
Figure 77 - Passive Female Mechanical Interface (PFMI) 3-D Model.....	82
Figure 78 – Passive Male Mechanical Interface (PMMI) 3-D Model. ....	83
Figure 79 – Active Female Interface (AFI) 3-D Model.....	83
Figure 80 – Electrical Interface Connector (EIC) Temperature and Current test.....	85
Figure 81 – (a) Buck converter 28 V to 5 V with ripple 30.22 mVpp; (b) Buck converter 28 V to 6 V with ripple 25.39 mVpp; (c) Buck converter 28 V to 12 V with ripple 37.22 mVpp; (d) Buck converter 28 V to 24 V with ripple 23.33 mVpp.....	86
Figure 82 – Boost Converter 48 V with ripple 425 mVpp.....	86
Figure 83 - Oscilloscope with lower threshold of the UV/OV window. ....	87
Figure 84 - Oscilloscope with upper threshold of the UV/OV window.....	87
Figure 85 - Accurate switching among prioritized power sources. ....	88
Figure 86 – (a) Switching time Ideal switch (1.96 $\mu$ s); (b) Switching time Non-ideal switch (2.01 $\mu$ s)... ..	89
Figure 87– Temperature Diagram over the PBIMS.....	89
Figure 88 – Standard Payload Module Frame.....	90
Figure 89 – Payload Module Drop Test. (a) 2.4 kg Load attached to the box; (b) Minor damages after four drops; (c) Field with medium grain gravel where the test was performed. ....	91
Figure 90 – NXP MCUXpresso BUS1_EN enabling .....	92

<b>Figure 91 – NXP MCUXpresso BUS1_SW1 and BUS1_SW2 enabling .....</b>	<b>92</b>
<b>Figure 92 – Oscilloscope measurement after BUS1 (24V) is activated. ....</b>	<b>93</b>
<b>Figure 93 – Oscilloscope measurement after BUS1_SW1 and BUS1SW2 are activated with 300 ms delay. ....</b>	<b>93</b>
<b>Figure 94 – Bluetooth input command handler calling the com_prot handler.....</b>	<b>94</b>
<b>Figure 95 – HTerm window with transmission of commands and reception of status via Bluetooth communication. ....</b>	<b>94</b>
<b>Figure 96 – Header file com_prot.h with the definitions of commands.....</b>	<b>95</b>
<b>Figure 97 – The structure of the command packet. ....</b>	<b>95</b>
<b>Figure 98 – Oscilloscope measurements of BUS1, BUS2 and BUS3. (a) BUS1 (24 V) is ON; (b) BUS2 (12 V) is ON; (c) BUS3 (5 V) is ON; (d) BUS1(24 V) is OFF.....</b>	<b>95</b>
<b>Figure 99 - Docking sequence with LRU-2, robotic arm, and payload boxes. ....</b>	<b>96</b>
<b>Figure 100 - Mating success rate (%) with the offset distance (mm) in the x-axis. ....</b>	<b>97</b>
<b>Figure 101 - Mating success rate (%) with the offset distance in the y-axis. ....</b>	<b>97</b>
<b>Figure 102 - Mating success rate (%) with inclination of top box in relation to the ground (degree).....</b>	<b>98</b>
<b>Figure 103 – LIBS payload box integrated to the robotic docking interface. ....</b>	<b>100</b>
<b>Figure 104 – KIT Hand Tool integrated to the robotic docking interface. (a) Hand open; (b) Hand closed; (c) Hand grasping object.....</b>	<b>101</b>
<b>Figure 105 - Setup of the integration of the PBIMS to the RCLOFA payload box.....</b>	<b>102</b>
<b>Figure 106 - Setup of the integration of the PBIMS to the LIBS payload box.....</b>	<b>103</b>
<b>Figure 107 – Simulated series of current peaks. (a) OS laser real shooting; (b) Oscilloscope screen of simulated laser shooting at 9.5 Hz frequency.....</b>	<b>104</b>
<b>Figure 108 – Setup PBIMS with Battery Pack and DC Power Supply Unit. ....</b>	<b>105</b>
<b>Figure 109 – Switching power between Power Supply and Battery Pack.....</b>	<b>106</b>
<b>Figure 110 – Inrush current when plugging the battery pack. ....</b>	<b>106</b>

## List of Tables

Table 1 - Summary of tools and components in each stage of the MBE.....	4
Table 2 - Criteria for Modularity Qualitative Assessment .....	10
Table 3 - MI Modularity Qualitative Assessment.....	10
Table 4 - PMDH Board Modularity Qualitative Assessment .....	13
Table 5 - Power Budget Satellite Example [45]. .....	33
Table 6 - Stakeholders vs Requirements.....	52
Table 7 - Power Budget Analysis for KN and OS payload carriers.....	52
Table 8 – Calculated values for the external resistances in the buck converter.....	58
Table 9 – Resistance values for EIC.....	84
Table 10 – Payload Module Frame Dimensions, Weight and Volume .....	90
Table 11 – Resistance values for EIC during Integration. ....	99
Table 12 – Voltage and Current levels during stacking of payload modules. ....	99
Table 13 – Electrical Measurements LIBS payload box integration with robotic end-effector. ....	100
Table 14 – Current Measurement for the KIT Hand Tool in operation. ....	101
Table 15 – Electrical Values with RCLOFA and PBIMS setup.....	102
Table 16 – Electrical Values with LIBS and PBIMS setup.....	104
Table 17 – Electrical Values with Power Sources and PBIMS setup.....	105
Table 18 – Summary of Test Results.....	107

## List of Acronyms

AC	Alternating current
ACK	Acknowledgement
ADC	Analog to Digital Converter
AFI	Active Female Interface
AOCS	Attitude and Orbit Control System
ARCHES	Autonomous Robotic Networks to Help Modern Societies
ASCII	American Standard Code for Information Interchange
ASI	Italian Space Agency
ATHLETE	All-Terrain Hex-Limbed Extra-Terrestrial Explorer
AWG	American Wire Gauge
BMS	Battery Management System
BMWi	German Ministry of Economy and Energy
CAD	Computer-Aided Design
CAN	Controller Area Network
CANH	Controller Area Network High
CANL	Controller Area Network Low
CCSDC	Consultative Committee for Space Data Systems
CDPI	Combined Data and Power Management Infrastructure
CEBOT	Cellular Robotics
CEP	Central Processing
ChemCan	Chemistry and Camera
CNES	National Center for Space Studies
COTS	Commercial off the Shelf
CPHA	Clock Phase
CPOL	Clock Polarity
CPU	Central Processing Unit
CRC	Cyclic Redundancy Check
CREX	Crater Explorer
DC	Direct Current

DFKI	German Research Center for Artificial Intelligence
DLC	Data Length Code
DLR	German Aerospace Center
DSP	Digital Signal Processing
EDA	Electronic Design Automation
EIC	Electrical Interface Connector
EM-1	Exploration Mission -1
EMI	Electromechanical Interface
EOF	End-of-Frame
EPS	Electrical Power System
ERA	European Robotic Arm
ESA	European Space Agency
FHSS	Frequency Hopping Spread Spectrum
FIFO	First-In First-Out
FLP	Flying Laptop
FPGA	Field Programmable Gate Array
GER	Global Exploration Roadmap
GND	Ground
GNSS	Global Navigation Satellite System
GPIO	General Purpose Input Output
HBA	High Band Antenna
HPC	High Priority Command
I2C	Inter-Integrated Circuit
IC	Integrated Circuit
IDE <sup>1</sup>	Integrated Development Environment
IDE <sup>2</sup>	Identifier Extension Bit
IMU	Inertial Measurement Unit
IR	Infra-Red
ISRU	In-Situ Resource Utilization
ISS	International Space Station
JAXA	Japanese National Aerospace and Space Agency

JPL	Jet Propulsion Laboratory
KIT	Karlsruhe Institute of Technology
KN	Communication and Navigation
LAN	Local Area Network
LBA	Low Band Antenna
LED	Light Emitting Diode
LF	Low Frequency
LIBS	Laser Induced Breakdown Spectrometry
LNA	Low Noise Amplifier
LOFAR	Low Frequency Array
LRU	Lightweight Rover Unit
MarCO	Mars Cube One
MASCOT	Mobile Asteroid Surface Scout
MAV	Micro Aerial Vehicle
MBE	Model-Based Engineering
MCU	Micro Controller Unit
MI	Mechatronics Infrastructure
MISO	Master In Slave Out
MOSI	Master Out Slave In
MSL	Mars Science Laboratory
NASA	National Aeronautics and Space Administration
NCLE	Netherlands Chinese Low Frequency Explorer
NCOSE	National Council on Systems Engineering
NORCAT	Northern Center for Advanced Technology
NUC	Next Unit of Computing
OBC	On-board Computer
OBSW	On-board Software
OLFAR	Orbiting Low Frequency Array
OS	Optical Sensor Systems
OV	Over-Voltage
PBIMS	Payload Box Infrastructure Management System

PCB	Printed Circuit Board
PCDU	Power Conditioning and Distribution Unit
PFMI	Passive Female Mechanical Interface
PMDH	Power Management and Data Handling
PMMI	Passive Male Mechanical Interface
PMS	Power Managements System
PoE	Power over Ethernet
POM	Polyoxymethylene
PPC	Power Path Control
PS	Power Source
PWM	Pulse Width Modulation
RAE	Radio Astronomy Explorer
RAFCON	RMC (Robotics and Mechatronics Center) Advanced Flow Control
RC	Resistance-Capacitance
RCU	Receiver Unit
RCLOFA	Radio Communication and Low Frequency Array
REIPOS	Relative Interferometric Position Sensor
RF	Radio Frequency
RESOLVE	Regolith & Environment Science and Oxygen & Lunar Volatile Extraction
RIMRES	Reconfigurable Integrated Multi-Robot Exploration System
RM	Robotics and Mechatronics
ROI	Region of Interest
RTG	Radioisotope Thermoelectric Generator
RTR	Remote Transmission Request
RX	Receiving Data
RW	Reaction Wheel
SCKL	Serial Clock
SCL	Serial Clock Line
SDA	Serial Data Line
SDR	Software Defined Radio
SIG	Bluetooth Special Interest Group

SLAM	Simultaneous Localization and Mapping
SOC	State of Charge
SOF	Start-of-Frame
SOH	State of Health
SPI	Serial Peripheral Interface
SS	Slave Select
TCP	Tool Center Point
TTL	Transistor-transistor Logic
TX	Transmitting Data
UART	Universal Asynchronous Receiver Transmitter
UHF	Ultra-High Frequency
USAF	United States Air Force
USB	Universal Serial Bus
UV	Under-Voltage
WLAN	Wireless Local Area Network

# 1 Introduction

This thesis presents how modular tools and payload carriers can be beneficial for robotic planetary exploration. It focuses on the design, construction and standardization of the complete mechatronics infrastructure (MI) which encompasses the standard docking interfaces, the payload mechanical container and the electronics inside these boxes. This approach will enable the extension of the capabilities of robotic units. This work took place at the Robotics and Mechatronics (RM) Institute in the German Aerospace Center (DLR) as part of the Autonomous Robotic Networks to Help Modern Societies (ARCHES) project. All the developed systems will be in operation during the analogue mission on Mount Etna, Sicily, in Italy in July 2020.

Three major applications of modular robotics in space are the construction of large structures, the exploration of craters and caves, and the exploitation of local resources on the surface of extraterrestrial bodies. These three activities require robustness and flexibility from the robot system, but at the same time achieving reduced mass, low cost, short development time and simple integration of the parts. The mechatronics infrastructure described in this thesis explores the strengths of this method and how these characteristics can be implemented in a multi-robot network.

## 1.1 Motivation

Planetary exploration with mobile robots has changed the way humans perceive the Solar System. From the lunar soil analyses carried out by the Soviet Rover LunoKhod-1 in the 1970s to the geological measurements performed recently by the NASA Mars Science Laboratory (MSL) Curiosity on Mars, the number of discoveries in the past fifty years has fascinated scientists and the general public. Countless images and several in situ scientific analyses provided the first hints about what is yet to be discovered. The infinite possibilities range from the potential bio signatures on Mars to the use of resources from lunar soil, from the desire of building the first extraterrestrial outpost to the dream of the creation of self-sufficient settlements on other planets. Regardless of the nature of future space missions, mobile robots will always be present either to support humans or to perform jobs astronauts cannot do [1].

The future sustainable presence of humans on the Moon and Mars will rely on the development of an infrastructure including habitats, power grids and mining facilities on the surface of these planetary bodies. The Global Exploration Roadmap (GER) [2] introduces a set of six sustainability principles. Among them, the principle of *Capability Evolution and Interoperability* foresees the use of common interfaces and modular architectures in the human space exploration endeavor. This will reduce mass, increase safety and allow new partners to integrate their technologies to the infrastructure in the future. Similarly, the mechatronics infrastructure (MI) presented in this work will provide flexibility and robustness to the ARCHES robot network. Its standardized docking interfaces, universal electronics systems and modular payload boxes will enable the

robot units to assemble and maintain complex structures as well as executing different scientific tasks.

Another important aspect is the rise of a new space competition between private companies, known as "NewSpace". Differently from the space race in the 1960s and 70s between the United States and the former Soviet Union, NewSpace allows private industry to have a significant participation in the space sector and facilitates the development of a space economy [3]. With lower budgets than space agencies and large private organizations, NewSpace companies can benefit from modularity in robotics because the use of low-weight, low-cost and scalable modules will provide them easier access to space. They will be able to start with their involvement in low to medium budget projects, and with time, scale up infrastructure with the introduction of additional scientific instruments and tools. According to the German Ministry of Economy and Energy (BMWi) [4], the survival of NewSpace companies in this competitive environment does not only depend on technology but also on speed. The modular approach proposed in this thesis ensures that new businesses can rapidly start with a simplified infrastructure and later expand upon it. They can begin with one low-weight rover and a few inexpensive tools. This would not impede them to become operational in a short period of time or perform tasks of exploration and soil sample collection. However, in the future, because of standardized interfaces and payload carriers, they will be able to add more rovers and complex scientific instruments in the original set, which would allow them to carry out more detailed geologic analysis and cover wider areas of exploration.

## **1.2 Problem Statement**

Heavy and fully integrated robotic units were developed in the past and sent to space. Examples include the 800 kg soviet rovers Lunokhod 1 and Lunokhod 2 which landed on the lunar surface in 1971 and 1973 [5], and the 900 kg NASA MSL Curiosity Rover which landed on Mars in 2012 [6]. Although those missions were successful, several limitations can be found. Such limitations include the high mass of these car-size machines and the lack of flexibility for future integration of new technologies or replacement parts to their systems.

In order to create a light-weight system, all the scientific instruments can be removed from the rover and be transformed into individual payload modules. The rover manages navigation and localization, while the payload units can be connected to the robotic arm or be deployed on the terrain to take the scientific measurements.

This modular mode depends on the standardization of mechanical and electrical interfaces of the rover and the payload boxes. The standard elements will connect and disconnect several times during the mission and the encapsulated payload shell will need to be flexible enough to incorporate different scientific instruments being placed on it. The use of an electromechanical docking interface to connect the parts and the mechatronics infrastructure in the interior of the modules to provide adequate power and data management to the scientific tools are key in this process.

Hardware and software integration can be a challenging task, especially when several actors are involved in a multi-robot project. Unlike previous endeavors that had scientific payloads built individually by different parts, the modularity and standardization aspects used in ARCHES guarantee a simplified and fast integration process.

### **1.3 Objectives**

The goal of this work is to design and build the mechatronics infrastructure (MI) which enables the integration of the scientific payload modules and dockable tools to the rover's robotic manipulator. This process will use the modular approach and can derive the following objectives:

- Design the electrical interface of the electromechanical docking mechanism and integrate it to the original mechanical structure.
- Design and manufacture the standard payload carrier.
- Design and create the standard electronics board to provide adequate power and data buses to the scientific instruments or basic infrastructure elements that will be incorporated into the payload units.
- Integrate all the components of the MI to the robotics systems of ARCHES multi-robot network

### **1.4 Hardware and Software Development**

This work used the Model-Based Engineering (MBE) methodology for the development of hardware and software components of the mechatronics infrastructure (MI). More specifically, the V-shaped model was chosen because it is simple and effective while also ensuring the quality of the development process during all phases. This model, which is detailed in section 2.4, is heavily used in industries with complex systems, such as the automotive, aerospace and robotics. Because of this increasing complexity, more interfaces are generated and the likelihood of having faults increases. To face these challenges, more tests must be performed, and more processes need to be validated. This ensures the mitigation of risks and the excellence of the product development.

With the purpose of standardizing the entire MI, the use of the V-Shaped model was beneficial to this project. The creation of a standardized and versatile structure which can accommodate different technologies of scientific instruments and embedded systems is not simple - particularly if there are conflicting requirements. However, the involvement of the stakeholders during all stages of the process was crucial for the MI's successful development. They provided relevant feedback, received information about the MI ongoing process results, and contributed

to the risk and opportunity assessment. This interactive process helped to reshape requirements, correct inaccuracies and clearly define the reason why the MI was built.

The details of the application of the V-shaped model to the development of the MI are shown in Chapter 5. Each stage of the model was supported by the use of a variety of tools: Computer-aided Design (CAD), Electronic Design Automation (EDA) and an Integrated Development Environment (IDE<sup>1</sup>) for modelling, simulating software platforms for simulation, additive manufacturing and evaluation boards for prototyping, and real robotic systems for testing and integration. Table 1 summarizes them:

*Table 1 - Summary of tools and components in each stage of the MBE*

Stages V-model	Mechanical	Electronics	Software
Concept	Sketches, diagrams	Sketches, diagrams	Sketches, diagrams
Model	PTC Creo 3.0	KiCAD, PADS	MCUXpresso
Simulation	PTC Simulate	LTSpice	MCUXpresso
Prototype	Ultimaker 2+	Evaluation boards	Evaluation boards
Test	Robotic Arm	Manufactured board	Manufactured board
Integration	Robotic Arm, Payload Boxes	Payload Boxes	Robotic Network

## 1.5 Thesis Outline

This thesis is organized as follows: Chapter 2 summarizes the background in modular robotics, small satellites architectures, model-based engineering process and important subsystems of embedded electronics systems that form the base of this work. Chapter 3 introduces the requirements for the ARCHES project and for this thesis with the focus on how they interrelated to each other. Chapter 4 describes the mechatronics infrastructure design and each of its components. In Chapter 5, the integration and testing of the mechatronics infrastructure elements are shown. Chapter 6 discusses the results of the integration and testing carried out in Chapter 5. Finally, in Chapter 7, conclusions and future work are presented.

## 2 Background

This chapter explores the related work in relevant topics to this thesis such as Modular Robotics, Small Satellites Architectures, Model-Based Engineering and other important systems. The design of the mechatronics infrastructure (MI) was developed based on these concepts.

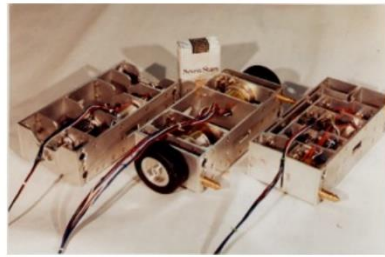
### 2.1 Modular Robotics

The payload mass limitation for the current launch vehicles has led to the modularity concept applied to space systems. One of the most memorable examples is the International Space Station (ISS) which was assembled on orbit after multiple launches during a period of 12 years. This concept makes space missions feasible and the construction of large structures possible.

For robotics, this approach started in the late 1980s with Fukuda and Kawauchi [7] in the development of cellular robotics (CEBOT). This innovative technology inspired subsequent research in the robotics community utilizing a similar concept. A few illustrative cases, including the pioneer CEBOT, are shown in this section. To conclude the related work in modular robotics, a qualitative analysis which compares the existing systems is performed. This evaluation identified potential points of improvement which has set the base of the MI's hardware and software development.

#### 2.1.1 CEBOT

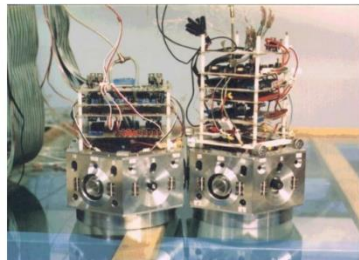
The initial idea for modularity in robotics starts with the concept of self-reconfigurable robots. Fukuda and Kawauchi [7] created CEBOT targeting modular industrial manipulators. They ensured that their system could build an adequate structure according to the purpose of the task or the environment where the cells were placed. This change of configuration could happen dynamically, autonomously and relying on a decentralized control system. In those early days of development, the first prototypes were already using the concept of docking and separating cells through a standardized interface, which is critical for this work. Figure 1 shows four different prototypes with this feature:



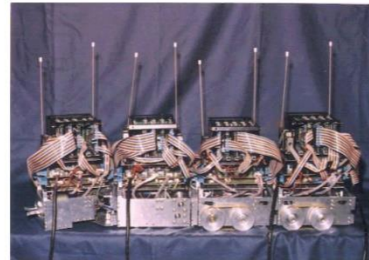
**CEBOT mark I (1985)**



**CEBOT mark II (1988)**



**CEBOT mark III (1989)**



**CEBOT mark IV (1992)**

*Figure 1: Four different CEBOT prototypes. The cells can be connected and separated with the use of a docking interface [7].*

### 2.1.2 ATRON

The ATRON system, developed by the Adaptronics group at Maersk McKinney Moller Institute, University of Southern Denmark, follows the same self-reconfigurable robot fashion. Its modules have nearly spherical shape, in which two hemispheres are linked by a single revolute joint and four connectors (two female and two male) are present on the surface of each half-module [8]. This design allows ATRON to have several modules connected to each other in a versatile manner. The variation of possible configurations is visible in figure 2:



*Figure 2: ATRON modules in different configurations: snake, cluster-walk and car [9].*

Although ARCHES project does not focus on self-reconfiguration, there are other characteristics in ATRON that are relevant. Its system is robust because it has redundant modules that can be easily replaced in case of failure without compromising the operation. It is flexible enough to execute different tasks with different configurations. It has a low cost since each module is standardized and can be produced in large-scale.

### 2.1.3 ATHLETE

The All-Terrain Hex-Limbed Extra-Terrestrial Explorer (ATHLETE) is a cargo handling and manipulation robot for lunar surface exploration. It has six limbs with a *wheel-on-leg* structure which provides advantages in mobility. Additionally, the limbs can be used as a manipulator where special end-effectors such as gripper, scoop and drill can be connected. The vehicle is heavy (850 kg) and wide (2.75 m), but has an incredible payload carrying capacity of 300 kg in Earth gravity [10]. It was developed jointly by the Jet Propulsion Laboratory (JPL), the NASA Johnson Space Center, the NASA Ames Research Center, Stanford University and the Boeing Company in 2005, and upgraded as Tri-ATHLETE in 2009. It can dock to similar ATHLETE vehicles with the use of a hook interface and expand their carrying capacity. Its electronics and computing capacity rely on seven distributed modular central processing units (CPUs). The main CPU is used as a central unit and the additional six are attached to each limb as peripheral units. Their tasks are to handle mobility, telemetry, system control, power management, and camera images. Figure 3 shows this system:

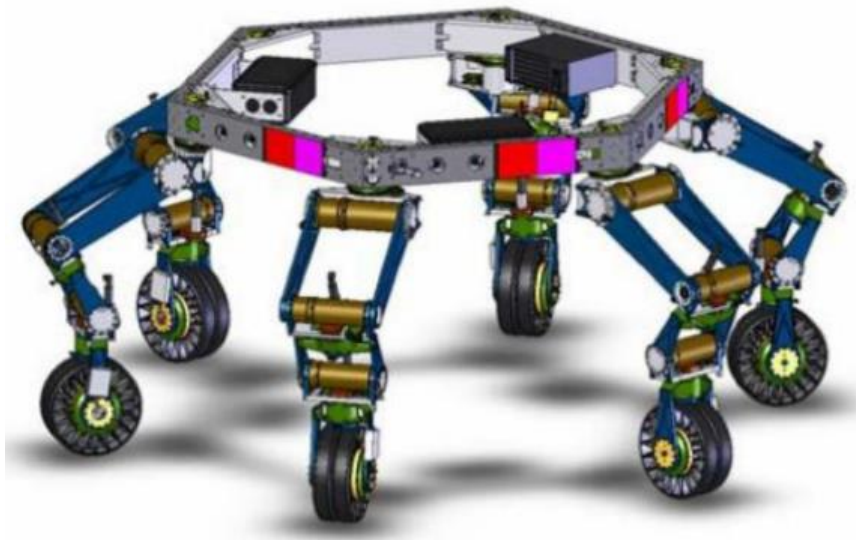
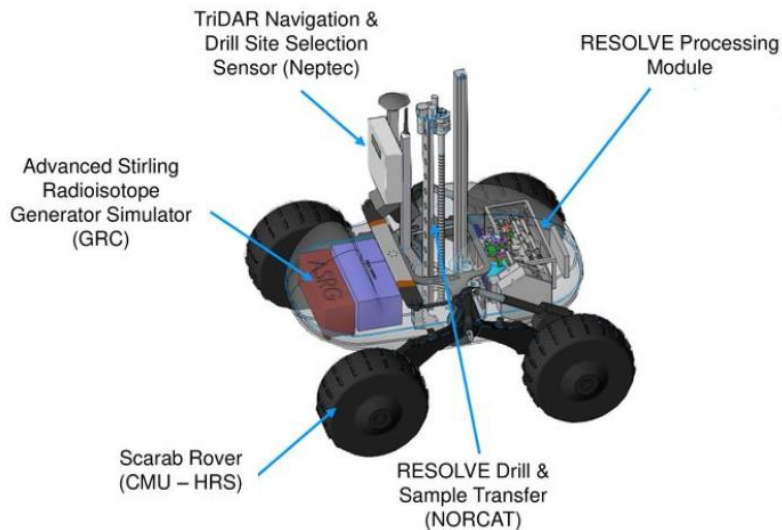


Figure 3- ATHLETE vehicle [10]

### 2.1.4 SCARAB

The Scarab rover is a prospecting vehicle developed by the Robotics Institute of Carnegie Mellon University with NASA collaboration in 2008 for future In-Situ Resources Utilization (ISRU)

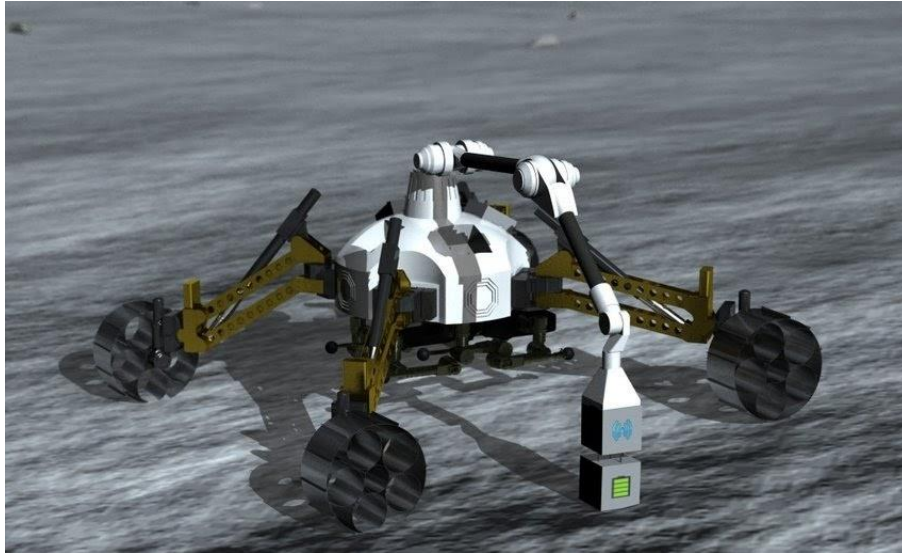
missions. Its original design incorporates several space resources modules such as the drill and sampling recovery tool from Northern Center for Advanced Technology (NORCAT) and the NASA Regolith & Environment Science and Oxygen & Lunar Volatile Extraction (RESOLVE) instruments for in situ processing of core samples [11]. While the drilling system is fixed, the RESOLVE payload is removable for servicing and calibration. This can characterize Scarab as a modular rover and open the possibility for incorporating other scientific payloads to the vehicle chassis in the future. Each module attached to the Scarab has its own avionics, power and thermal management system. Figure 4 introduces the rover system:



*Figure 4- Scarab rover and RESOLVE modules [11]*

### **2.1.5 DFKI RIMRES**

The Reconfigurable Integrated Multi-Robot Exploration System (RIMRES) [12] was developed by DFKI Bremen in 2009 as expansion of previous multi-robot cooperation projects. It is constituted of a team of robots, represented by the four-wheeled Sherpa rover and the six-legged scout Crater Explorer (CREX), and payload units that can be scientific tools or infrastructure components. The rover and the crawler can be connected through an electromechanical interface (EMI) to form a combined structure. The same EMI is also used to attach the payload modules to the manipulator of the Sherpa rover. Each payload module has a standardized Power Management System (PMS) which allows external consumers and power sources to use common power buses. Figure 5 illustrates the RIMRES system:



*Figure 5 -The DFKI RIMRES system encompasses the four-wheeled Sherpa rover, the legged scout CREX and immobile payload units. [12]*




The concept used in RIMRES is the closest to that used in ARCHES. Rather than having the body of the mobile robots subdivided in several pieces to be reshaped in different configurations, both have robots that can cooperate with each other and payload modules that can extend the capabilities of the rover. However, ARCHES intends to go further in exploring the benefits of modularity with the development of its MI.

#### **2.1.6 Modularity Qualitative Assessment**

This subsection brings a qualitative assessment of the modular robotics systems introduced in section 2.1. With the purpose of evaluating how well each modular system performs, this study considers six modularity characteristics. Three of them (standardization, versatility and maintainability) are described in the NASA framework for modular assembly systems [13] and were adapted to planetary robotic exploration. The three additional attributes (integration capability, manipulability and operability) were included considering how these robots interact with external systems and how they operate in the field.






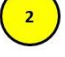




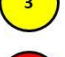
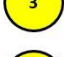



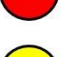
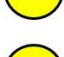



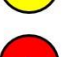
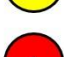





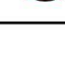


To understand how they can be assessed, the following table describes the criteria for each modularity sub-attribute:

Table 2 - Criteria for Modularity Qualitative Assessment

Attributes	Sub-Attributes	Comments	Qualitative Assessment		
			0-1 	2-3 	4-5 
Standardization	Standard Interface	Qty Different Interfaces	> 5	3 - 4	1 - 2
	Standard Modules	Qty Different Payloads	> 5	3 - 4	1 - 2
	Plug and Play	Change HW no need to redesign	Never	Sometimes	Always
Versatility	Multi-Function	Variety of functionalities	1 - 2	3 - 4	> 5
	Multi-Level	Modularity in several levels	1	2	3
	Reconfigurable	Disassembled and recombined	Never	Sometimes	Always
	Upgradable	Accommodate new technologies	None	Few	Several
Maintainability	Scalable	Add modules to grow the system	Small	Medium	Large
	Serviceable	Scheduled Events (maintenance)	Hard	Medium	Easy
	Repairable	Unscheduled Events (repair)	Hard	Medium	Easy
Integration Capability	HW external systems	HW integration external payloads	Low	Medium	High
	HW sub-systems	HW integration internal modules	Low	Medium	High
	SW external systems	SW integration network (external)	Low	Medium	High
	SW sub-systems	SW integration internal modules	Low	Medium	High
Manipulability	Docking Process	Flexibility ( angular/linear tolerances)	Low	Medium	High
	Payload Portability	Ability to carry payload boxes	Low	Medium	High
Operationality	Payload Operating Independently	Internal electronics for self-sustaining Operation. No dependency on rover.	Low	Medium	High

Although the Mechatronics Infrastructure (MI) is a concept created in this thesis for the ARCHES project, it will be associated with the robotics systems presented in section 2.1 with the purpose of comparing their modularity characteristics. The result is presented as follows:

Table 3 - MI Modularity Qualitative Assessment

Attributes	CEBOT	ATRON	ATHLETE	SCARAB	REMRIS
Standardization					
Versatility					
Maintainability					
Integration Capability					
Manipulability					
Operationality					

The evaluation was carried out based on the publications available about each robot and their subsystems.

CEBOT is a pioneer system in modular robotics. However, it does not mean it is the system which provides most of the benefits in modularity. Standardization was evaluated as medium (3.3) because interfaces and modules were upgraded during series I to IV without the consistency of its geometry. This also led to the redesign of the modules and interfaces in the upgraded versions [14]. Versatility was assessed as low-medium (2) because CEBOT has only mobility functions, a single modularity level in the external hardware, and not well-defined purpose of its different geometries. Maintainability received a medium score (3) because the system has weaknesses in how the software can be maintainable and how easy it is to access or replace damaged parts in the interior of the modules. Integration Capability got a low value (1.75) because CEBOT has poor interaction with external systems such as scientific instruments, no indication of network among different modules, and limited functionalities for internal data transfer. Manipulability had a low-medium result (2) because the robot has no capacity to manipulate objects, has few millimeters of tolerance in docking, and cannot carry external payloads. Finally, Operationality was assessed as low (1) because its modules were not designed to operate independently and there are no payloads to be interconnected to it.

ATRON is a great example of how robots can be reconfigurable through their bodies. However, it presents limitations regarding tasks to be performed in planetary exploration such as manipulation and scientific measurements. The Standardization aspect of ATRON was evaluated as high (4) because its docking mechanisms are fully standardized, and the modules are exactly a replica of each other. Interfaces to accommodate new technologies might need redesign. For Versatility it received a low-medium score (2.4) because it has only mobility functions, a single modularity level in the external hardware, and need of redesign if technologies are upgraded. Maintainability received a medium score (3) because the system has weaknesses in how the software can be maintainable and how easy it is to access or replace damaged parts in the interior of the modules. Integration Capability got a low-medium value (2.25) because ATRON has poor interaction with external systems such as scientific instruments and no indication of network among different modules. Internally, HW and SW appear to have reasonable interconnection when considering the power management between modules for instance [15]. Manipulability had a medium result (2.5) because the robot has no capacity to manipulate objects and cannot carry external payloads. Angular and linear tolerances for docking are good with 45 and 4 cm [16]. Finally, Operationality was assessed as low (1) because its modules were not designed to operate independently and there are no payloads to be interconnected to it.

ATHLETE is a marvelous reconfigurable robotic system to support human exploration on planetary surfaces. For Standardization it was evaluated with a medium score (2.7) because its interfaces will possibly need redesign to include future technologies. The interfaces are basically hooking and docking tools [10]. Modules are the limbs and the interchangeable tools. For Versatility the evaluation was a medium value (3) because ATHLETE has reasonable multi-functionality (drilling, scooping, gripping and carrying) and it can be scalable with the connection to other ATHLETES. However, it possesses only one level of modularity. Its Maintainability aspect was assessed as high (4) because ATHLETE's geometry is favorable to the replacement

of parts with its six identical limbs and seven onboard CPUs. Integration Capability was evaluated as low-medium (2.3) because the robot does not interact with the payloads it carries or any external sensors. Also, there is no evidence of software networks with external systems. Manipulability had a high-medium score (3.5) because it has sufficient tolerances in the docking process and high capability of carrying payloads. Finally, Operationality was evaluated as low (1) because its modules were not designed to operate independently and there are no payloads to be interconnected to it.

The SCARAB rover carries the RESOLVE sensing payload for ISRU missions, but it does not show flexibility for accommodating other scientific payloads. Standardization was evaluated as low-medium (2) because it is not clear how the rover is interconnected to the RESOLVE system. Also, the RESOLVE modules, which were designed differently according to each ISRU task [17], are not standardized. Its Versatility aspect was accessed as low (0.8) because Scarab is limited to the functionality of the ISRU mission. It cannot be scaled up nor reconfigured itself. Maintainability had a medium score (3) because the system has weaknesses in how the software can be maintainable and how easy it is to access or replace damaged parts in the interior of the RESOLVE system. Integration Capability got a low value (1.75) because it is not clear how Scarab interacts with external systems such as RESOLVE and there is no indication of a modular software networking. Internally, HW appears to have reasonable interconnection between each ISRU sub-system. The Manipulability was also evaluated as low (1.5) because Scarab has no manipulator, docking interfaces are not specified, and it is unclear if other payloads could be adapted to the rover structure. Finally, Operationality was accessed as low (1) because RESOLVE was not designed to operate independently and there are no additional payloads to be interconnected to it.

RIMRES is one of the robotic systems that can be highly benefited by modularity attributes. However, some points can be improved. Standardization was evaluated as high (4.3) because of its standardized EMI, PMS board and payload modules. The standardization of interfaces for new technologies is not specified and the system needs special design for upcoming payload items such as Relative Interferometric Position Sensor (REIPOS) and drilling sub-system [12]. Versatility had a high-medium (3.4) score because RIMRES has a reasonable multi-functionality with its two payload modules: battery module and scientific camera module. It has two levels of modularity (payloads and electronics), but the PMS has no modular components. It can be upgradeable, but the small volume of the payload carriers can be a challenge to incorporate new scientific instruments. Maintainability got a high value (4.5) because RIMRES has the possibility to be maintained and replace parts when damaged. However, there are no specifications about how easy it is to access the interior of the payload items. Integration Capability was evaluated as high-medium (3.8) because the system has good interconnection with external components or internal subsystems. There is a basic WLAN network for data transfer to control station. Manipulability was accessed as high (4) because the docking process has sufficient angular and linear tolerances with 5 mm and 40 degrees [18], and the payload portability is good. Finally, Operationality was evaluated as high (5) because the payload items can operate independently from the rover systems.

Regarding the electronics power management and data handling (PMDH) board in the interior of the modules, not all the systems disclosed detailed information. Therefore, only a few of them were considered and evaluated. The result is described as follows:

*Table 4 - PMDH Board Modularity Qualitative Assessment*

Attributes	ATRON	SCARAB	REMRIS
Standardization	4	1	4
Versatility	1.2	1.2	1.8
Maintainability	3	3	3
Integration Capability	2.3	1.8	3.8

The analysis was performed based on the publications available about each robot electronics power and data handling system.

The ATRON PMDH board was accessed as high (4) for *Standardization* because its interfaces and modules (upper and low hemisphere) are highly standardized, but the interfaces for incorporating future technologies are not present. The *Versatility* was accessed as low (1.2) because the ATRON PMDH is limited to perform the power management and the actuators control [15]. Also, because it is not designed to accommodate newly developed components and it is not possible to be scaled up. *Integration Capability* got a medium (2.3) score because it has good interconnection with internal subsystems, but poor with external systems (no external sensors or scientific instruments are integrated to ATRON).

The SCARAB/RESOLVE avionics system was designed specifically for the ISRU demonstration mission. There is no indication that the systems were designed similarly for different scientific modules. Therefore, *Standardization*, *Versatility* and *Integration Capability* were evaluated as low.

The RIMRES PMS board was evaluated as high (4) for *Standardization* because its interfaces and modules are highly standardized, but the interfaces for incorporating future technologies are not present. The *Versatility* was accessed as low (1.8) because the RIMRES PMS is limited to the power management system and offers a restricted amount of different power buses [19]. *Integration Capability* got a high-medium (3.8) result because it has good interconnection with internal subsystems and reasonable with external systems (Ethernet, RS-422 and Wi-Fi).

After the MI and PMHD board qualitative assessments were performed, it is possible to conclude that existing modular robotic systems lack a wider versatility and capability to

integrate internal and external components to their systems. With this gap identified, the hardware and software development of the ARCHES MI is an opportunity to demonstrate that current systems can be improved and diversified. Also, it can create a benchmark for future space robotic systems, which is essential for the desired sustainable space exploration with the construction of large structures on planetary surfaces.

## 2.2 Small Satellites

Small satellites, such as CubeSats or NanoSats, are very common technology used in space today. According to ESA [20], the fixed dimensions of these miniaturized satellites allows a high level of modularity and system integration by the use of commercial-off-the-shelf (COTS) products to develop subsystems that can be stacked to each other depending on the nature of the mission. This modular approach can bring several benefits as flexibility to satisfy multiple functions, short development time to reduce costs, and less complexity in integration. These advantages are in line with the goals of this study. A few examples are illustrated in this section.

### 2.2.1 Mars Cube One (MarCO)

MarCO is a CubeSat that was launched in 2018 as part of the Mars Insight mission. Two units of this CubeSat were deployed, and they supported with telecommunications during atmospheric entry of the Mars Insight lander. Each spacecraft has six-unit CubeSat (6U), which is 6 x 10 cm x 10 cm x 11.35 cm. Their modular architecture includes a Command and Data Handling board, a Power System with solar panels and lithium ion batteries, a Communications System with Ultra-high Frequency (UHF) antenna and X-Band transponder, and Attitude, Control and Propulsion system with gyros, star trackers, 3-axis reaction wheels and cold gas thrusters [21]. Figure 6 presents the compartments of the CubeSat with their different functionalities.

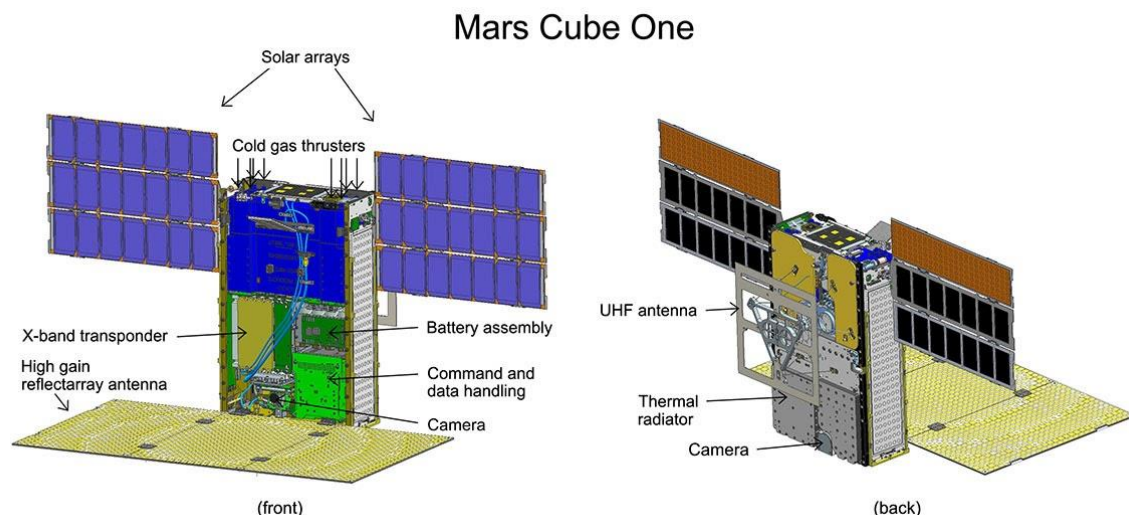
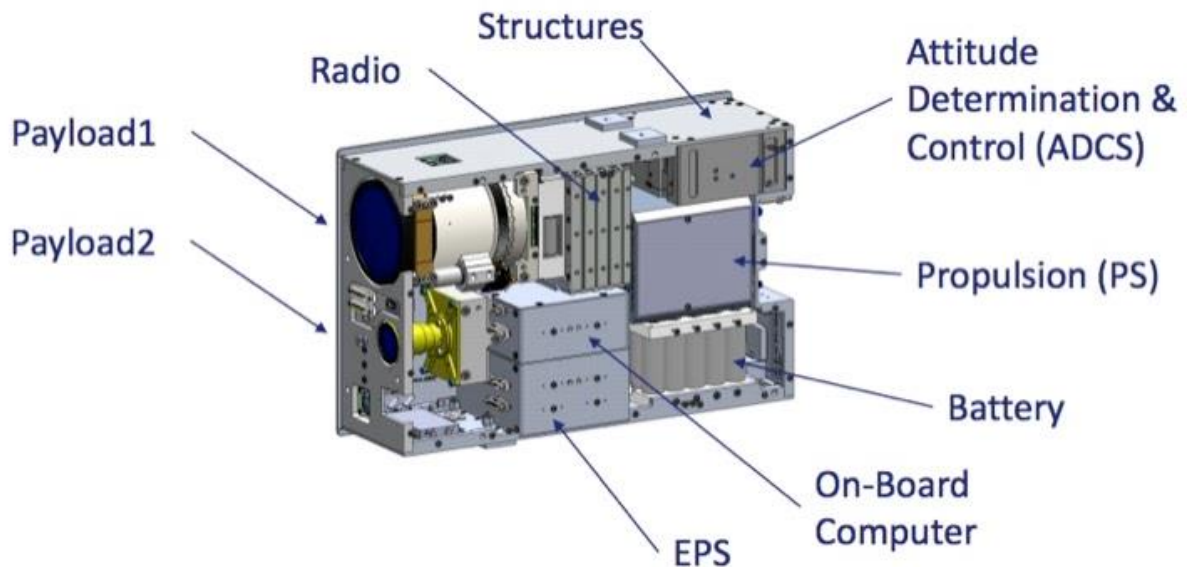


Figure 6 - Marco CubeSat [22]

### 2.2.2 ArgoMoon

ArgoMoon is a 6U cubesat developed by the Italian company Argotec. It is part of the Italian Space Agency (ASI) project with NASA to capture images of the Orion Exploration Mission-1 (EM-1) that will fly in 2020 [23]. Its subsystems are similar to MarCO CubeSat, however it has more power supplied through solar panels, more memory capacity and two narrow and wide field of view cameras. The modularity of each subsystem is still present and can be observed in figure 7:



*Figure 7 - ArgoMoon [23]*

### 2.2.3 Flying Laptop from University of Stuttgart

Researchers from the University of Stuttgart developed a mini satellite called Flying Laptop (FLP) that was launched in 2017 as part of the Small Satellites Program [24]. With the challenging task of designing a satellite with reduced mass and low power consumption, they came up with the idea of combining the On-board Computer (OBC) and the PCDU. This innovative technology was named Combined Data and Power Management Infrastructure (CDPI) [25]. The CPDI was built in a modular way to provide flexibility while being compliant to the technical constraints of the project. Its configuration is illustrated in figure 8 as follows:

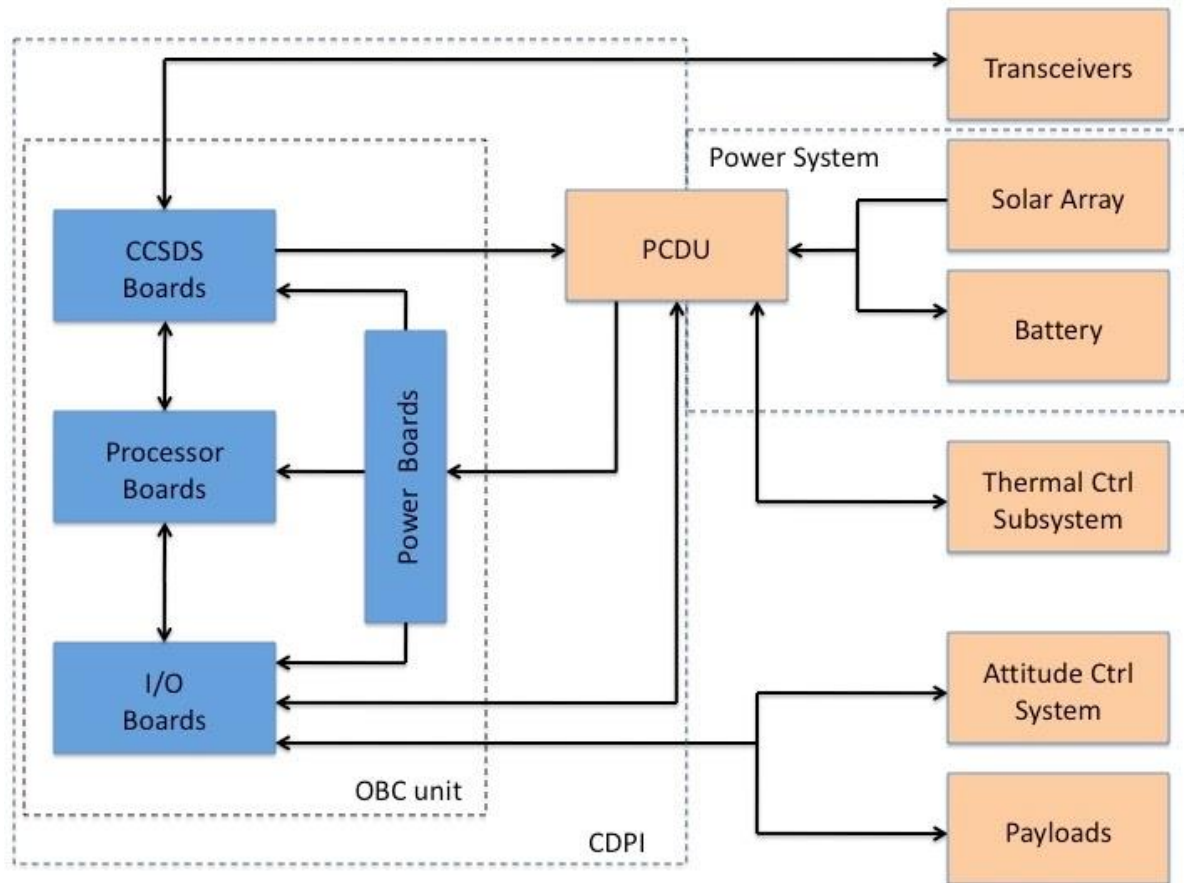


Figure 8 - CDPI adapted diagram [25]

The OBC encompasses four different stacked boards that are present twice for redundancy purpose [26]. They are: the Processor board which is responsible for data processing and control, the I/O board which has the digital interface for data transfer and telemetry data storage capacity, the Consultative Committee for Space Data Systems (CCSDC) board which performs communication with the satellite ground station, and the Power Supply board which supplies extra-low voltages to the other six OBC boards.

The PCDU is built in five stacks which are individual Printed Circuit Boards (PCBs) assembled in a single unit. Besides executing the conventional power regulation and distribution, it also acts as a combined controller which measures data, currents and voltages from most of the satellite subsystems [27]. Additionally, in case subsystems fail or the on-board software (OBSW) crashes, the CCSDC boards will send High Priority Commands (HPCs) directly to the PCDU which will keep the satellite operational and controllable. These extended functionalities show the importance of the PCDU for the satellite system.

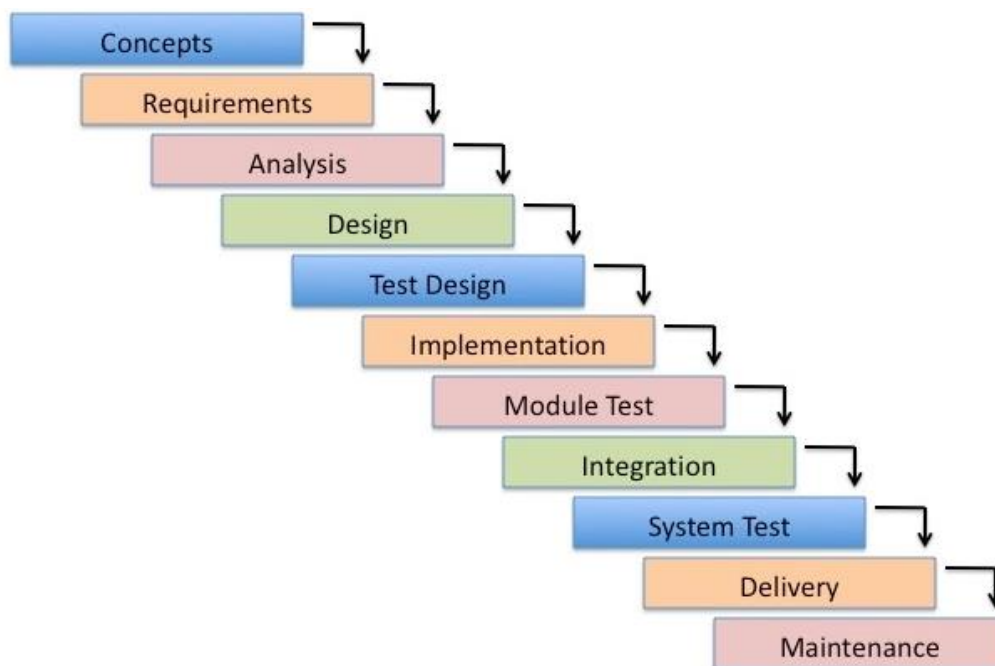
In this thesis, the design of the Payload Box Infrastructure Management System (PBIMS) is based on some features of the CPDI such as its modular structure, compactness, versatility and safety during operation.

## 2.3 Model-Based Engineering

Model-Based Engineering (MBE) is a method for managing complex systems and projects [28]. It adopts an approach in which the process is decomposed into a few phases that range from the specifications' definition to the delivery of the final product. The flawless application of the method is achieved with the execution of tests to meet the defined requirements, the adequate system integration and the acceptance of the product by the user. Although there are several MBE methodologies, this work will present the three most used in the automotive and aerospace industry: Waterfall, V-shaped and Spiral.

### 2.3.1 Waterfall

The Waterfall methodology was developed by Benington in 1956 [29] and modified by Winston Royce in 1970 [30]. It is a linear and sequential application model for software development and manufacturing. The process is broken down into successive phases. This is a very straightforward approach which is easy to execute. However, there is the disadvantage that previous phases are not revisited after they are finalized which would not allow verification and validation of the process. This was criticized by Royce [30] in his own paper in which he pointed out that the implementation could be risky, and failures could happen. Therefore, he suggested an iterative model by adding arrows that connect each stage back to its antecessor. This modified model is also emphasized by Barry Bohem [31] in 1986 when he created the Spiral methodology. Figure 9 shows this methodology as follows:



*Figure 9 - Waterfall Model [30]*

### 2.3.2 V-Shaped

The V-Shape methodology was developed by NASA for satellite systems and was presented in 1991 at the National Council on Systems Engineering (NCOSE) conference [32]. It is a derivation from the Waterfall model, but it focuses on iterative stages to perform verification and validation. While the descending branch of the model represents the product or project definition, the ascending branch concentrates on the integration, test and verification. If observed from top to bottom, the model can be decomposed from system to component level. This hybrid approach including sequential and concurrent development has stakeholders and users involved in its entire process which leads to an enhanced final product and more unlikely to have failures. The NASA space missions Clementine in 1994 and Mars Pathfinder in 1997 had their project management process based on the V-shaped model. This made them successful examples of concurrent engineering application, adequate project cycle implementation, risk mitigation and cost reduction [33]. Figure 10 presents the representation of this model:

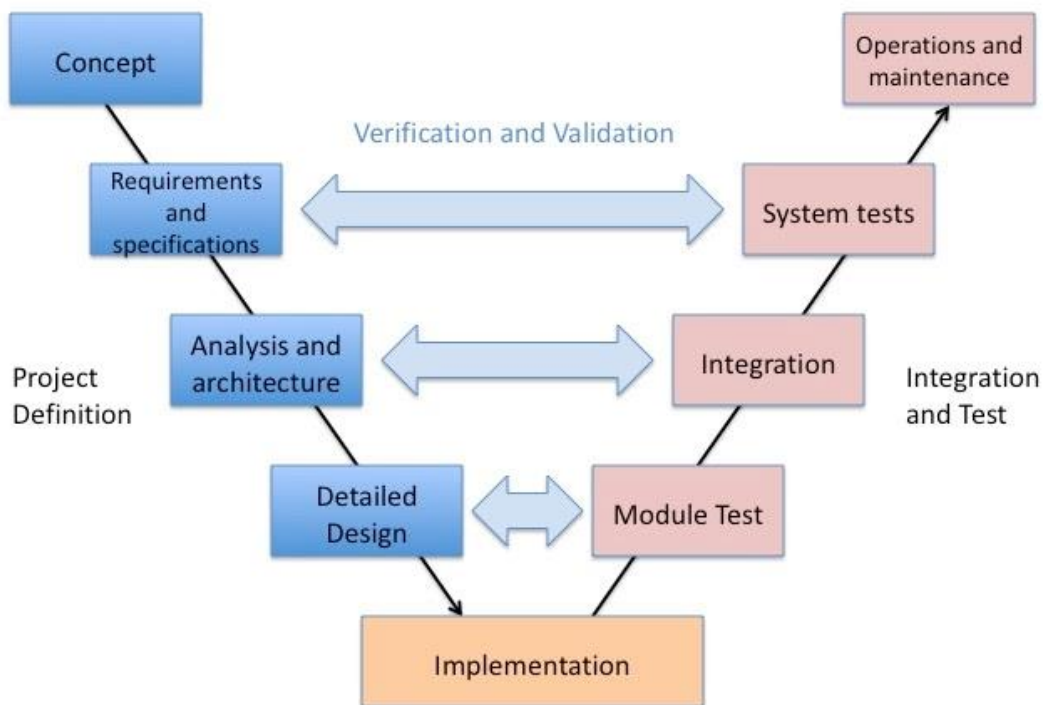


Figure 10 - V-Shaped model [34]

### 2.3.3 Spiral

The Spiral methodology is a risk-driven process model created by Barry Boehm [31] in 1986 for the development of software-intensive systems. This cyclic approach emphasizes concurrent engineering, reassessment of critical stakeholder needs, constraints and risk mitigation at each cycle, level of effort and detail under the risk perspective, degree of stakeholder commitment during the entire process, and overall system importance. Although it was initially

designed for software development, it can also be used for any engineering complex systems. For instance, the United States Air Force (USAF) and NASA use a slightly modified version of this model for the design of spacecraft systems. Farr et al. [35] saw an opportunity to continuously accommodate new technologies to NASA's space transportation system by the combination of this methodology with the modularity in the spacecraft design and manufacturing process. In this manner they ensure that innovative solutions are always considered which put them at the forefront of the space industry. The following figure introduces the original Boehm's model:

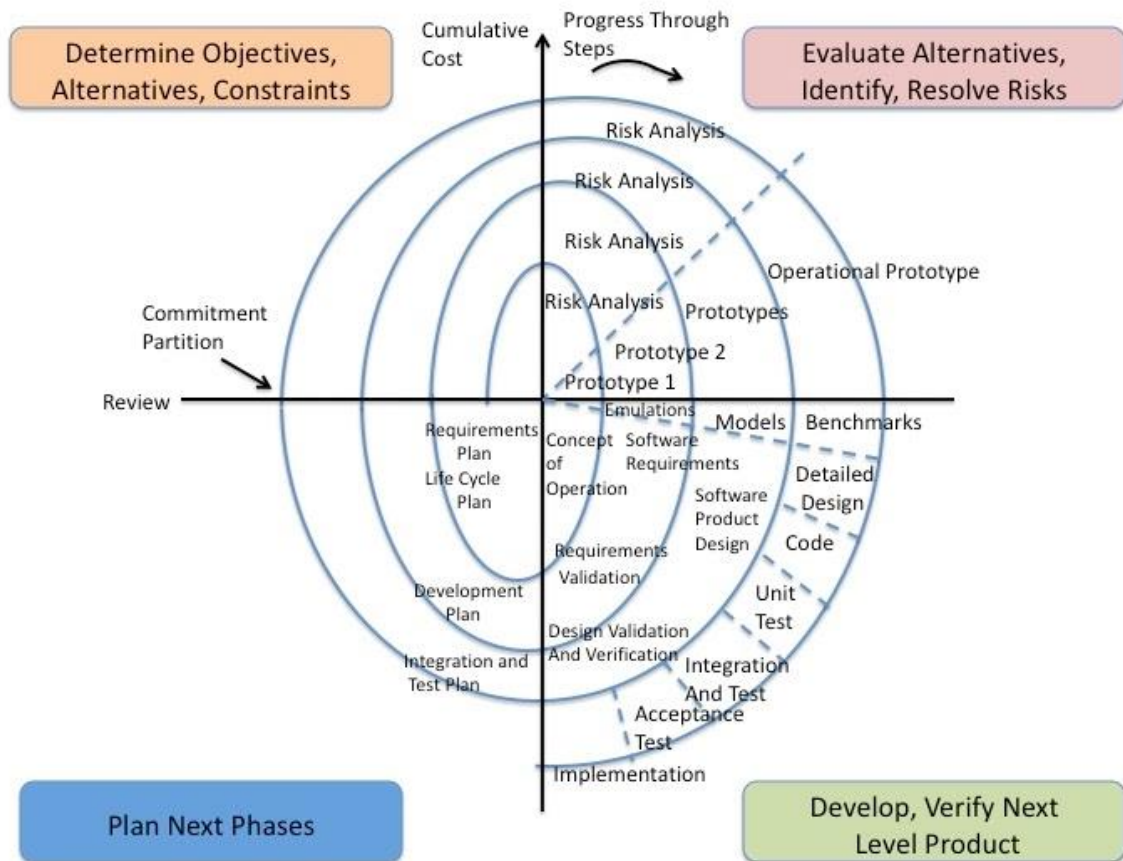


Figure 11 - Spiral Model [31]

## 2.4 Docking Interfaces

Docking interfaces are key to build modular structures and allow exchange of power, data, fluid and thermal flow between the parts. It was heavily used in railway systems in the past and in space it started with Gemini VIII in 1966 [36]. Followed by the first Russian docking with two Soyuz modules in January of 1969 and Apollo 9 in March of 1969 [37]. Many subsequent missions happened after the prominent beginning - the Russian space station Salyut in 1971 [38], the American space station Skylab in 1973 [39], the improbable Apollo-Soyuz project in 1975 brought Americans and Soviets together during the Cold War [40]. Other missions include the MIR station in 1986 [41], the MIR/Shuttle 11-mission program from 1993 to 1998 that made

international cooperation in space possible. And finally, the ISS that had its first module launched in 1998 and has been a test bed for docking and berthing mechanisms.

For robotic systems, docking interfaces played a significant role in the development of modular robotics as it was shown in section 2.1 in this chapter. Regarding future missions and applications, they will undoubtedly continue to be important because the vision for future space exploration is to create a sustainable human presence on the Moon and Mars as stated in the Global Exploration Roadmap (GER) [2]. This endeavor will aim for huge architectures and in-situ resource utilization (ISRU). Therefore, robots will need to be modular to execute these operations, and consequently, attachment mechanisms on their end-effectors and bodies will be necessary. There are mainly four types of mechanical docking mechanism as shown in [42]: Hook, Clamp, Carabiner and Roto-Lock.

### 2.4.1 Hook

The movable hooks of one module will latch the pins or bar of the target module. Figure 12 (a) demonstrates the hooking mechanism while figure 12 (b) shows an example applied to modular robotics with two ATRON modules connecting to each other:

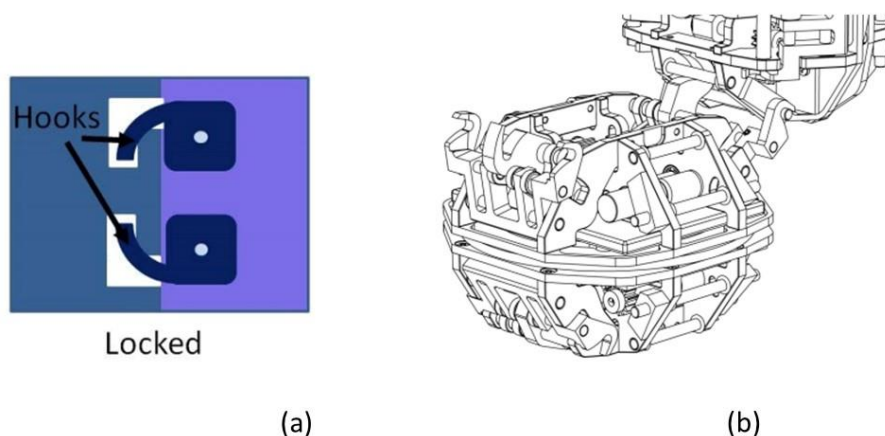


Figure 12 – (a) Docking mechanism with hooks [42]; (b) ATRON hook docking mechanism [15].

### 2.4.2 Clamp

Two or more chucks or spring-loaded devices will close at the same time to attach the two surfaces of the connectors together. The mechanism and the example of the European Robotic Arm (ERA) can be seen in figure 13.

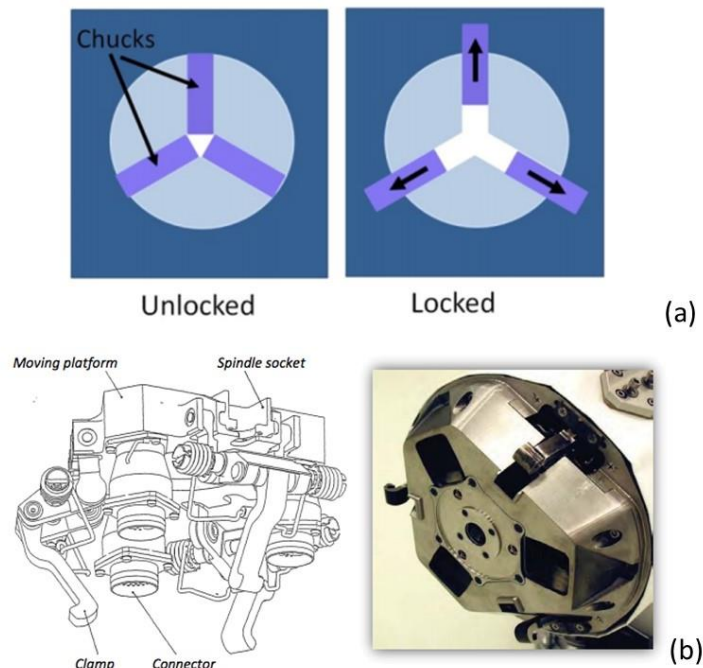


Figure 13 – (a) Clamping Docking Mechanism [42]; (b) Grapple mechanism showing three clamps and three connectors in the ERA [43].

### 2.4.3 Carabiner

The male part pushes the female counterpart that will retract. Then, the male part will continue forward until it reaches a threshold. After passing this point, the female piece will recover its original position and the system will be locked. The decoupling will happen with active force to unlock the system.

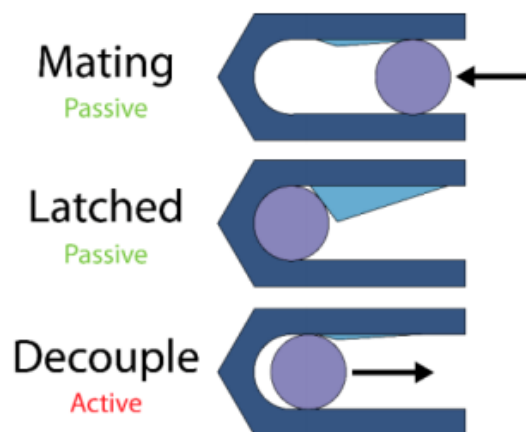


Figure 14 – Carabiner Docking Mechanism [42].

### 2.4.4 Roto-Lock

In this mechanism the male and female interfaces will couple to each other and then a motor initiates a rotation to lock the system. It is possible to see this in the iBoss modular satellite.

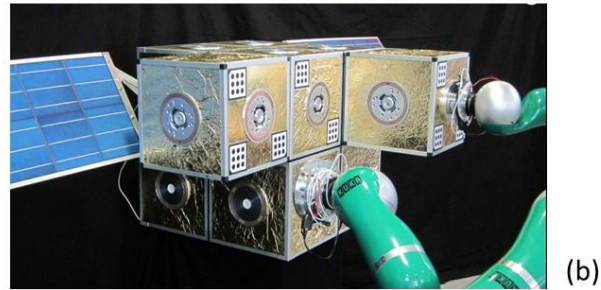
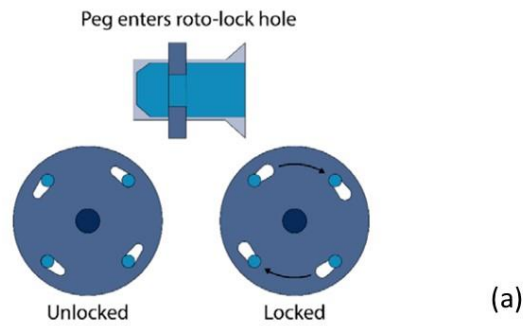


Figure 15 – (a) Roto-Lock Docking Mechanism [42]; (b) iBoss modular satellite [44]

In the ARCHES project the electromechanical docking interface is a clamping system composed by an active and a passive part. The active part has nine springs that are extended and retracted by an actuator. The passive coupling can be guided by the extended springs until both active and passive parts are mated. The retraction of the springs will ensure the system is latched and locked.

## 2.5 Power System

Electrical Power System (EPS) is possibly the most important system for a spacecraft or a rover because if this system fails or shutdown, with no possibility of recovery, the space mission will be terminated [45]. A recent example is the NASA Opportunity Rover that had its solar panels covered by regolith after a heavy dust storm. It entered hibernation mode and could not re-establish contact with Earth even after NASA sent more than 1,000 signals to the rover. This demonstrates how critical this system is in any space mission.

The three main components of the spacecraft and rover EPS are the primary and secondary power sources, and the power management, control and distribution network. The following diagram shows how they are interconnected:

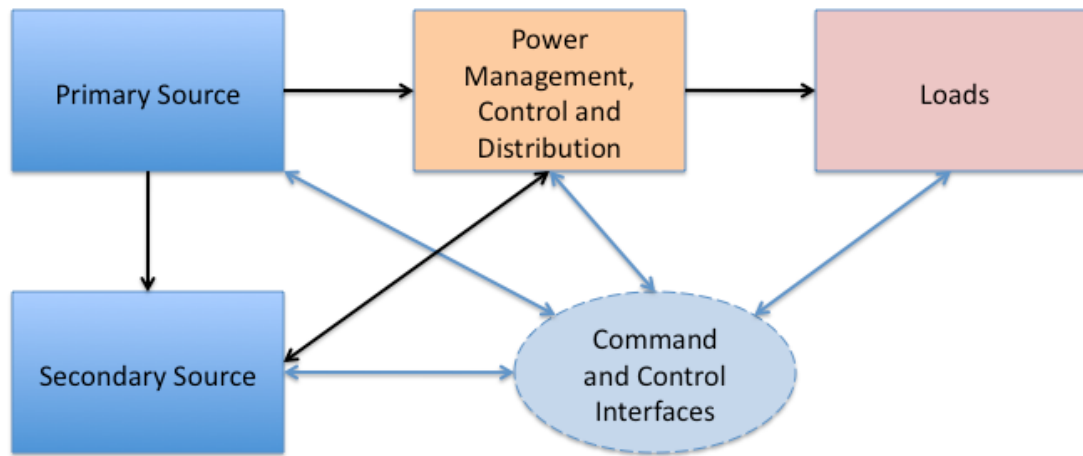


Figure 16 - Diagram of Spacecraft Electrical Power System [46]

### 2.5.1 Primary and Secondary Power Sources

The primary power sources perform conversion of fuel into electrical power. The fuel can be solar, nuclear, chemical or mechanical energy. Solar energy is heavily used in today's spacecrafts and rovers with the implementation of solar arrays. The solar cells are made of semiconductor p-n junctions that in the presence of solar illumination and radiation will allow current flow [45]. Examples of their applications are not only in satellites, but in rovers such as the Mars Sojourner in 1996, Spirit and Opportunity in 2004, and ExoMars to be launched in 2020. Nuclear energy in space is commonly represented by Radioisotope Thermoelectric Generator (RTG), which converts the heat produced by the decay into electrical energy. Its utilization is seen mainly in missions which solar arrays become inefficient because of the distance to the Sun. Pioneer 10 and 11 in 1972, Voyager 1 and 2 in 1977, Cassini in 2005 and New Horizons in 2006 are a few examples. The Mars Curiosity rover also uses RTG as a power source. Chemical energy is converted into electricity by the oxidation reaction of oxygen and hydrogen in the case of fuel cells technology implementation. They were used in Gemini, Apollo and the Space Shuttle orbiter. And finally, the mechanical energy of Reaction Wheels (RW) can be converted into angular motion of the spacecraft about its own axis. It is often used in telescopes and it was present in Kepler, Hayabusa and Hubble missions.

The secondary power sources are responsible for energy storage. These storage systems include mainly batteries and capacitors. The batteries can be classified into primary or rechargeable. Primary batteries are non-rechargeable and will generate power for short period missions that will last a few hours or days. A few examples of these batteries are: Lithium-sulfur dioxide (Li-SO<sub>2</sub>), which were utilized in Huygens probe, lithium-thionyl chloride (Li-SOCl<sub>2</sub>), which backed up Mars Sojourner solar panels during its mission, and silver-zinc (Ag-Zn), which were

used in the Soviet satellite Sputnik and the NASA Apollo Lunar lander. Rechargeable batteries provide power when the primary power source is not available. They are often used in missions with solar arrays or RTG. Mars Curiosity is currently using lithium-ion (Li-ion) batteries and the Hubble Telescope nickel-hydrogen (Ni-H<sub>2</sub>). Finally, capacitors are used to attend power peak demand by providing high pulses during a short period of time. They were present in the Cassini and Galileo spacecrafts.

In ARCHES, there are three power sources available: The External Battery, located in the energy payload box, the Internal Battery, placed in the interior of each payload carrier, and the Arm power, which comes from the batteries inside the LRU rover. Each of these sources are selected in order of priority by the Power Path Control (PPC) circuit.

### **2.5.2 Power Management, Control and Distribution**

The Power Management, Control and Distribution module is designed to allocate the correct power levels to the diverse loads of a rover or a spacecraft [45]. The power sources alone are not able to deliver the energy to all the subsystems. Therefore, this unit, often called Power Conditioning and Distribution Unit (PCDU), is responsible to regulate, control and distribute the power through a regulated main bus. Also, it guarantees the protection of the system with continuous operations even in the presence of an eventual failure.

#### **Power Conditioning and Regulation**

The Conditioning and Regulation subsystem is responsible for: the conversion of alternating current (AC) power generated by the primary power source into direct current (DC) power with the use of inverters or rectifiers, the maintenance of voltage and current levels steady, and the regulation of battery charges and discharges through the Battery Management System (BMS).

#### **Battery Management System (BMS)**

The BMS enables that batteries can be used efficiently and safely [47]. Its main functions include:

- Protection of battery cells by the identification of malfunctions such as extreme high temperatures, overcharging and electric leak
- Monitoring the capacity of the battery, voltage and temperature
- Checking the state of charge (SOC) and state of health (SOH)
- Regulation of voltage levels
- Control proper charging and discharging
- Isolate the battery from source and load

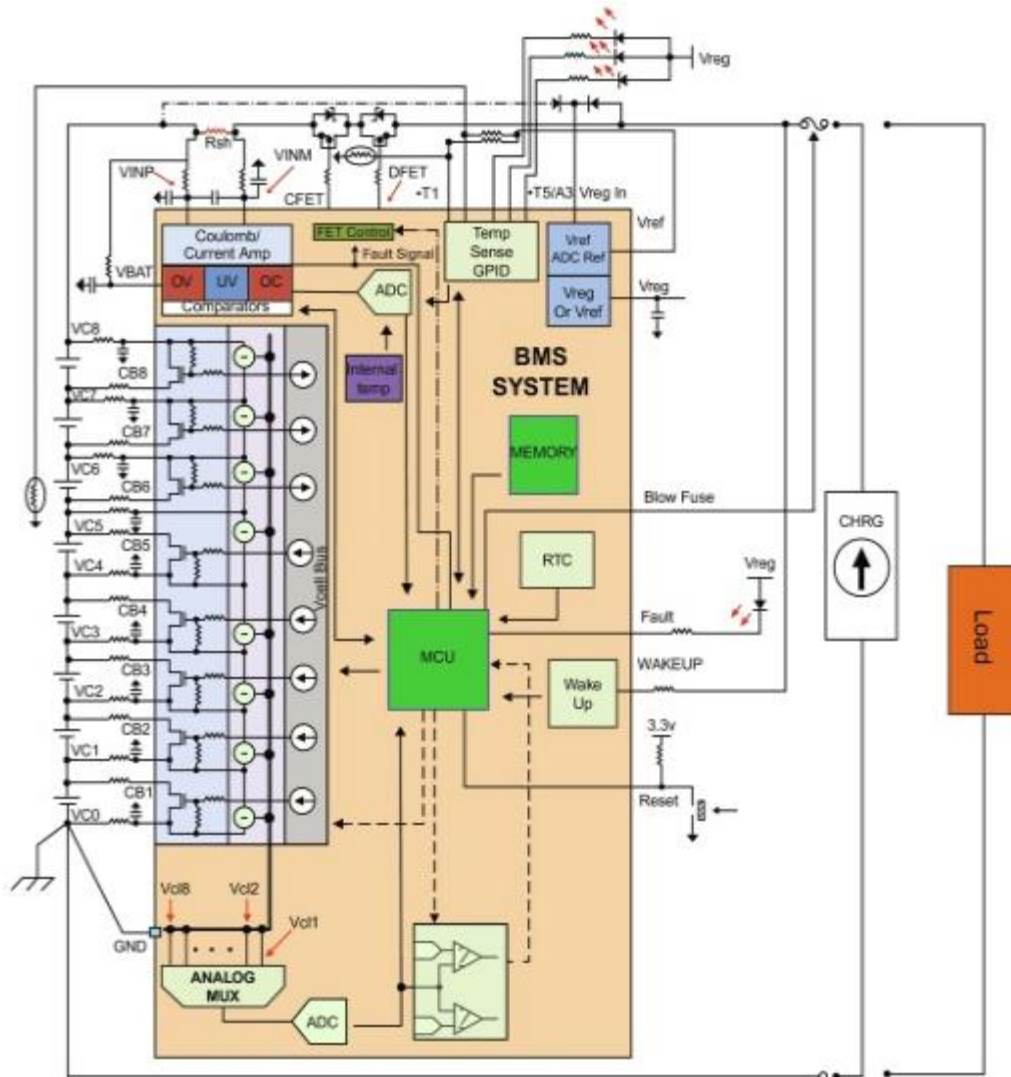


Figure 17- Diagram of BMS [47]

### Prioritized Power Path Control (PPC)

The prioritized Power Path Control (PPC) is a circuit that selects one valid power source among two or more available (V1, V2, etc.). This selection is performed based on priority which is defined by pin assignment. For instance, in the case of three power supplies in the circuit, V1 has the highest priority while V3 has the lowest. There is a range called Overvoltage (OV)/Undervoltage (UV) window which determines the validity of the power source. The channel must have its voltage for at least 256ms inside the window to be considered valid. The loss of priority happens when a valid input with the highest priority goes outside the OV/UV window. In this situation, the next highest priority will take place. The replacement of an invalid channel with a valid channel occurs almost instantaneously (8μs) [48].

Figure 18 shows an example from [48] with three available power sources. It is possible to observe the main parts of the circuit: the IC LTC4417 which does the logic, the three power sources (a), the resistors which define the OV/UV window (b), the P-channel MOSFETs which

allow the load current to flow or be blocked between the input supply and the load (c), the output voltage ( $V_{out}$ ) (d) and the VALID pins which indicate if the input supply is valid or not (e).

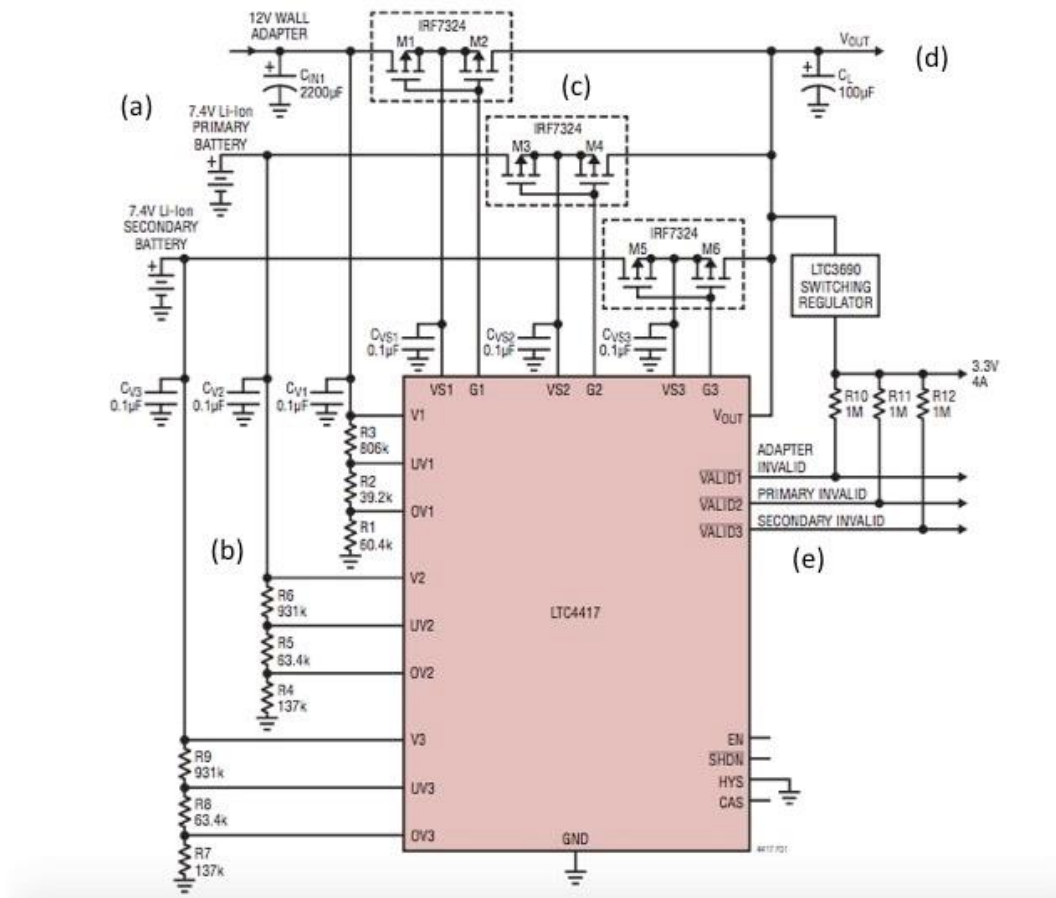


Figure 18 - Prioritized Power Path Control example with three power sources [48]

Considering the circuit displayed on figure 19, an example of how it would have the input voltages switching is presented. In this case, the highest priority (V1) is a wall adapter voltage of 12V. Followed by two Li-ion battery packs of 7.4 V (V2 and V3). Figure 17 shows on tag (1)  $V_{out}$  (purple) following the highest priority V1 (red). On tag (2), V1 goes out of the OV/UV window which leads to the immediate switch of  $V_{out}$  to V2 (green). On tag (3), V2 falls out of the OV/UV window which takes  $V_{out}$  to follow V3 (blue). On tag (4), V3 is out of its OV/UV range and the only valid supply is V1. Therefore,  $V_{out}$  starts to follow V1. Then, the example is completed with tag (5) where V1 is stabilized on its nominal voltage and  $V_{out}$  continuous to follow it.

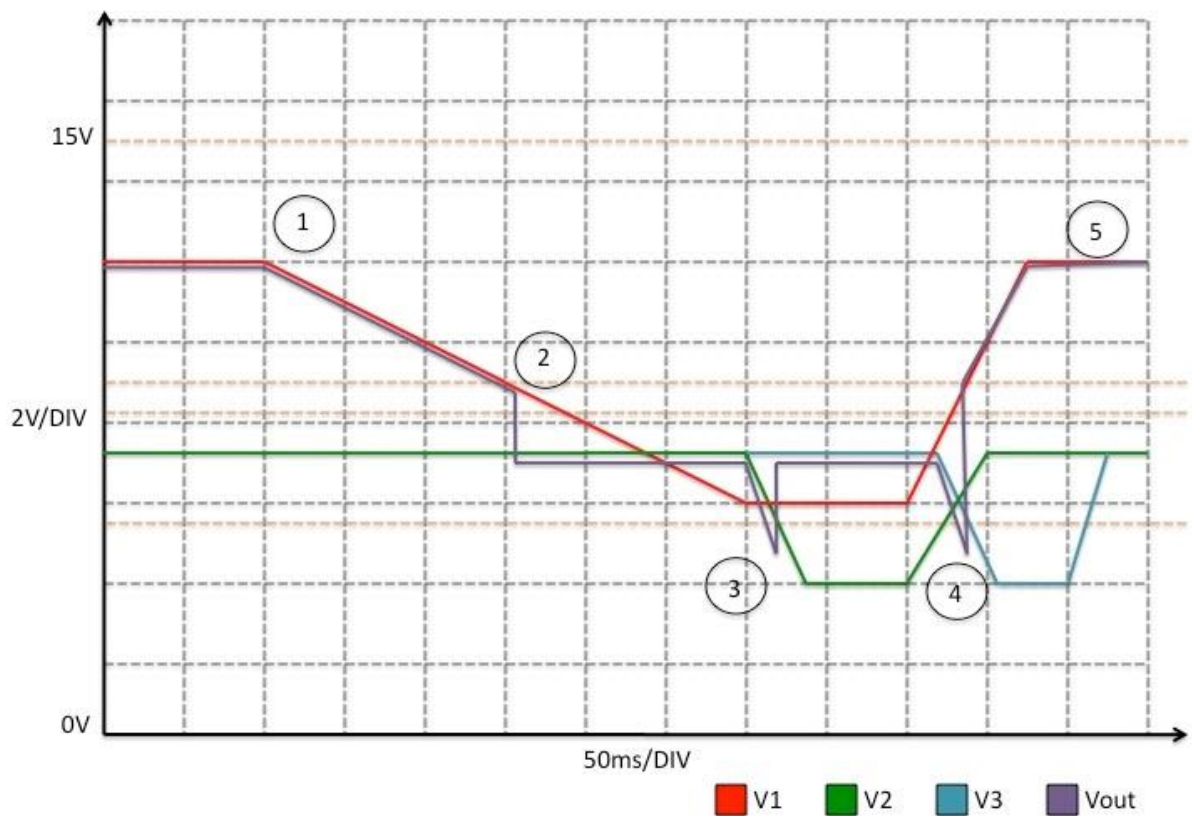


Figure 19 - Switching voltage between V1, V2 and V3.

## Power Distribution and Protection

This part of the system is responsible for the power distribution to the other subsystems of the spacecraft/rover and their circuits safety. Power switches and DC-DC converters will ensure the power distribution is performed adequately. Regarding protection, components of the circuit will prevent propagation of failures to the entire system and will provide protection against short-circuits.

## Switches and DC-DC converters

Switches are components of a circuit that allows the current to flow or to be blocked. This is important because it is possible to control the output voltage delivered to the load and protect subsystems from damage. Figure 20 shows a Power MOSFET switch to control DC motors. When the output voltage from the Transistor-transistor Logic (TTL) is 0V the MOSFET is OFF. If the voltage applied to the gate (G) is positive, the MOSFET is ON.

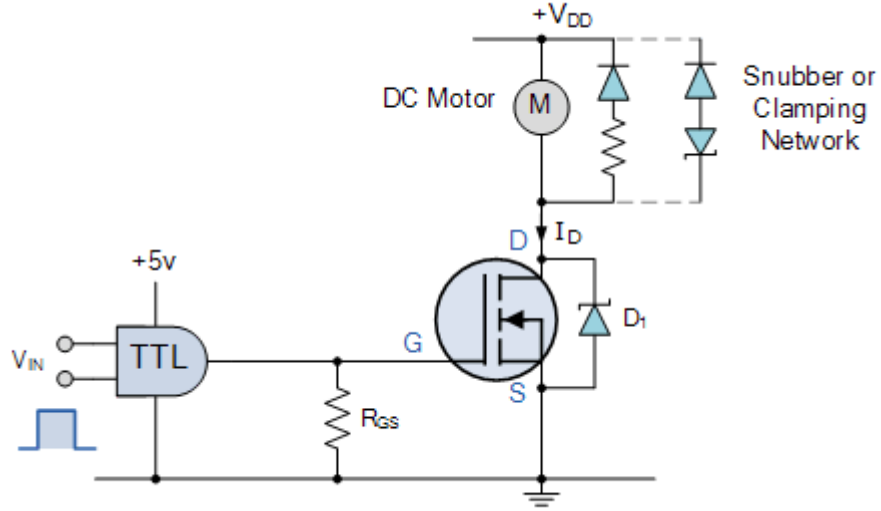


Figure 20 - Power MOSFET switch to control DC motor [49].

DC-DC converters are circuits designed to lower or increase the level of the DC output voltage and regulate it. Among the several existing topologies, the Buck and Boost converters will be presented because they are used in the PBIMS developed in this thesis.

The Buck converter is used to step-down the input DC voltage into a lower DC voltage. It is used when there is a need to lower down the voltage of a power source into lower levels to be utilized by diverse components or devices in the circuit or in the network. Figure 21 illustrates this circuit (a) which is mainly composed by a switch, a diode, an inductor and a capacitor. When the switch is ON (b), the input current  $i_{IN}$  flows through the circuit and the inductor current  $i_L$  increases with slope  $(V_{IN} - V_{OUT})/L$ . This stores energy in the inductor. When the switch is OFF (c), the inductor releases the energy and  $i_L$  decreases with slope  $-V_{OUT}/L$ . The current on the load  $i_{OUT}$  is equal to  $i_L$ . If the comparison between  $i_{OUT}$  and  $i_{IN}$  is carried out, it is possible to notice that the average value of  $i_{OUT}$  is higher than the average value of  $i_{IN}$  (d). Considering the conservation of energy, if  $i_{OUT} > i_{IN}$  then  $V_{OUT} < V_{IN}$ .

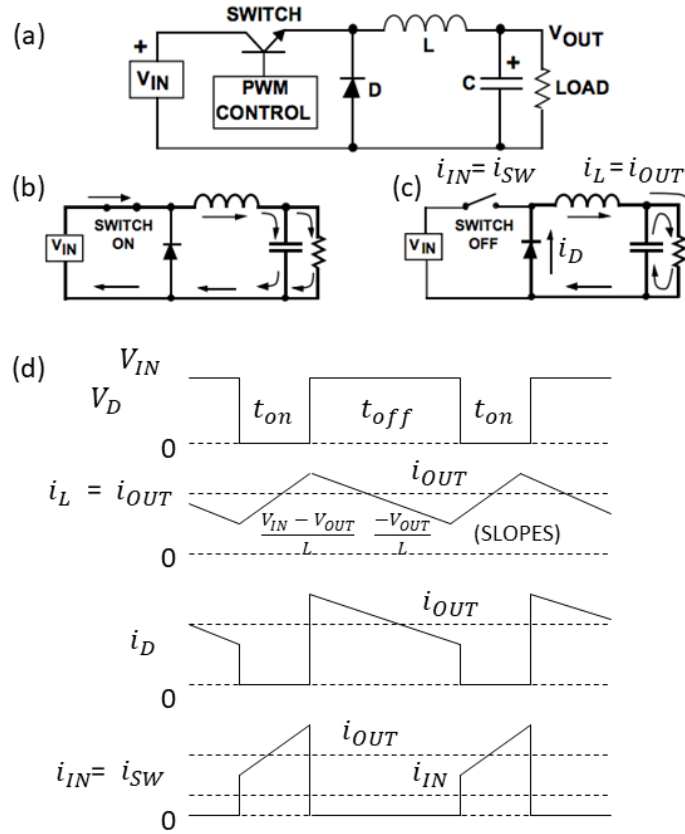


Figure 21 - (a) Buck Converter Circuit. (b) Flow Switch ON (c) Flow Switch OFF (d) Waveforms [50].

The Boost converter is used to step-up the input DC voltage into a higher DC voltage. It is used when the power source voltage needs to be increased to a higher voltage demanded by a device in the network. Figure 22 illustrates this circuit (a) which is mainly composed by a switch, a diode, an inductor and a capacitor, but with a different configuration compared to the Buck converter. When the switch is ON (b),  $i_L$  increases with slope  $V_{IN}/L$ . When the switch is OFF (c), the inductor releases the energy and  $i_L$  decreases with slope  $(V_{OUT} - V_{IN})/L$ . The current from the supply source  $i_{IN}$  is equal to  $i_L$  and the current on the load  $i_{OUT}$  is equal to the current on the diode  $i_D$ . If the comparison between  $i_{OUT}$  and  $i_{IN}$  is carried out, it is possible to notice that the average value of  $i_{OUT}$  is lower than the average value of  $i_{IN}$  (d). Considering the conservation of energy, if  $i_{OUT} < i_{IN}$  then  $V_{OUT} > V_{IN}$ .

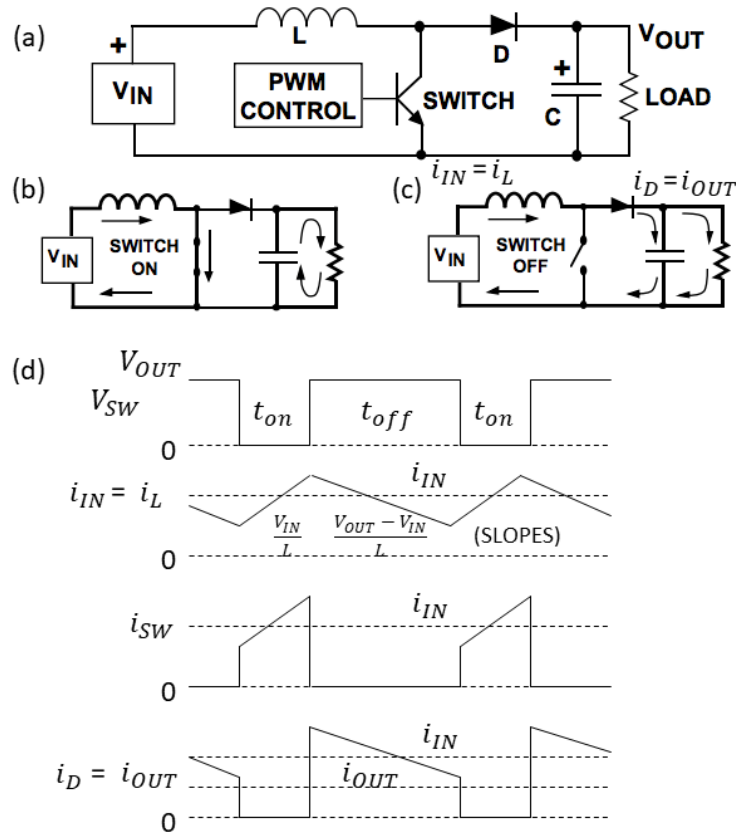


Figure 22 - (a) Boost Converter Circuit. (b) Flow Switch ON (c) Flow Switch OFF (d) Waveforms [50].

## Control Interface

The Control Interface monitors parameters such as voltage, current, temperature and status. All the acquired data will be transmitted to the OBC. This information will be essential for the accurate monitoring of the Power System and to take actions for enabling/disabling switches and power buses.

## Pulse Width Modulation (PWM) for Control

A technique used to control the amount of power delivered to a load is called Pulse Width Modulation (PWM). It is basically a generation of an analog signal using a digital source [51]. Its applications include the ability to control the speed of small DC motors or the intensity of light-emitting diodes (LEDs). The PWM signal has two main components: *duty cycle* and *frequency*. Duty cycle (D) is the ratio between the amount of time the signal is high (ON state) by the total time of a complete cycle. Frequency (f) is how fast the PWM cycle is completed. The following figure describes the characteristics of the PWM signal and how the variation of the duty cycle impacts on the level of voltage delivered to the load:

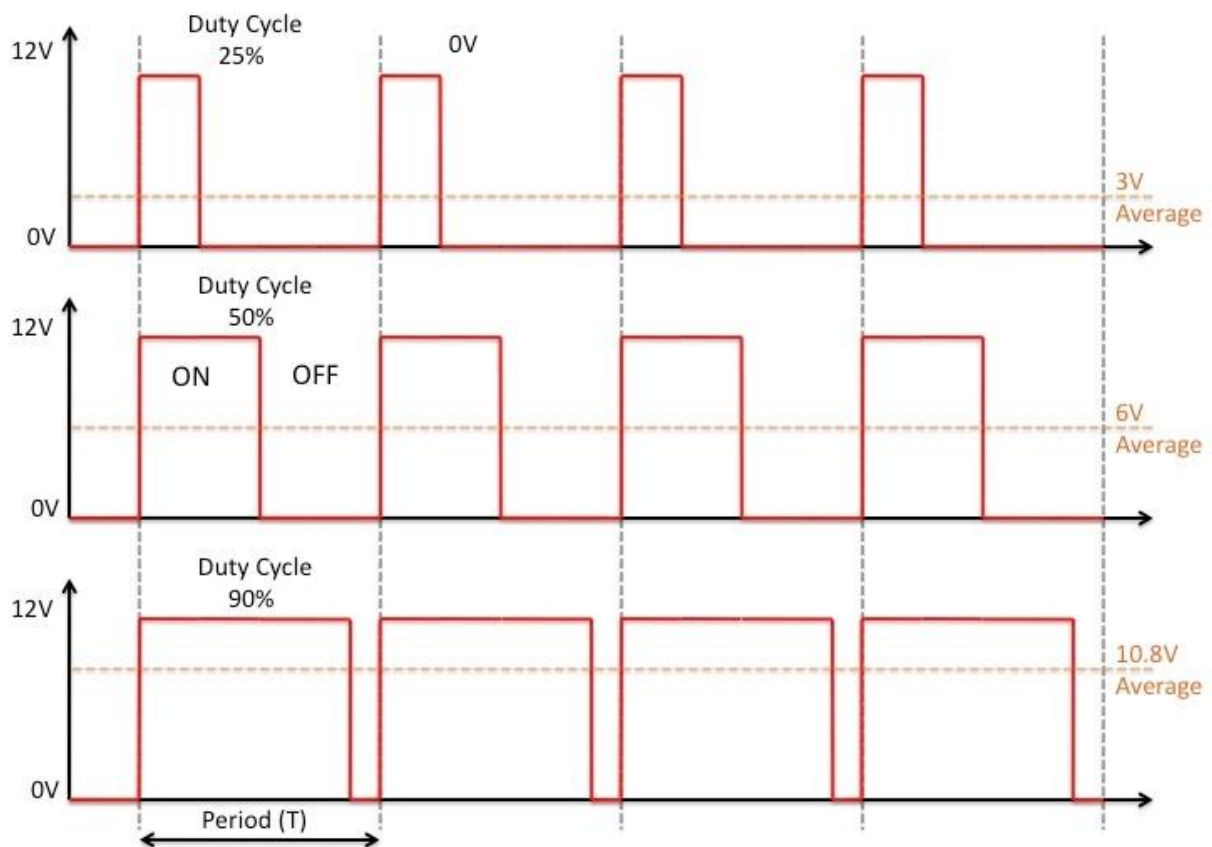


Figure 23 - PWM signal in 25%, 50% and 90% duty cycle [52].

The basic circuit that generates the PWM signal is composed of an Astable Multivibrator integrated circuit (IC), a switching transistor, a potentiometer, resistors, diodes and capacitors. Figure 24 represents this circuit:

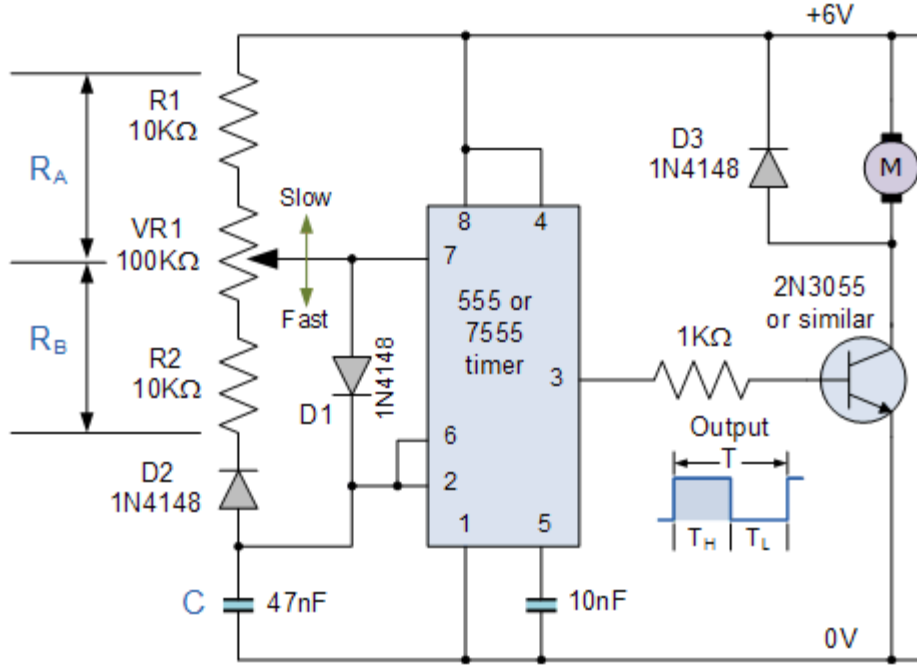


Figure 24 - PWM generator circuit [51].

The capacitor C is charged and discharged by the current flowing through the resistors  $R_A$  and  $R_B$ . When charging, the current flows in the direction  $R_A$ -D1-C and the output voltage at pin 3 will be equal to the supply voltage (6V) which will turn ON the transistor. During the discharging phase the flow is C-D2- $R_B$ -pin 7. In this case the output voltage at pin 3 will be 0V which will turn OFF the transistor. This modulated signal generated at the output can be controlled by the duty cycle (D).

The calculation of D can be performed with the time ( $T$ ) for the capacitor to complete one charge-discharge cycle and its individual times for charging ( $T_H$ ) and discharging ( $T_L$ ). These variables depend on the values of  $R_A$ ,  $R_B$ , and C.  $R_A$  is composed by the resistor R1 and the top part of the variable resistor VR1, while  $R_B$  is represented by R2 and the bottom part of VR1. Their values can be tuned by the potentiometer. The C value is chosen by the designer.

The computation of  $T_H$  and  $T_L$  is given by the equation of the half-life capacitor charge decay:

$$t_{1/2} = R * C * \ln(0.5) \quad (2.1)$$

Then,

$$T_H = R_A * C * \ln(0.5) \quad (2.2)$$

$$T_L = R_B * C * \ln(0.5) \quad (2.3)$$

As  $T = T_H + T_L$  and the results of  $T_H$  and  $T_L$  are determined, the duty cycle can be calculated by:

$$D = T_H / T = R_A * C * \ln(0.5) / (R_A + R_B) * C * \ln(0.5) = R_A / (R_A + R_B) \quad (2.4)$$

The PBIMS includes a microcontroller unit (MCU) that can generate PWM signal for activation of actuators or speed control of motors. The Radio Communication and Low Frequency Array (RCLOFA) payload box, which will be described in Chapter 4, has an antenna that must be deployed. The release mechanism includes a small actuator that is activated by PWM signal.

### 2.5.3 Power Budget

The power budget analysis is crucial for the design of the EPS. The understanding of the size of the power system impacts the component selection and the development of the circuitry. First, all the loads or subsystems need to be listed. Then their respective currents and voltages with minimum, nominal and maximum values are stated. Finally, the power for each subsystem and the system total power consumption are calculated. This analysis will give the designer a view about which subsystem demands more power. With this information, he/she will design the EPS considering the worst case which is the maximum power consumption. Table 5 illustrates the power budget analysis for a satellite system:

*Table 5 - Power Budget Satellite Example [45].*

Subsystem	Nom. Current (A)	Max. Current (A)	Nom. Voltage (V)	Max. Voltage (V)	Nom. Power (W)	Peak Power (W)	Duty Cycle (%)
AOCS	0.2	0.24	5	5	1	1.2	100
Power	0.4	0.48	5	5	2	2.4	100
Thermal control	0.2	0.24	5	5	1	1.2	-
Communication	0.06	0.07	3.3	3.3	0.2	0.24	100
Data Handling	0.06	0.07	3.3	3.3	0.2	0.24	100
Payload	3.12	3.74	5	5	15.6	18.7	50
Total					20	24	

## 2.6 Data Communication Buses

Data communication buses are frameworks to allow communication. It is important to differentiate the Physical layer to the Data Link layer. The former includes the electronic circuit transmission technologies while the latter provides the set of rules on how the communication will proceed (protocol). Diverse types of buses are introduced in this section.

### 2.6.1 I2C

Inter-Integrated Circuit (I2C) is a synchronous, half-duplex, multi-master, multi-slave serial bus developed by Phillips in the 1980s [53]. The bus has only two lines which are called serial data line (SDA) and serial clock line (SCL). Both lines need to be pulled up to Vdd (positive power supply pin) with resistors being able to generate low and high signal. While the first state occurs when the resistors are driven and connect the line to ground, the latter happens when the drive is removed, and the line receives a high voltage. The following diagram shows how the devices are physically connected:

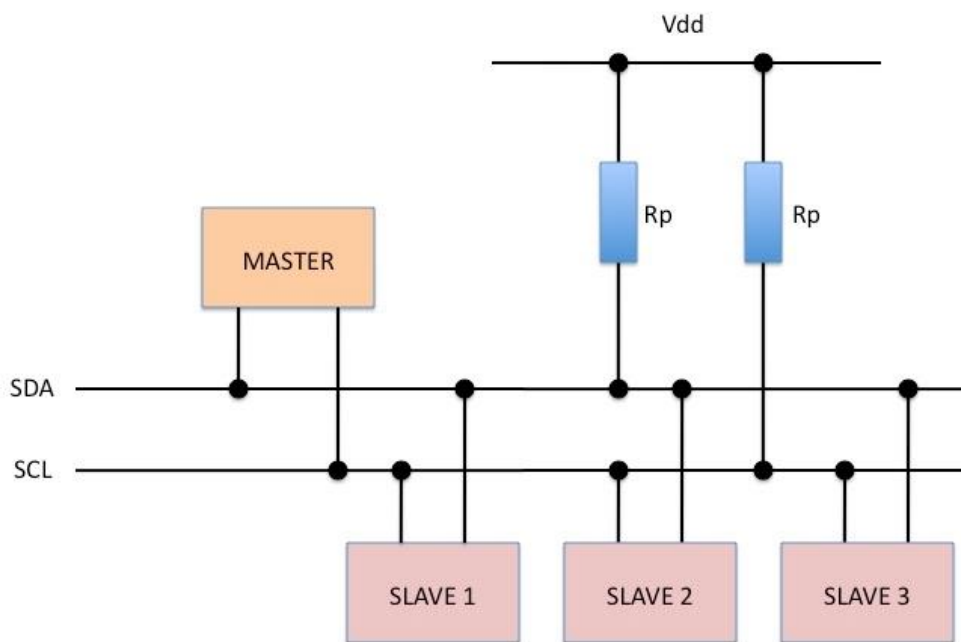


Figure 25 - Generalized I2C connection diagram [54].

The clock frequency can vary from standard-mode (100 kHz) to fast-mode (400kHz) and high-speed-mode (3.4MHz). The maximum capacitive load limit in the line is 400pF.

The communication operation sequence [53] illustrated in figure 26 happens as follows:

1. The Master initiates with the *Start Condition*. SDA goes low (0) and immediately after SCL goes low (0) as well
2. Then the seven address bits will come, to be able to identify which integrated circuit (IC) will receive or send the message
3. The 8th bit (R/W) will tell if the Slave will read (1) or write (0) data. Slave uses SCL to sample Data
4. The Slave pulls the SDA line low (ACK=0) by acknowledging the address is related to it and it is ready to read or write data
5. Then, depending on the 8th bit (R/W), either the Master will write the eight data bits and the Slave will read them or the Slave will write the eight data bits and the Master will read them
6. The Slave pulls the SDA line low (ACK=0) again by acknowledging the data is correctly read or written
7. Finally, the Master will drive the *Stop Condition*. SCL goes high (1) and immediately after SDA goes high (1) too

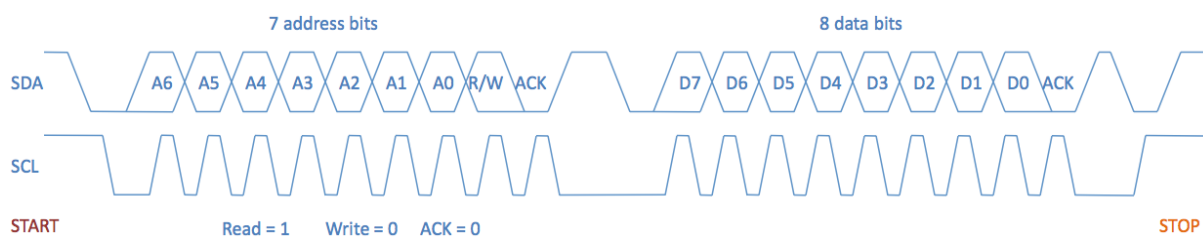


Figure 26 - Communication sequence [53].

## 2.6.2 SPI

Serial Peripheral Interface (SPI) is a synchronous, full-duplex, single-master, multi-slave serial bus developed by Motorola in the 1980s [55]. The bus has four lines which are referred to Serial Clock (SCKL), Master Out Slave In (MOSI), Master In Slave Out (MISO) and Slave Select (SS). Since communication happens simultaneously, the Master can send data through MOSI at the same time the slave is also sending data via MISO. There is no need of address to identify each slave. In this case, the pin SS when in low (0) will select which slave is communicating to the Master. The SCKL signal comes from the master and synchronizes the data transfer. This operation has a speed of up to 1 Mbps and is performed in eight/sixteen bits block. The following scheme describes the connections of this bus:

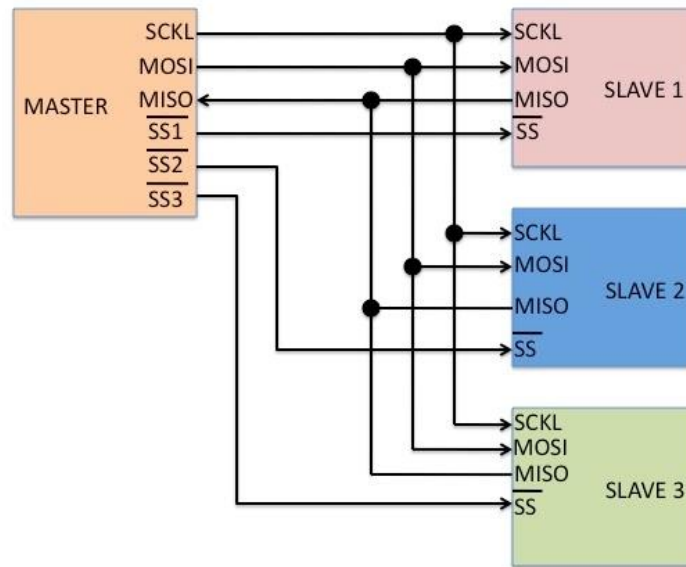


Figure 27- SPI in Daisy Chain connection [55].

The SPI bus has four clock modes that are defined by the clock polarity (CPOL) and clock phase (CPHA). While CPOL dictates if the idle state is low (0) or high (1), the CPHA determines if the rising or falling edge of the clock will put new data on the line.

### 2.6.3 UART

The Universal Asynchronous Receiver Transmitter (UART) is a circuit created in the 1960s for allowing data conversion from parallel to serial bit-stream asynchronously and in full-duplex [56]. It has three lines called Receiving data (RX), Transmitting data (TX) and Ground (GND). Because there is no clock involved in the communication, there is an introduction of a Start and Stop bit, so the receiving IC can understand when the message begins and finishes. Also, both ICs communicating to each other need to be in the same Baud rate, or else, the same speed of data transfer expressed in bits per second (bps). Common baud rates are 9600, 57600 and 115200.

The following figure illustrates the connection between two devices and how the eight bits of data are transmitted including start, parity and stop bits:

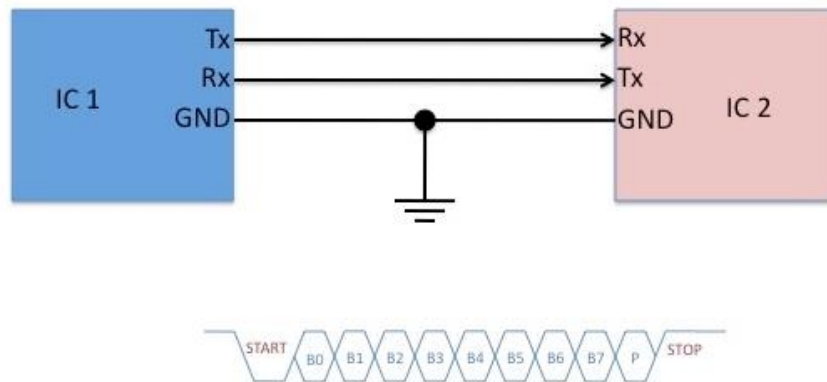


Figure 28 - UART Diagram [57]

#### 2.6.4 CAN

The Controller Area Network (CAN) is an asynchronous, half-duplex, multi-master priority-based serial bus invented by Bosch in the 1980s particularly for automotive and industrial applications [58]. It has two lines named CAN High (CANH) and CAN Low (CANL). The logical state of the bus is determined by the voltage difference between the two lines. If CANH is at 5V and CANL at 0V it means, there is a dominant voltage and the logical state is 0. If both CANH and CANL are at 2.5V there is a recessive voltage and the logical state is 1. This behavior is exemplified in figure 29.

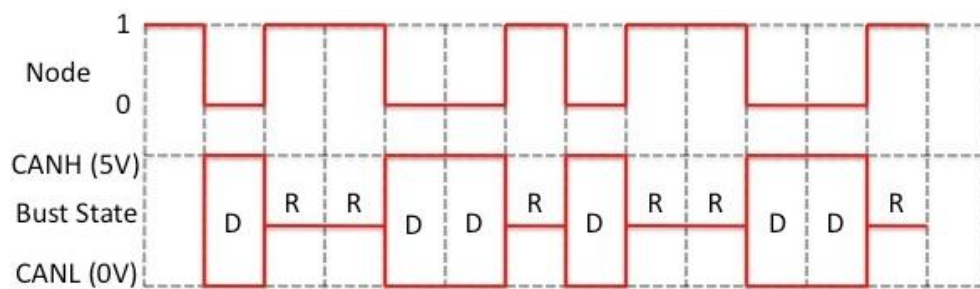


Figure 29 - CAN Bus state [58]

The data transmission is prioritized allowing messages coming from nodes to have precedence over others according to their addresses. If two nodes need to transmit data at the same time, through arbitration they will confront bit by bit from their message addresses until they find one bit which has priority over the other. This mechanism is shown in figure 30. Three nodes try to send the message simultaneously but only Node 3 will transmit while the other nodes will only listen.

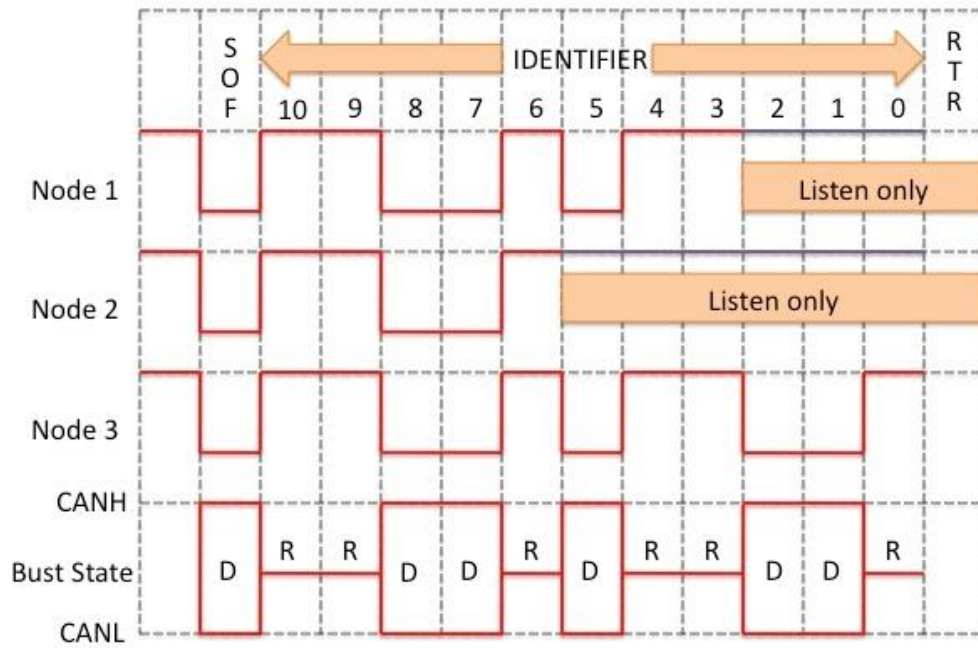


Figure 30 - Arbitration between three nodes [58]

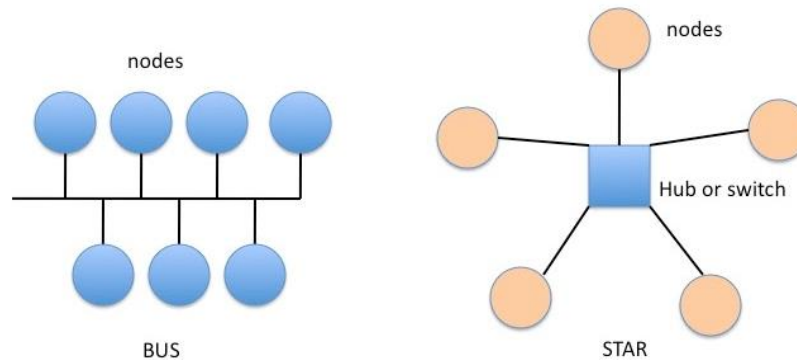
The CAN data frame includes the start-of-frame (SOF) with one bit, the identifier with 11 bits if base and 29 bits if extended, the remote transmission request (RTR) with one bit, the identifier extension bit (IDE<sup>2</sup>) with one bit, the reserved bit with one bit, the data length code (DLC) with 4 bits, the data field with up to 64 bits, the cyclic redundancy check (CRC) with 15 bits, the CRC delimiter with one bit, the acknowledgement (ACK) slot with one bit, the ACK delimiter with one bit and the end-of-frame (EOF) with seven bits.

## 2.6.5 USB

The Universal Serial Bus (USB) is a synchronous, half-duplex/full-duplex, single-master serial bus that was created by seven companies (Compaq, DEC, IBM, Intel, Microsoft, NEC and Nortel) in 1996 with the objective to standardize the connection between personal computers and peripherals (up to 127 devices) [59]. It has four pins named Vbus (+5V), Data- (D-), Data+ (D+) and Ground (GND). Vbus and GND are for power supply while D- and D+ for data transmission. The transfer speed varies from 1.2 Mbps (USB 1.0) to 40Gbps (USB4). The data transfer operation happens with network packets between the host and the device. It has four different types: *control* (for status queries and command), *isochronous* (periodic and streaming), *interrupt* (infrequent and bounded latency) and *bulk* (non-periodic for large data transfer).

### 2.6.6 ETHERNET

The Ethernet is a computer networking technology developed in the 1970s by Bob Metcalfe and Xerox PARC for high-speed data communication among digital devices in a Local Area Network (LAN) [60]. It can have different topologies such as bus and star illustrated in figure 31.



*Figure 31 - Bus and Star configurations [60].*

The data transmission rates can vary from 10Mbps to 100Gbps and different wires can be used to interconnect the LAN: coaxial, twisted-pair, copper or fiber optics. The ethernet frame structure includes the preamble (8 bytes), the destination address (6 bytes), the source address (6 bytes), the type field (2 bytes), the Data field (46 to 1500 bytes) and the CRC (4 bytes). As in the USB, the data is sent in packets which will be received by devices according to their addresses.

### 2.6.7 Wi-Fi

The Wi-Fi is a standard wireless network communication developed for high-speed communication between devices connected in a Wireless Local Area Network (WLAN). It was introduced in 1998 by the Wi-Fi Alliance and it is part of the IEEE802.11 family of standards for wireless communication [61]. It operates in both 2.4 GHz and 5 GHz bands and its range varies with the power of the transmitter, the modulation type and the gain of the antenna. Its data transmission is very similar to the Ethernet, but it includes additional address fields in its frame structure. This frame format leads to much more complex addressing system than to the Ethernet frame. However, it allows for wider networks including more devices.

### 2.6.8 Bluetooth

The Bluetooth is a standard wireless network communication with short range, low power and low-cost characteristics. It was developed in 1998 by the Bluetooth Special Interest Group (SIG) which had as pioneer companies Intel, IBM, Ericsson, Nokia and Toshiba [62]. It operates with short Radio Frequency (RF) in the 2.4 GHz band and can achieve typically 1-10 m in range. However, this range can be extended to 100 m depending on the antenna. It is considered a replacement of serial communication interfaces. The data transferring uses a packet-based protocol for efficient transmission. It breaks down longer data packets into data packet units that are feasible to be transmitted in the bandwidth. The communication occurs through a small

network called Piconet. This elementary network is a master-slave architecture with one device set as master and seven additional slaves connected to it. Because the operating band is divided into several channels of 1 MHz with 1 Mbps data transferring rate, the devices of the Piconet must synchronize to each other with the agreement of the selected frequency. This process will happen after each packet transmission. Therefore, the devices are always changing from channel to channel, which is known as Frequency Hopping Spread Spectrum (FHSS). The FHSS will avoid interference between devices and guarantee the robustness of the system. The Bluetooth is particularly important in this work, because it will be the main communication network type used for the communication between the Payload Box Infrastructure Management System (PBIMS) and external users. Considering that the users are the LRU-2 and the Scientific Instruments, which are within 1- 2 m to the PBIMS, the short range is not a barrier for the accurate communication.

## 2.7 Scientific Instruments

There is an enormous variety of scientific instruments used in space exploration missions. However, this work will be limited to the instruments used in rover planetary missions and, more specifically, to those that relate to the ARCHES project.

### 2.7.1 Chemistry and Camera (ChemCam)

The ChemCam is one of the scientific instruments incorporated into the NASA Mars Rover Curiosity, which can identify specific elements on rocks and soils. It uses the laser-induced breakdown spectroscopy (LIBS) to measure the chemical composition of its targets. Once the laser is fired, part of the target is converted into ionized plasma and the light wavelengths emitted are captured by a Curiosity's optical system [63]. The data is then analyzed by a spectrometer and the high content of a specific element is indicated by the peaks in intensity of light as can be seen in figure 32.

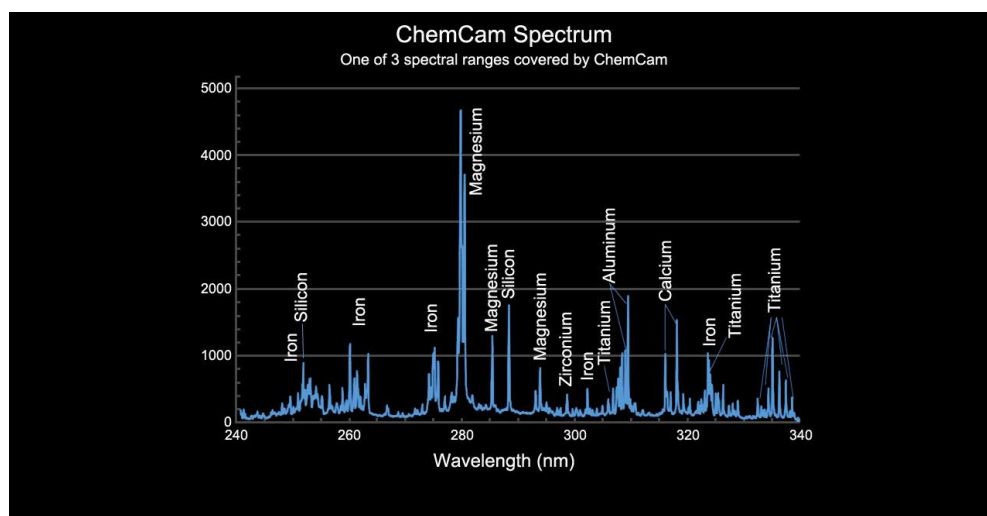


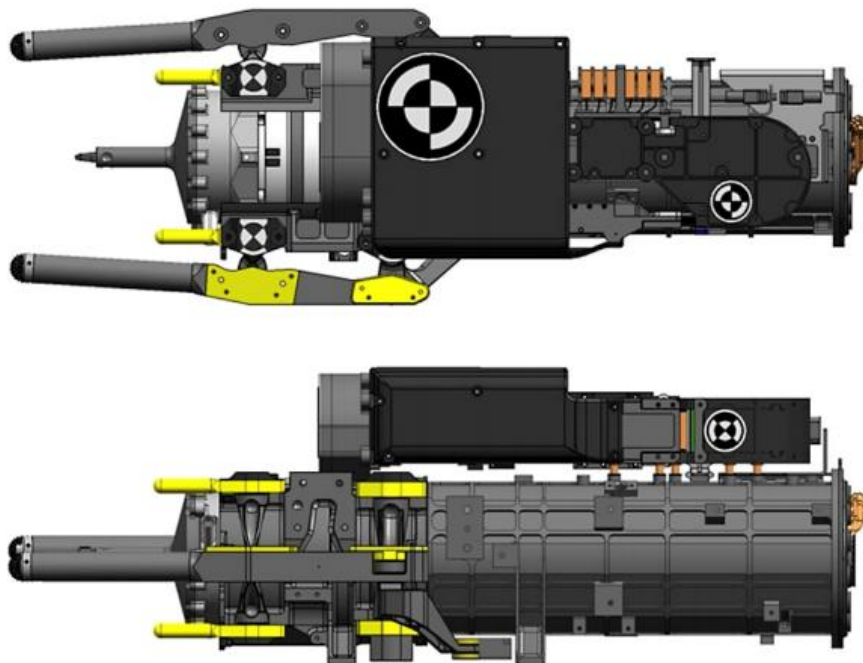
Figure 32 - Example of type of data collected by the ChemCam instrument on the Mars Curiosity rover (NASA/JPL-Caltech/LANL).[64]

The ChemCam can identify a broad variety of elements such as oxygen, hydrogen, carbon, fluorine, lithium, rubidium, strontium, barium, sodium, magnesium, aluminum, silicon, potassium, calcium, titanium, iron, phosphorus, sulfur, chlorine, chromium, manganese, nickel and zinc. However, it is limited to only sense elemental composition. It cannot distinguish the arrangement of these elements into minerals, which means that rocks with different mineralogy and geologic histories can be classified as identical [63].

Unlike the ChemCam, the LIBS system used in this project is not measured remotely. The payload module is connected to the LRU robotic arm and will be placed near the surface of the rock to make the measurements. Further details will be explained in subsection 4.4.2.

### 2.7.2 Robotic Sample Acquisition

Sample acquisition is essential for scientific analysis of soil and rock from planetary surfaces. Understanding the characteristics of the regolith of extraterrestrial bodies, such as Mars or the Moon, can reveal potential minerals to be exploited in situ or biological traces that could possibly indicate the presence of life. To acquire samples the rover or lander normally uses a robotic manipulator, a scoop and a drilling system [1]. However, not necessarily all these items are always present. The drilling system, for instance, was included in more recent missions such as the Mars Rover Curiosity in 2012 and will be part of the future missions ESA ExoMars and NASA Mars2020 to be launched in 2020. The combination of articulated manipulator and scoop was present in the NASA Mars lander missions Viking-1 and Viking-2 in 1975 and Phoenix in 2007. It is possible to observe these systems in figures 33 and 34:



*Figure 33 - Schematic of NASA MSL Curiosity Drill and Drill bit (NASA JPL) [65].*

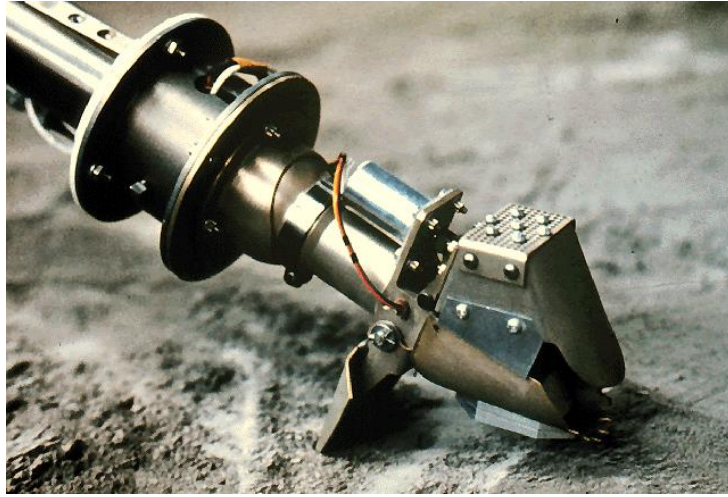


Figure 34 - Viking lander soil sampler (NASA JPL) [66].

In ARCHES, neither the LRU rovers nor the payload modules have a drill bit, but the presence of a standardized electromechanical interface provides the flexibility for a future inclusion if required. The shovel and the soil sample payload box can be connected to the robotic arm through the passive and active docking couplings. Thus, the rover can sample the terrain and store the specimens in individual compartments of the payload module.

### 2.7.3 Radio Telescope

Radio telescopes are astronomical instruments able to measure radio waves emitted from distant galaxies or other celestial bodies in the universe. Core components of radio telescopes include: a radio antenna, which is normally a parabolic dish, a feed horn, which is a funnel to select specific radio waves, a radio receiver, an amplifier and a processor [67].

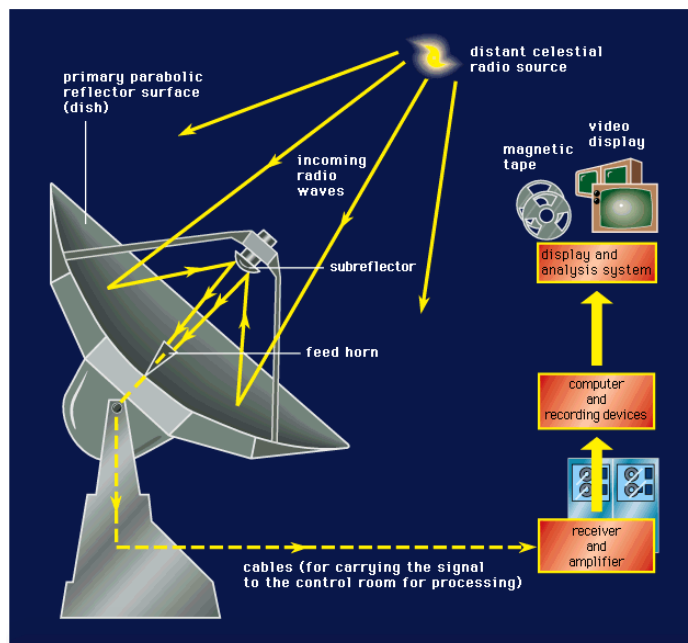


Figure 35- Radio telescope diagram [68]

Several radio telescopes have been launched into space. Zond-3, which was launched by the Soviets in 1965 to do a flyby of the far side of the Moon [69]. The NASA spacecrafts Radio Astronomy Explorer RAE-1, which was launched in 1968 and performed measurements in the spectrum of 0.4 to 6.5 MHz [70], and RAE-2, which was deployed in lunar orbit in 1973 and analyzed astronomical radio sources in the range between 25 kHz to 13.1 MHz [71]. HALCA, a Japanese mission launched in 1997 with the objective of conducting radio-wave observations in combination with ground-based radio telescopes [72]. Spektr-R, a Russian spacecraft, part of the RadioAstron program, launched in 2011 to Earth orbit, also used combined radio interferometry techniques [73]. And most recently, the Netherlands Chinese Low Frequency Explorer (NCLE) launched in 2018 as part of the Chang'E 4 lunar mission and sensitive to radio frequencies of 80kHz to 80MHz [74].

Looking into the modularity aspect, the radio interferometry plays an important role. The amount of radio telescopes can be scaled-up and the combination of the radio waves will create a higher resolution image with the increase of units in the array. A few examples are the Low Frequency Array (LOFAR) and the Orbiting Low Frequency Array (OLFAR).

LOFAR is an innovative radio interferometer network developed by ASTRON in the Netherlands in 2012 [75]. It operates in the frequencies between 10-250 MHz. Each array constitutes of two types of low-cost antennas: The Low-band antennas (LBA) which operate between 30-80 MHz and the High-band antennas (HBA) which operate in the range of 110-250 MHz. Besides the antennas, there are also the receiver unit (RCU) to digitize the signal and the digital signal processing (DSP) hardware to process the data acquired locally. This pre-processed signal coming from several stations distributed in the Netherlands and Northern Europe is sent to a Central Processing (CEP) facility that will correlate and combine each one of them to reproduce the effect of a conventional antenna. Figure 36 illustrates the LOFAR infrastructure:

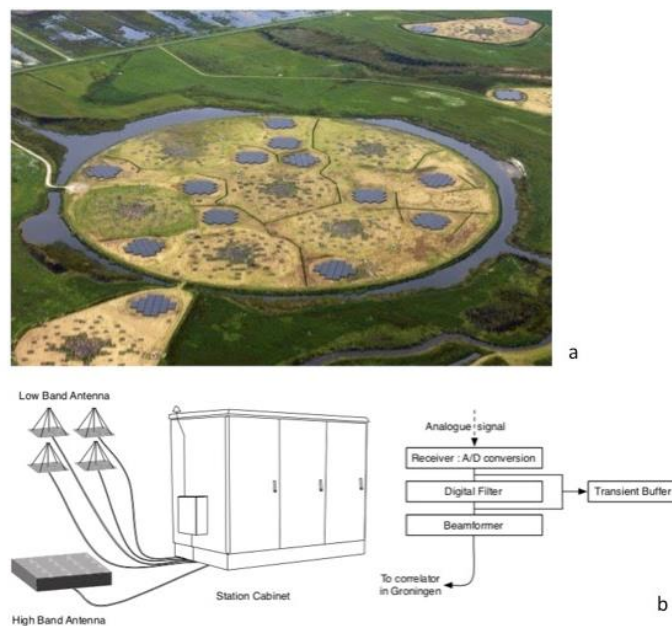
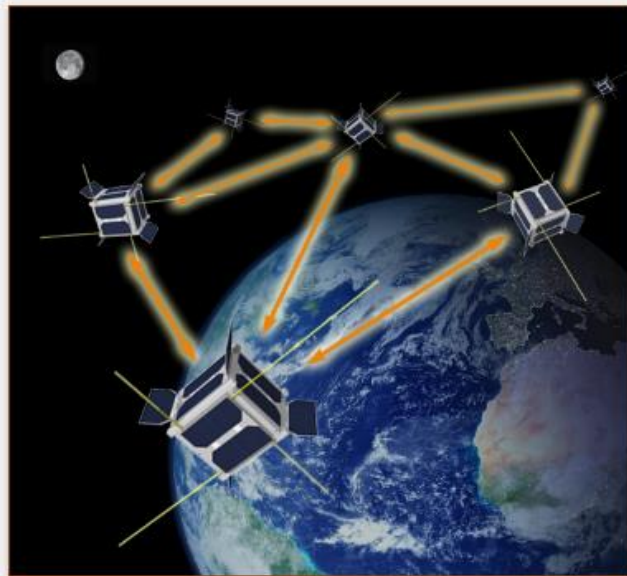


Figure 36 - a. Aerial photograph of Superterp, the heart of LOFAR core; b. Schematic illustrating the signal connections at station level [75]

OLFAR has its application in space and relies on the deployment of a network of low frequency radio telescopes installed in small satellites. This new concept has been developed by ASTRON, University of Delft and ISIS in the Netherlands. The swarm of 50 nanosatellites will orbit the Moon and will operate in the range of 1-30 MHz. This electromagnetic spectrum region is considered under-explored and of great value for scientific research [76].



*Figure 37 - OLFAR network [77]*

For this project, one of the payload modules uses similar technology as LOFAR. It uses the superposition of signals coming from different boxes and creates a unique image. However, it is a simplified version of the Dutch array. It operates in the range of 10 to 20 MHz and, instead of detecting faraway galaxies, it is meant to observe Jupiter or the Sun.

### 3 ARCHES and Thesis Requirements

This chapter will put the thesis in context with the DLR ARCHES project. With the introduction of the ARCHES mission, it will be possible to understand its goals and how the thesis requirements can be derived from them. The mechatronics infrastructure, which is the core of this work, will have its design constrained by the robots' characteristics and tasks to be performed during the mission.

#### 3.1 ARCHES

ARCHES has three mobile robots with different characteristics: Ardea, LRU-1 and LRU-2. Ardea is a micro aerial vehicle (MAV) which operates autonomously and can scan the terrain with a flight time of about 10 minutes [78]. It will create maps that will be shared with the two LRUs. This will improve their navigation. LRU-1 is a rover with an advanced scientific camera set which can differentiate and analyze different rocks on the terrain. It is also equipped with a platform on which Ardea can land and be transported. LRU-2 is a rover which is capable of manipulating objects as it is equipped with a robotic arm. Its manipulator has a mechanical docking interface which can dock to all the payload modules and measurement devices necessary for the scientific tasks. Figure 38 illustrates all three robot platforms:

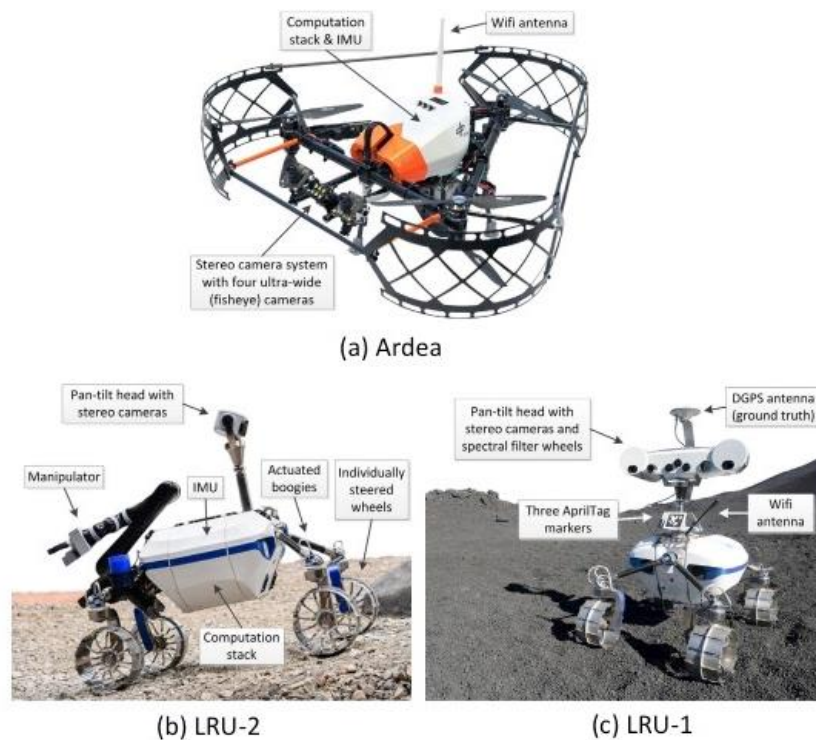


Figure 38 - ARCHES robotics platforms [79].

### 3.1.1 ARCHES Mission Scenario

The ARCHES analogue mission, also known as Demo-mission, will be carried out at Mount Etna in Sicily, Italy, in July 2020. This demonstration of the robot network on the field is a simulated geologic mission in an environment which imitates extraterrestrial worlds such as Mars. Mount Etna volcanic characteristics provide some of the challenges which robots would face in real robotic space missions, therefore it is a suitable location for scientists and engineers to test software and hardware devices developed in the last three years. The mission scenario considers that the mobile robots will perform several tasks to provide the necessary information to the scientists. The sequence of the most important tasks to be performed by the multi-robot system is listed as follows:

1. With the three robots located initially by the side of the lander mockup, Ardea will fly over the terrain and will map the area. This will provide better resolution images for the scientists that can decide which region of the terrain is considered a region of interest (ROI). Additionally, the two LRUs will receive the 3D-mapping information which will support their navigation.
2. Then, LRU-1 and LRU-2 will drive to the first selected ROI. While LRU-1 will analyze the different types of rocks, LRU-2 will take the LIBS payload box from the lander, dock it to the arm and take measurements of the selected rocks. The information will be transmitted to the scientists who will confirm the geological value of the sample.
3. In the subsequent task, LRU-1 and LRU-2 will advance to the second selected ROI. LRU-1 will perform new rock analysis with the cameras. Prior to driving to the ROI, LRU-2 will return to the lander and pick up the Sample box. Once LRU-2 reaches the ROI, it will use the Segregation Tool to separate the rocks. Then, it will use the KIT Hand to measure the rock sizes, collect them and store them in the Sample container. Finally, LRU-2 will use the Sampling Shovel to collect soil samples and deposit them in the Sample box.
4. After carrying out geological activities, the next task will involve communication and radio astronomy. LRU-2 will carry four Power boxes and four Communication modules from the lander to a designated area. These boxes will be deployed and stacked on top of each other. The antennas from the Communication modules will be released and the system will be fully operational. From this moment, the part of the internal circuitry that is specified to the communication tasks will establish a network including all the robot platforms. The other part of the circuit that is designated to capture low frequency radio waves will seek to measure the signals from Jupiter.

As it is possible to notice, these activities require a considerable amount of manipulation effort. Therefore, the use of the robotic arm and the docking interface is essential. However, these two elements by themselves are not enough for the adequate operation of the payload modules and tools. The mechatronics infrastructure presented in this work will ensure that these extended parts of the multi-robot network are fully functional after the complete integration of all systems.

### **3.1.2 ARCHES Goals**

According to Wedler et al. [80] the ARCHES mission main goals are:

- To explore unknown terrains and marine environment with autonomous mobile robots
- To deploy and maintain scientific instruments and basic infrastructure elements (power and communication)
- To use the heterogeneous autonomous robots in a cooperative manner with the combination of their capabilities
- To enhance the efficiency of the multi-robot network with the exchange of information among the agents

From the four goals presented, it is possible to notice that the second is particularly important for the development of this work. The utilization, deployment and maintenance of devices on the terrain can be accomplished using standardized interfaces, docking mechanisms and modular architecture. The design of the Mechatronics Infrastructure will consider these elements.

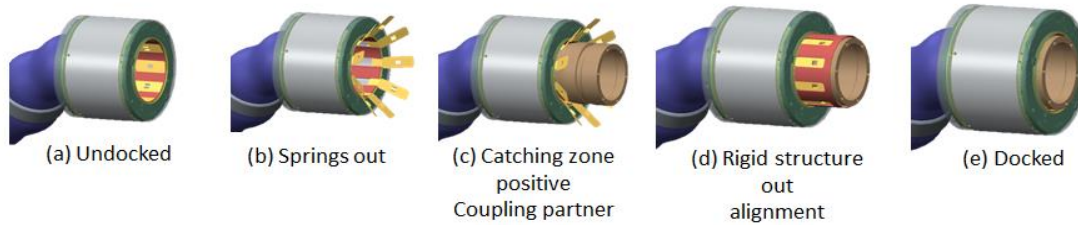
### **3.1.3 Light Weight Rover Unit (LRU)**

The two Lightweight Rover Units (LRUs), named LRU-1 and LRU-2, are planetary rover prototypes with dimensions of 114 cm x 74 cm x 94 cm, approximate weight of 40 kg, speed of 4 km/h and battery life expectancy of about two hours [81]. As described previously in this chapter, while LRU-1 has enhanced capabilities of rock analyses using its camera set, LRU-2 is equipped with a robotic arm which can manipulate and deploy objects. Both rovers have online Simultaneous Localization and Mapping (SLAM) system for 3D Mapping navigation [79]. They also are capable of computing visual and wheel odometry [82]. The combination of all these inputs will ensure an accurate navigation on the terrain.

### **3.1.4 Electromechanical Docking Interface**

The Electromechanical Docking Interface is a key element for the payload modules and toolsets manipulation. This mechanism is a standardized component in the system and can be either active or passive. The active part is located on the end-effector of the LRU-2 arm. It has nine springs which are extended and retracted by an actuator. When extended, they create a catching zone which has tolerance to misalignments. After catching the passive coupling, the retraction of the springs and the release of a rigid structure will ensure alignment of the parts. When they

are completely pulled back, the system will be locked. At this moment the docking process is completed. Unlike its counterpart, the passive part has a much simpler design. It is a mechanical piece which is machined to facilitate the grasping movement of the active part. The docking sequence is illustrated in figure 39:



*Figure 39 - Docking Sequence [83]*

### 3.1.5 Payload Modules Constraints

The Payload Module is a standard box which will incorporate the scientific instruments and the basic infrastructure elements. It was inspired by the shoe-box-sized Mobile Asteroid Surface Scout (MASCOT) lander deployed on the Ryugu asteroid in October 2018 as part of the DLR-JAXA-CNES joint mission Hayabusa-2 [84]. Its constraints are in size, weight and power. Each one of them is described as follows:

- **Size:** As MASCOT, the payload box dimensions are 340 mm x 200 mm x 237 mm. These measurements ensure that essential electronics, mechanical parts and scientific instruments can be inserted in the box interior. They also are adapted to the proportions of the LRU body and can be carried on top of the platform located on the back of the rover.
- **Weight:** The maximum weight for the payload module is 3 kg. This weight is limited by the maximum load supported by the LRU-2 robotic arm.
- **Power:** The power limitations are dependent on the three different power supply sources: the robotic arm, the external power box and the internal battery. They operate in 24 V and 2 A. The battery capacity varies from 50 to 200 Wh depending on the configuration.

## 3.2 Thesis Requirements

The thesis requirements are derived from the constraints introduced by the ARCHES mission. With the intention of extending the capabilities of the robotics systems and make them fully operational, the Mechatronics Infrastructure will be designed and implemented in this work. It shall:

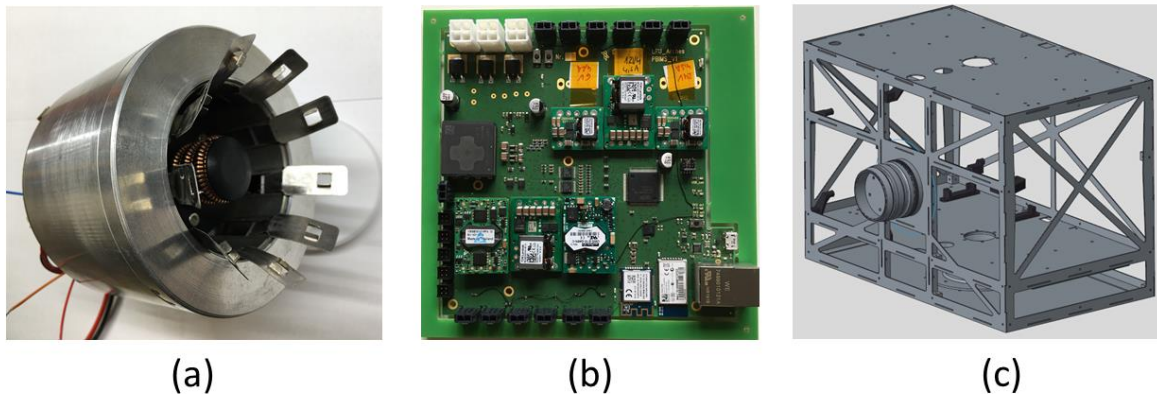
- Have standard interfaces (Hardware and Software) in all its components.
- Be compliant to the payload module limitations in size, weight and power.
- Provide adequate power and data buses required by the scientific instrument designers.
- Observe power saving specifications to be able to extend the autonomy of the payload carriers and toolsets.
- Incorporate a robust electrical interface that can provide power and data transfer.
- Consider the integration of the electrical interface to the existing mechanical docking mechanism.
- Have its software integrated to the scientific payloads and the multi-robot network.
- Be tested and integrated to the LRU-2, scientific measurement devices and communication network.
- Be flexible enough to include new scientific instruments in the future.

## 4 Mechatronics Infrastructure Design

This chapter introduces the design and implementation of the mechatronics infrastructure (MI). It starts with the presentation of the MI's main components and subcomponents. Then, it explores the versatility of this framework. Finally, it associates the MI's design process to the descending branch of the V-shaped Model.

### 4.1 Mechatronics Infrastructure Outline

The mechatronics infrastructure (MI) encompasses the electromechanical docking interface, the standard payload module and the Payload Box Infrastructure Management System (PBIMS) Board. These three elements are essential for the extension of the capabilities of the ARCHES robot network. They will allow the autonomous robots to manipulate objects in the field, take important geological measurements, enhance their navigation and communication, and maintain the infrastructure deployed on the terrain. Figure 40 presents these three fundamental elements:



*Figure 40 - The three main elements of the Mechatronics Infrastructure. (a) Docking interface with electrical connector; (b) PBIMS board; (c) Payload Box.*

### 4.2 Payload Box Infrastructure Management System (PBIMS) Board

The PBIMS is an electronic board which provides adequate power and data buses for all the scientific instruments and basic infrastructure devices present in the interior of the payload modules. It is the power management system combined with the OBC in a compact fashion. This ensures that the PBIMS functionalities are met while flexibility and light weight are also guaranteed. The modular power electronics allow the assembling of DC-DC converters according to the need of the power buses. For instance, the 48 V is required only for the LIBS Payload Module. Therefore, the Boost converter is mounted only in the PBIMS dedicated to the LIBS Payload box. However, the future possibility of upgrading the additional boards with the Boost converter is present. The main parts of the PBIMS are the PCDU, the MCU, the Actuator

Driver, the Communication buses and the Integrated sensors. The following figure shows the PBIMS diagram with its main components:

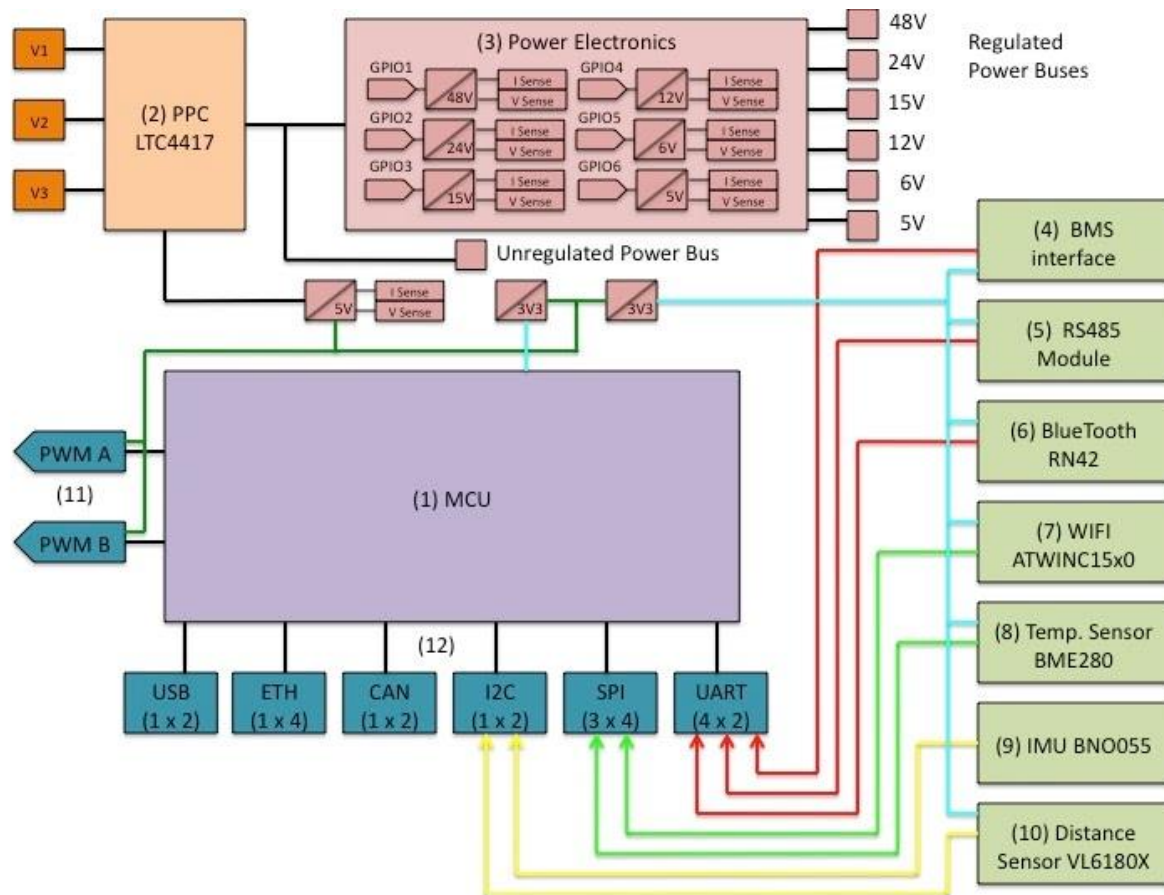


Figure 41 - PBIMS Diagram

Considering the PBIMS development process, it is important to highlight the main stakeholders, the requirements, and the Power Budget Analysis.

The main stakeholders for the PBIMS are: DLR Optical Sensor Systems (OS) institute, DLR Communication and Navigation (KN) institute, RM Manipulation Team, RM Navigation team.

Table 6 summarizes the requirements provided by the main parties involved:

Table 6 - Stakeholders vs Requirements

Stakeholders	Power Buses	Data Buses	Monitoring	Scientific Data
KN Institute	5V, 6V, 12V, 24V	USB, UART, Ethernet	V & I Levels, Channel status, Sensors data	Localization, LF signal
OS Institute	5V, 48V	USB, UART, Ethernet	V & I Levels, Channel status, Sensors data	Target Image, LIBS measurement
RM Manipulation	-	-	V & I Levels, Channel status, Sensors data	Target Image
RM Navigation	-	-	-	Localization

The Power Budget Analysis in Table 7 shows that either for the KN or OS payload modules a total of about 80 W must be supplied to guarantee their operability. Even if the highest power consumption does not happen during one hundred percent of the time, the PBIMS was designed for the critical case.

Table 7 - Power Budget Analysis for KN and OS payload carriers

Components	Nom. Current (A)	Max. Current (A)	Nom. Voltage (V)	Max. Voltage (V)	Nom. Power (W)	Peak Power (W)	Duty Cycle (%)
<b>KN</b>							
LNA	0.06	0.1	5	5	0.3	0.5	100
Ethernet Switch	0.4	0.5	5	5	2	2.5	100
Raspberry Pi	2	2.4	5	5	10	12	100
LOFAR SDR	1.25	1.42	6	6	7.5	8.5	100
Intel NUC idle	1.5	1.6	12	12	18	20	88
Intel NUC process	3.5	3.75	12	12	42	45	12
PoE Injector	0.42	0.5	24	24	10	12	100
Total					48-72	56-81	
<b>OS</b>							
Control Unit	1.6	2.4	5	5	8	12	100
WebCam	0.4	0.48	5	5	2	2.4	100
Spectrometer	0.2	0.24	5	5	1	1.2	10
QC-Laser	1.2	1.3	48	48	57.6	62.4	1
Total					10-69	14-78	

## 4.2.1 Power Control and Distribution Unit (PCDU)

The concept of the PCDU was introduced previously in Chapter 2. Now, the details of the PCDU implemented in the PBIMS and its main parts will be explained.

### Prioritized Power Path Control (PPC)

The PPC is responsible for the selection between the three power sources available on the network: Robotic Arm, Power Payload Box and Internal battery. The highest priority is given to the Power Payload box followed by the Robotic Arm, and then the Internal battery. The model of this circuit is shown in the KiCAD/PADS schematics as follows:

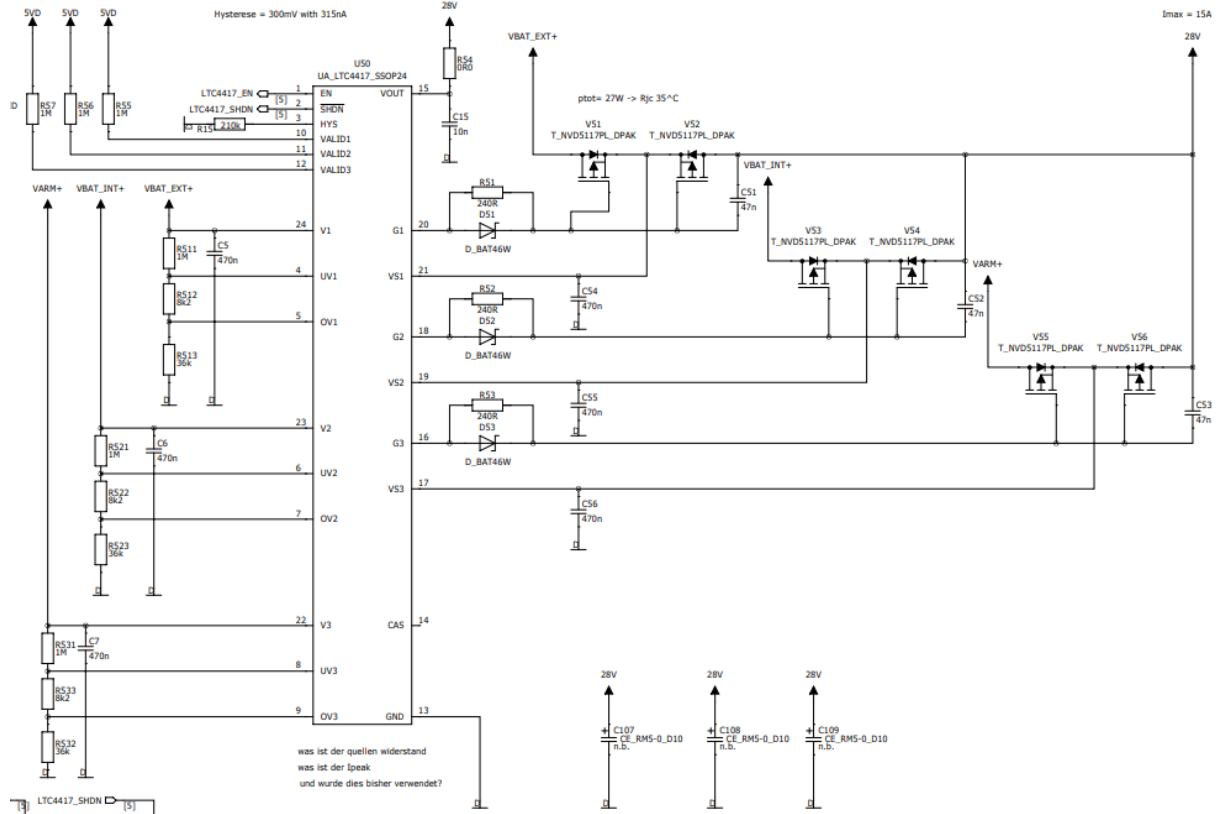


Figure 42 - PADS electronic schematics of the PPC

The choice of the resistors (R511, R512, R513, R521, R522, R523, R531, R532, R533) which set the OV/UV range is determined according to the following equations [48]:

$$R_3 = \text{Desired Hysteresis} / I_{OVUV(hys)} \quad (4.1)$$

$$R_3 = 300\text{mV} / 300\text{nA} = 1000 \text{ K}\Omega$$

$$R_{1,2} = R_3 / (UV_{TH(falling)} - V_{OVUV(THR)}) \quad (4.2)$$

$$R_{1,2} = 1000 \text{ K}\Omega / (23 \text{ V} - 1 \text{ V}) = 45.4 \text{ K}\Omega$$

$$R_1 = (R_{1,2} + R_3) / OV_{TH(rising)} \quad (4.3)$$

$$R_1 = (45.4 \text{ K}\Omega + 1000 \text{ K}\Omega) / 28 \text{ V} = 37.4 \text{ K}\Omega$$

$$R_2 = R_{1,2} - R_1 \quad (4.4)$$

$$R_2 = 45.4 \text{ K}\Omega - 37.4 \text{ K}\Omega$$

In this case, the target OV/UV range chosen was between 23V and 28V. This led to the approximated values of the resistors that were adjusted to the availability of standard 1% resistor values.

Additionally, the inrush current which occurs when the system is turned ON was calculated according to the equation [48]:

$$I_{INRUSH} = (V_1 - V_{OUT(init)}) / (R_{SRC} + ESR_{(CL)} + 2 * RDS_{(ON)}) \quad (4.5)$$

$$I_{INRUSH} = (28.8 \text{ V} - 19.6 \text{ V}) / (36 \text{ m}\Omega + 50 \text{ m}\Omega + 44 \text{ m}\Omega) = 71 \text{ A}$$

Where  $R_{SRC}$  is the internal resistance of the power source (in this case, Li-ion batteries),  $ESR_{(CL)}$  is the resistance of the electrolytic capacitor, and  $RDS_{(ON)}$  is the resistance of the switches.

The simulation for the PPC circuit was performed in LTSpice. The results of the simulation are presented:

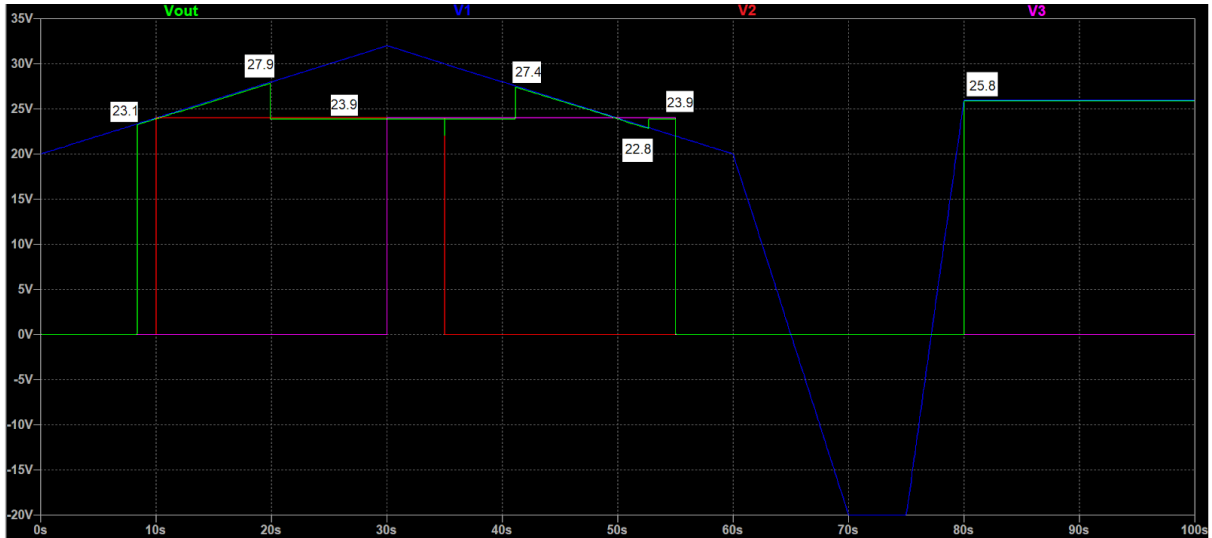
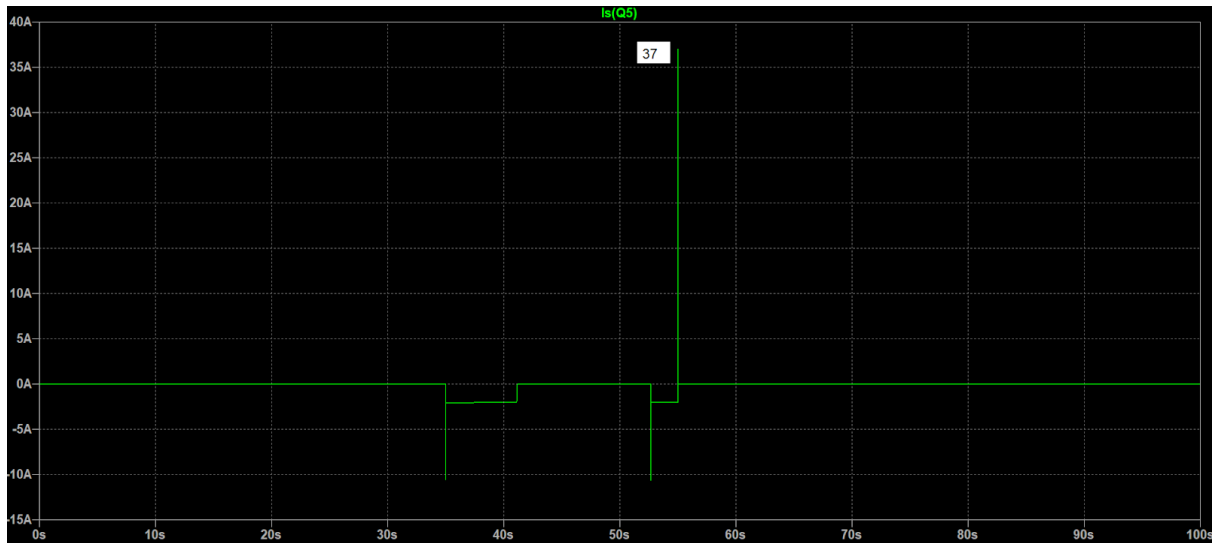


Figure 43 - Demonstration of the accurate switching of power sources.  $V_{out}$  (green line),  $V_1$  (blue line),  $V_2$  (red line) and  $V_3$  (violet line). OV/UV window between 23-28 V  $\pm$  5%.

The OV/UV range is achieved with minor errors (below 5%). Also, it is possible to point out the correct switching of power sources according to their priorities. The highest priority V1 (blue line) is activated first within the OV/UV window. Then, it is switched to V2 (red line) when V1 is out of the range, followed by a change to V3 (violet line), and finally, back to V1.

The maximum current observed in the circuit occurs over the external FETs connected to V3 (Q5 and Q6). The value measured in the simulation is 37 A over a period of 15  $\mu$ s, which is below the calculated inrush current value (71 A). Thus, the circuit is safe.



*Figure 44 - Maximum current through the FET.*

After the simulation with LTSpice, the circuit was implemented using the evaluation board DC1717A from Analog Devices. This demonstration circuit uses the LTC4417 IC and comes with a default setting for power sources of 12V, 5V and 8V. For the implementation, the resistors were changed with the purpose of obtaining the proper OV/UV window for three supply sources of about 24V. The results of the switching process according to the priority of the sources are shown as follows:

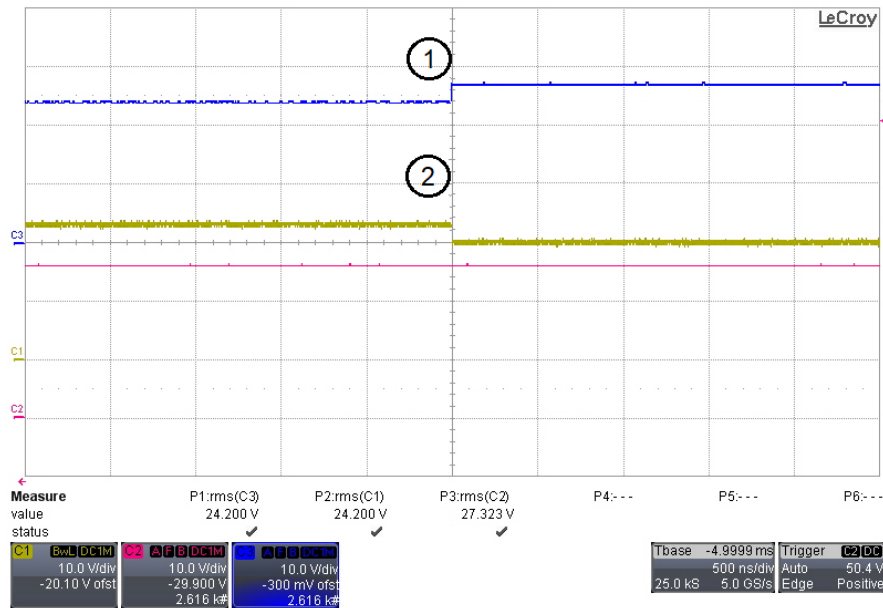


Figure 45 - DC1717 A oscilloscope measurements

As it can be noticed, C1(yellow) represents the highest priority power source V1, C2 (pink) the lowest priority power source V2, and C3 (blue) the output voltage Vout. Initially, both V1(24.2 V) and V2 (27.3 V) are within the UV/OV window, but Vout follows V1. When V1 is lowered to 20 V (2), outside the UV/OV range, Vout starts to follow V2 at 27.3 V (1).

## DC-DC converters

The DC-DC converters function is to lower or increase the output DC voltage. This is determined by the power buses requested by the stakeholders. Since the voltage levels specified are 48V, 24V, 15V, 12V, 6V and 5V, the DC-DC converters used are Buck and Boost converters.

The Buck converter utilized is the i3A series from TDK. It has output voltage range between 5 to 30 V, fixed switching frequency of 400 KHz, output ripple of 40mVpp, efficiency between 95-98 %, output current of 4.5 A, and maximum power of 100 W. Temperature operation is between -40° C and +125° C [85].

The Boost converter chosen is the DCM2322 from Vicor. It has output voltage of 48 V, output ripple of 474mVpp, efficiency of 88.5 %, output current of 1.25 A, and maximum power of 60 W. Temperature operation is between -40° C and +125° C [86].

The models of each circuit were designed with KiCAD/PADS and are shown as follows:

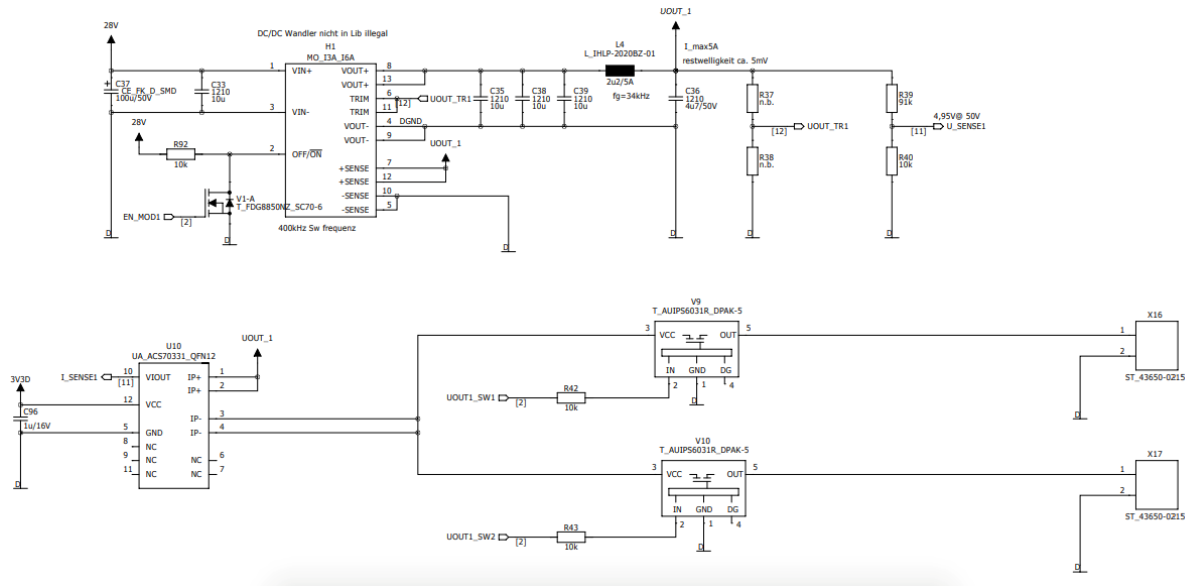


Figure 46 - PADS electronic schematics of the Buck converter

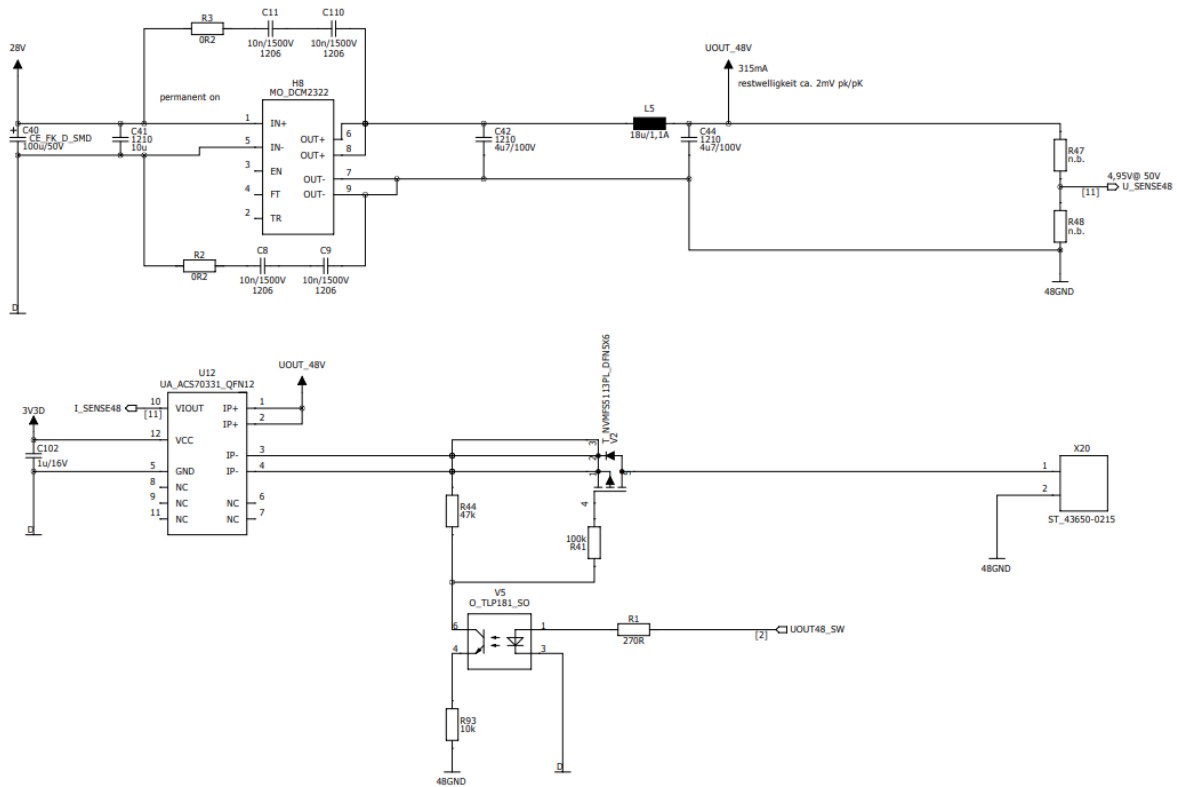


Figure 47 - PADS electronic schematics of the Boost converter

To control the output voltage of the buck converter it is necessary to select an external resistance between the VOUT+ and TRIM pins (figure 46). This resistance, which is represented by R37 in figure 46, will drive the current that will change the duty cycle of the PWM in the interior of the TDK i3A circuit. The selection is carried out with the following equation [85]:

$$Ru = [(V_{REF} * F)/(V_{o,up} - V_{o,nom})] - G \quad (4.6)$$

Where  $R_u$  is the external resistance,  $V_{REF}$  is 0.6 V,  $F$  is 36500  $\Omega$ ,  $V_{o,nom}$  is 2.59 V,  $G$  is 511  $\Omega$  [85], and  $V_{o,up}$  is the desired output voltage in the buck converter. The values of the resistances calculated for the planned output voltages in the PBIMS are presented in the following table. The resistance values were approximated to the 1% standard resistance available in the market.

Table 8 – Calculated values for the external resistances in the buck converter.

Desired Output Voltage (V)	Resistance (k $\Omega$ )
5	8.66
6	5.9
12	1.82
15	1.27
24	0.511

The circuit of the buck converter was implemented in a breadboard in load (2A) and no-load condition. The results of the DC voltage conversion are shown as follows:

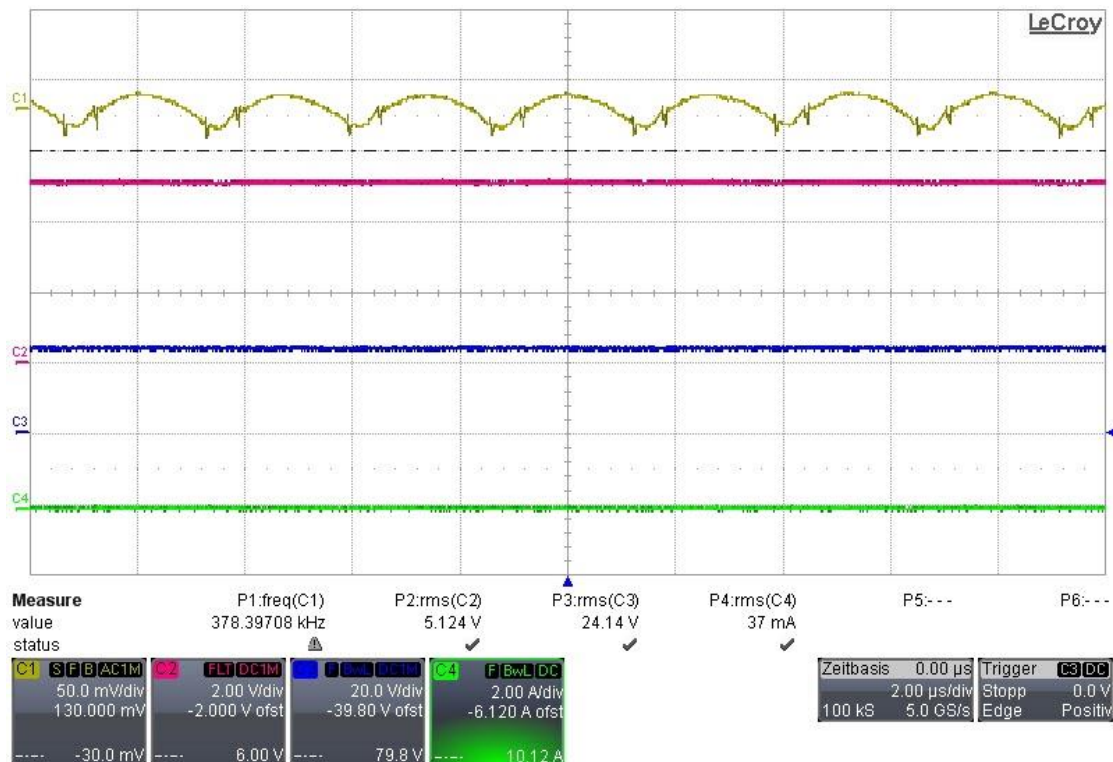


Figure 48 – No-load condition step-down conversion from 24V to 5V. Measurements performed with oscilloscope.

It is possible to notice that yellow signal (C1) represents the ripple with frequency of 378 KHz and amplitude of about 40mVpp. The pink signal (C2) is the Output Voltage with 5.1 V, the blue signal (C3) is the Input Voltage with 24.1 V, and the green signal (C4) is the Load Current with

37mA. The measure values show the expected no load condition and they are in accordance with the specification of the i3A buck converter.

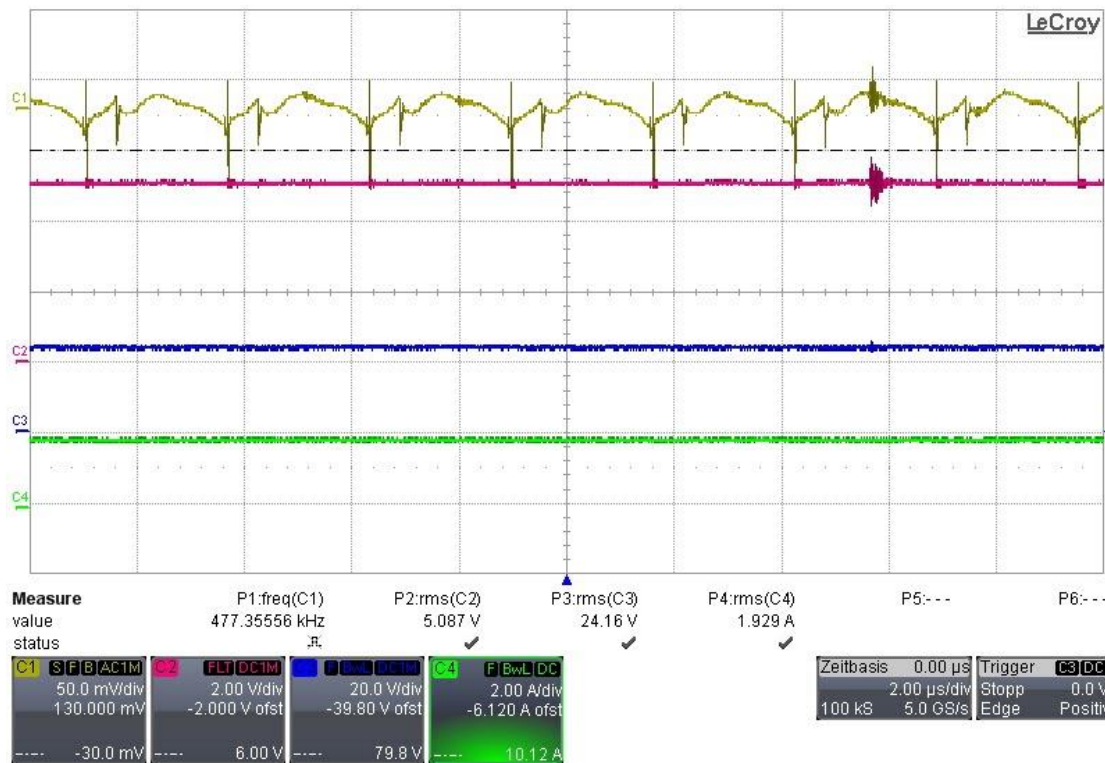


Figure 49 - Load condition step-down conversion from 24V to 5V. Measurements performed with oscilloscope.

In load condition, the ripple signal (C1) has frequency of 477 KHz and amplitude of about 70mVpp. The Output Voltage (C2) is 5.1 V, the Input Voltage (C3) is 24.1 V, and the Load Current (C4) is 1.9 A. Although the ripple amplitude is high if confronted with i3A specifications, this is caused by the lack of filtering. When this buck converter was integrated to the PBIMS, the filter was included, and the spike effects disappeared. The other values are in accordance with what was expected.

## 4.2.2 Microcontroller Unit (MCU)

The MCU chosen for this project is the NXP LPC1769 ARM Cortex®-M3 with high level of integration and low power consumption at frequencies up to 120 MHz. This is a versatile MCU with a variety of communication network buses (SPI, I2C, UART, CAN, USB, ETHERNET), pins for ADC and PWM purposes, and up to 70 general purpose input output (GPIO) pins. Temperature operation is between -40° C and +85° C [87].

The model of the circuit of the MCU was developed in PADS and it is presented:

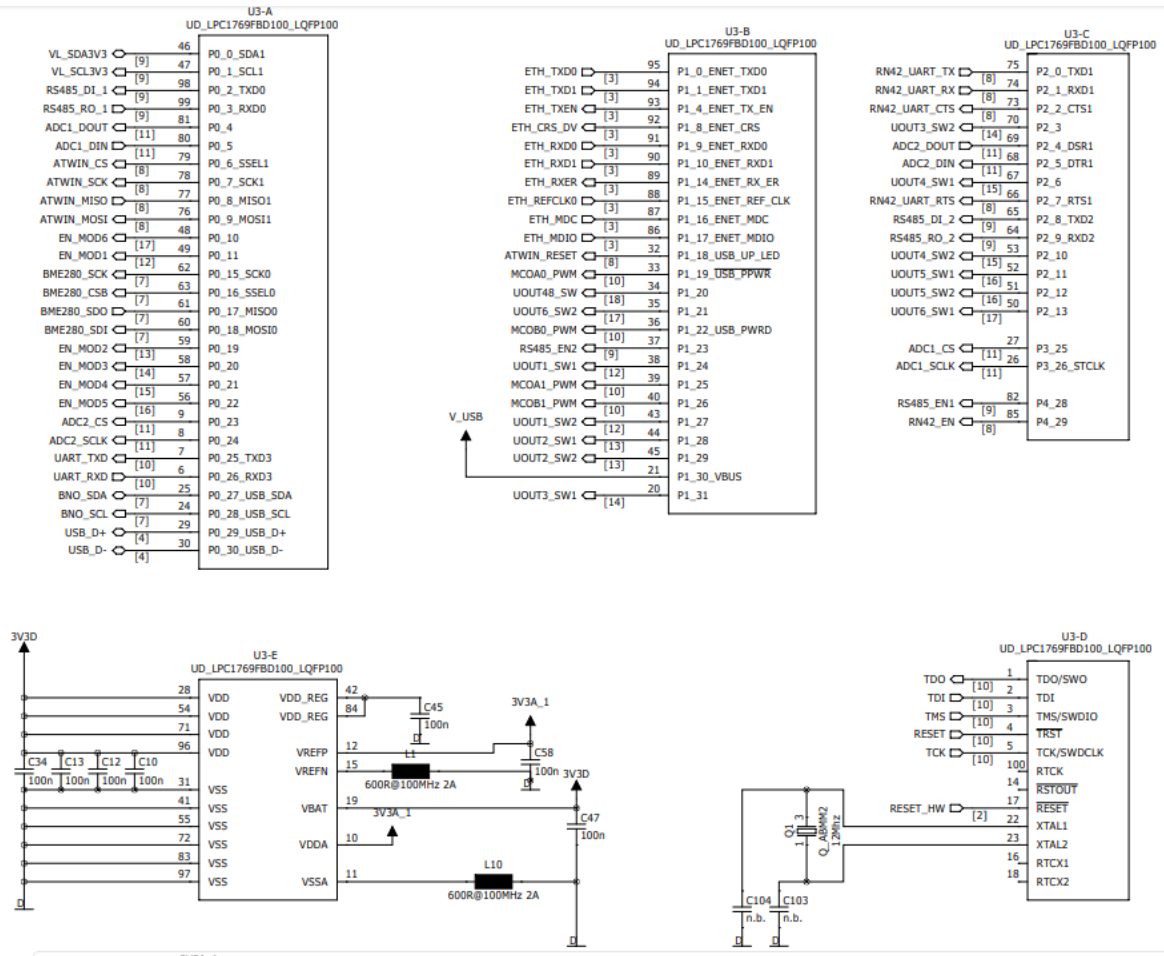


Figure 50 - Schematics of the MCU

The implementation of the MCU was carried out using the evaluation board ARM Keil MCB1700. This board includes the LPC1769 microcontroller and allows to check the functionalities of the GPIOs and communication digital interfaces. More details of the implementation are provided on the software development (section 4.3).



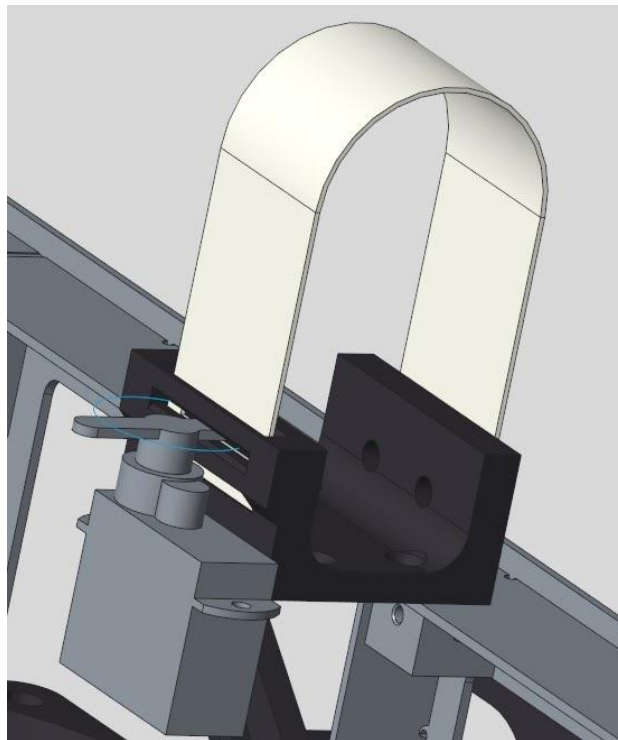
Figure 51 - ARM Keil MCB1700 evaluation board [88].

### 4.2.3 Actuator

The PBIMS has four channels dedicated to PWM signal for controlling actuators. It can control up to four motors spinning in only one direction or up to two motors with bi-directional rotation. In ARCHES, the Radio Communication and Low Frequency Array (RCLOFA) payload module has a mechanism to deploy the LOFAR antenna which includes a servo motor. In this case, the PWM signal is used to spin the motor and release a locking device that holds the folded antenna in place. There is no need to control the speed of the motor but operate it in an ON/OFF fashion. For future operations, the actuator speed control can be used for the automatization of new payload carriers.

The actuator used is the Sub Micro-Servo S03610 from Blue Arrow. It has torques of 0.27 Kg-cm (at 3.3 V) and 0.35 Kg-cm (at 4.2V), speeds of 1.28 rad/s (at 3.3 V) and 1.51 rad/s (at 4.2V), input voltage of 6V, and weight of only 3.9g [89].

The LOFAR antenna release mechanism is shown in the following figure:



*Figure 52 - Servo motor mechanism*

### 4.2.4 Communication Buses

The communication buses implemented in the PBIMS are: I2C, UART, SPI, USB, Ethernet, Bluetooth and Wi-Fi. Taking advantage of the versatility of the MCU regarding the digital communication interfaces and considering the broad requirements coming from the other

institutes (OS and KN), the buses were selected to attend their necessities while allowing integration for new technologies in the future.

I2C and SPI were implemented to connect the integrated sensors. There are no actual circuits representing the communication channels, but it is possible to observe how they are used in the upcoming section (4.2.5).

The UART circuit model is represented in the KiCAD/PADS electronic schematics as follows:

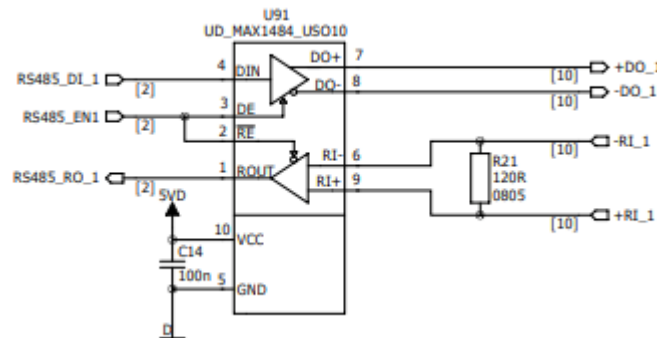


Figure 53 - UART circuit

The USB circuit model is shown in figure 54:

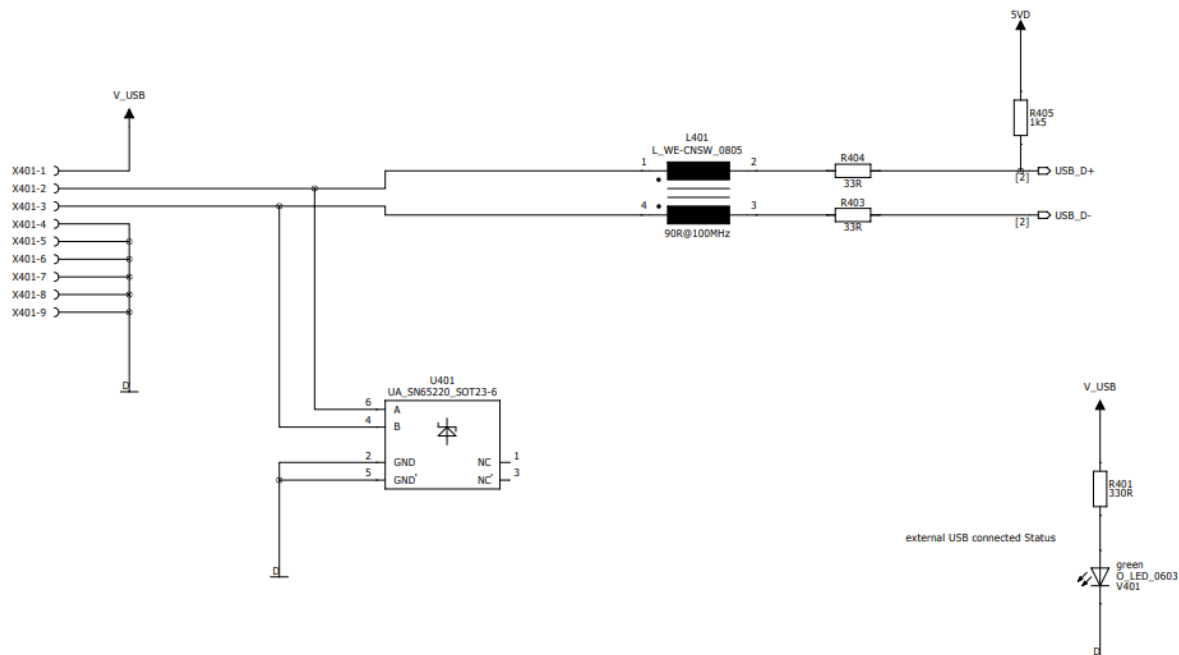


Figure 54 - USB circuit

The Ethernet circuit model is presented in the following figure:

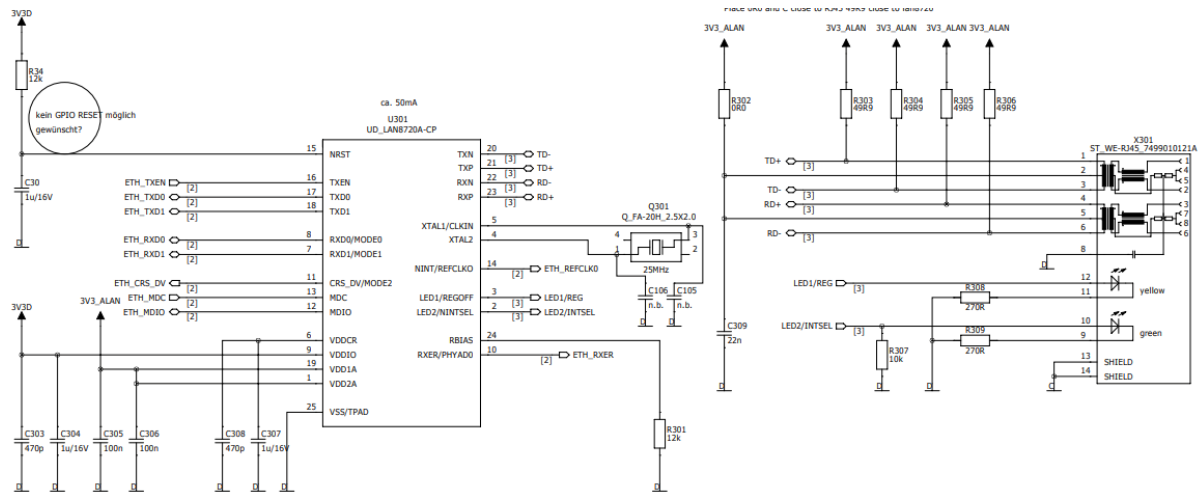


Figure 55 - Ethernet circuit

The Bluetooth circuit model is illustrated in the following figure:

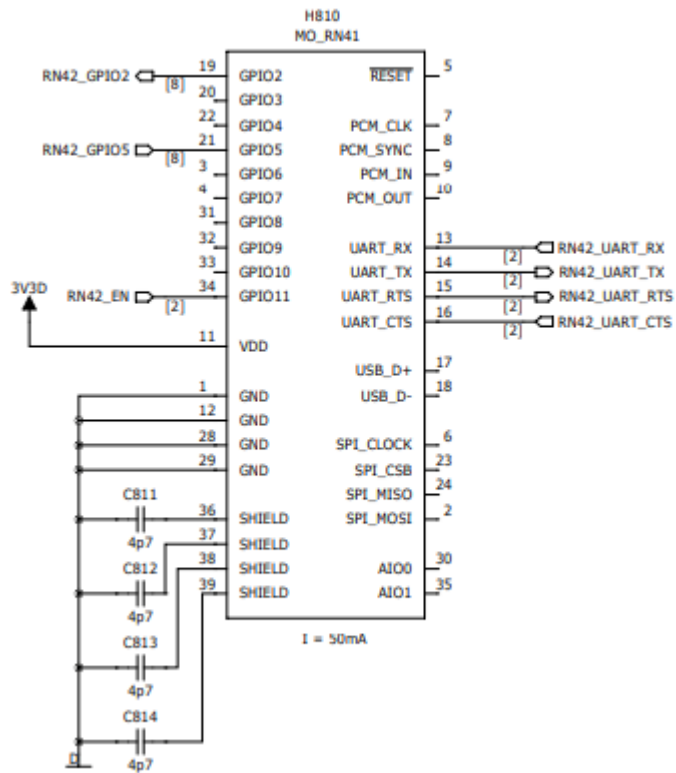


Figure 56 - Bluetooth circuit

The Wi-Fi circuit model is shown as follows:

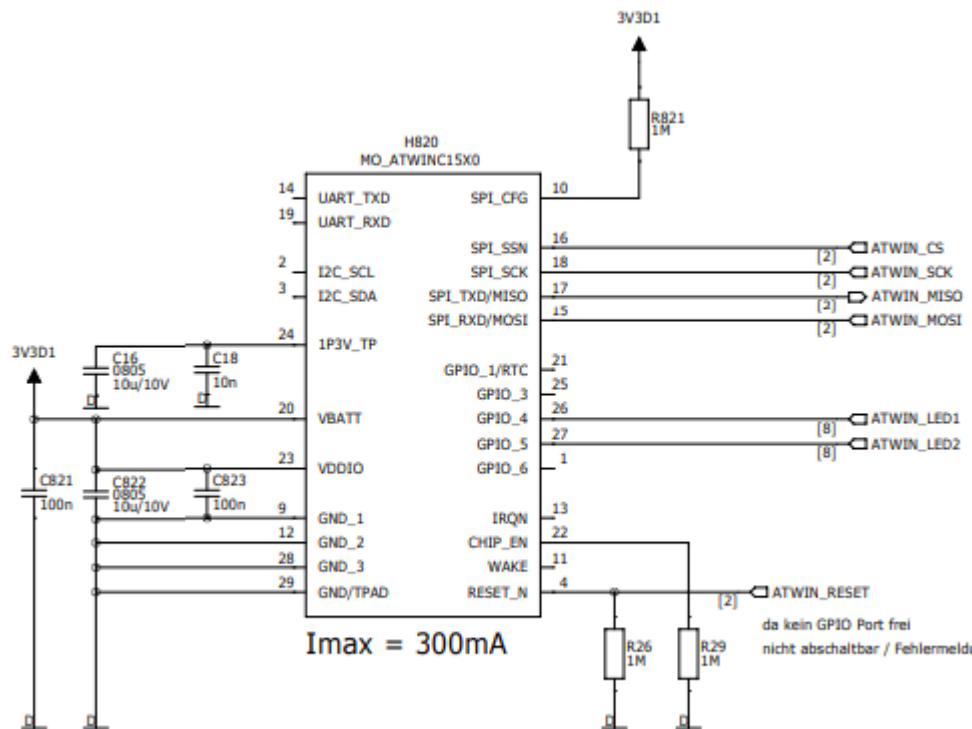


Figure 57 – Wi-Fi circuit

## 4.2.5 Integrated Sensors

The integrated sensors are not only fundamental pieces for the PBIMS correct operation but also for supporting the scientific tasks to be carried out during the demo mission at Mount Etna. The Inertial Measurement Unit (IMU) will be used during manipulation tasks. Particularly during the operation of the LIBS payload box, because it needs the accurate orientation of the laser beam before the shooting process starts. The distance sensor is also utilized during the LIBS geological task. Because the payload module needs to touch the surface of the selected rock before it is activated, it is crucial that the robot knows the distance from the box to the target. The temperature, pressure and humidity sensor is responsible for indicating the internal conditions of the box and if they are affecting the internal electronics or the scientific instruments. For example, the laser source of the LIBS system cannot operate in temperatures higher than 40°C. The feedback of the temperature values will limit when the LIBS operation can happen or not.

### IMU

The IMU selected for the PBIMS is the BNO055 from BOSCH Sensortec. It is a device with three sensors combined: gyroscope, accelerometer and geomagnetic sensor. It has digital interface I2C and UART, operates with 2.4 V to 3.6 V, and works in a wide temperature range (-40°C to +85°C) [90]. Its data will support the manipulation operations executed by the LRU-2.

The model of the circuit is seen in the following figure:

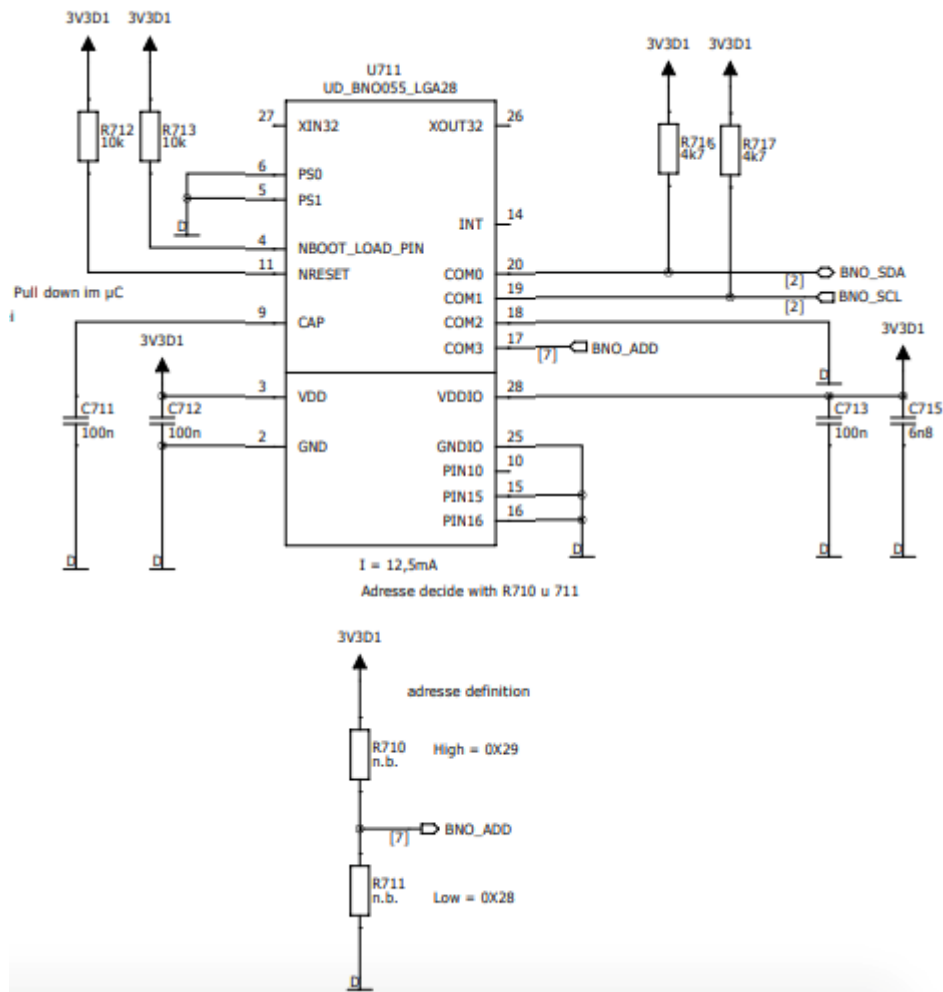


Figure 58 - BNO055 circuit schematics

## Temperature, Pressure and Humidity Sensor

The Temperature, Pressure and Humidity Sensor used in the PBIMS is the BME280 from BOSCH Sensortec. It has digital interface I2C and SPI, operates with 1.7 V to 3.6 V, and maximum consumption current of 3.6  $\mu$ A (when the three sensors are measuring) [91]. Its data will be important to understand the environment conditions in the interior of the payload module and how it can affect the operation of the scientific instruments or electronics.

The model of the circuit is shown as follows:

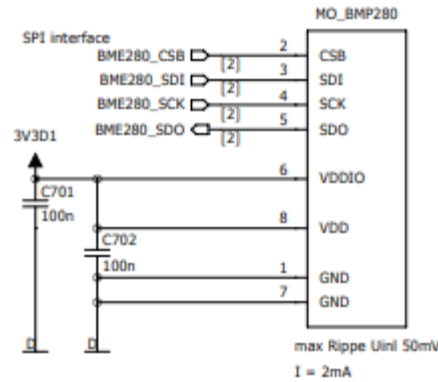


Figure 59 - BME280 circuit schematics

## Distance Sensor

The Distance Sensor included in the PBIMS is the VL6180X from ST technologies. It has a digital interface I2C, operates with 2.6 V to 3.0 V, and works with the temperature range between  $-20^{\circ}\text{C}$  to  $+70^{\circ}\text{C}$ . It combines an Infra-Red (IR) emitter, a range sensor and a light sensor to precisely measure the time the light takes to travel to the target object and return [92]. The measurements taken by this sensor will support the operation of the LIBS task.

The model of the circuit is presented as follows:

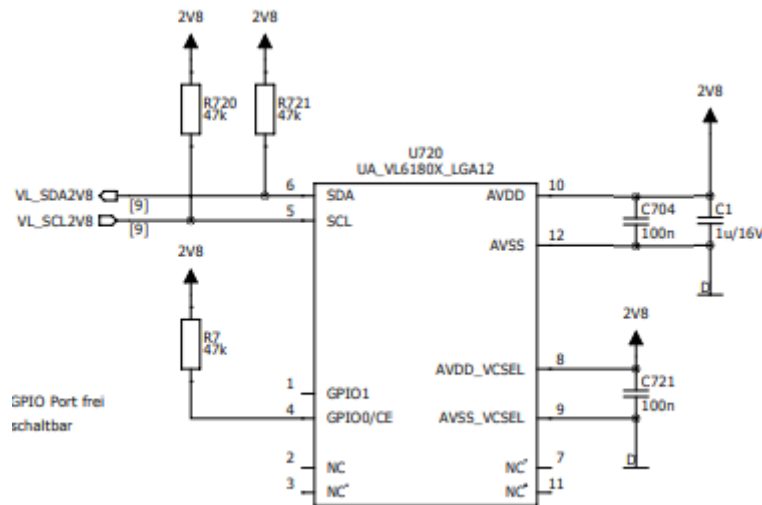


Figure 60 - VL6180X circuit schematics

## 4.2.6 External Analog to Digital Converters (ADCs)

Two external Analog to Digital (ADC) converters were installed in the PBIMS because of the limited number of channels available in the internal ADC from the NXP MCU. The ADC converters chosen for the PBIMS were the Texas Instruments ADC128S102 [93]. They are 12-bit analog-

to-digital converter with eight channels each. The data communication occurs through standard serial communications such as SPI and digital signal processing (DSP). The model of the circuit which represents these external ADC converters is shown as follows:

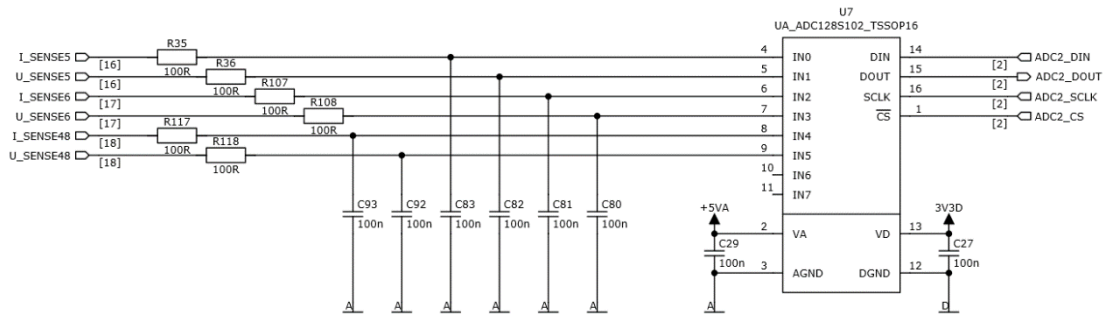


Figure 61 – External ADC converter circuit schematics

There are twelve analog signals to be converted to digital signal and then to be monitored by the MCU. They are the current and voltages values from the DC-DC converters present on the PBIMS. This monitoring is important not only for the control of the accurate functionality of the buck and boost converters, but also to set a safety threshold that can switch off the channel in case overvoltage or very high currents occur. This safety limit will be considered in the basic software implemented in the MCU.

The current values are converted to analog voltage output through a Hall-effect sensor Allegro ACS70331 [94]. It will sense the magnetic field generated by the flow of the current and will generate an analog signal proportional to the current. This signal is then sent to the ADC for analog to digital conversion.

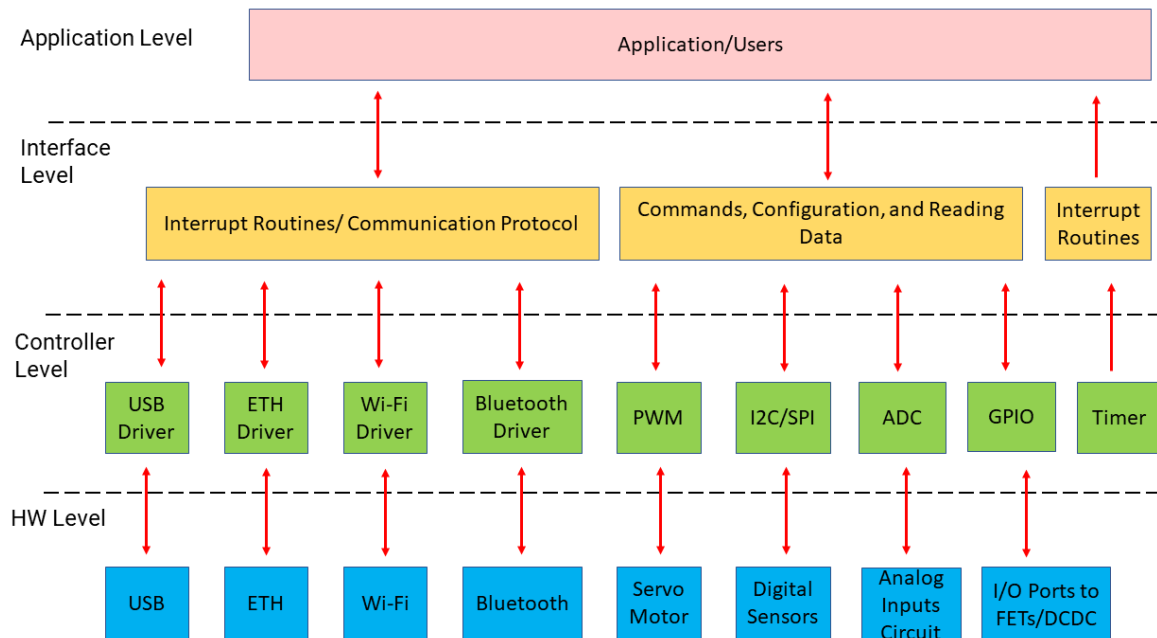
The analog to digital conversion occurs according to the following equation:

$$D_{OUT} = [(2^N - 1)/V_{CC}] * V_{IN} \quad (4.7)$$

Where  $D_{OUT}$  is the binary output converted,  $N$  is the number of bits for the ADC,  $V_{CC}$  is the power supply, and  $V_{IN}$  is the input analog value. In this case,  $N$  is 12 and  $V_{CC}$  is 5 V. The maximum voltage for voltage levels is 4.95 V, which is correspondent to 50 V (maximum level for the Boost converter). The limit voltage for current levels is 2.5 V, which is proportional to 5 A (maximum level for the Hall-effect ACS70331).

### 4.3 Software Architecture

This section introduces the software architecture that makes the PBIMS functional and enables the scientific instruments to be in operation during the analogue mission. The following diagram illustrates it and highlights its main elements:



*Figure 62 - Software Architecture Diagram*

The software was developed with C programming language in the MCUXpresso IDE from NXP Semiconductors. This platform enables the creation, editing, compiling and debugging of the code targeting the MCU operation.

The basic functions of the software are:

- Basic communication to internal sensors and external users
- Monitoring current and voltage levels in the PCDU (ADC)
- Monitoring batteries capacity and state (BMS)
- Control FET switches and DC-DC converters (GPIOs ON/OFF)
- Control servomotor (PWM)

They are represented in the following diagram:

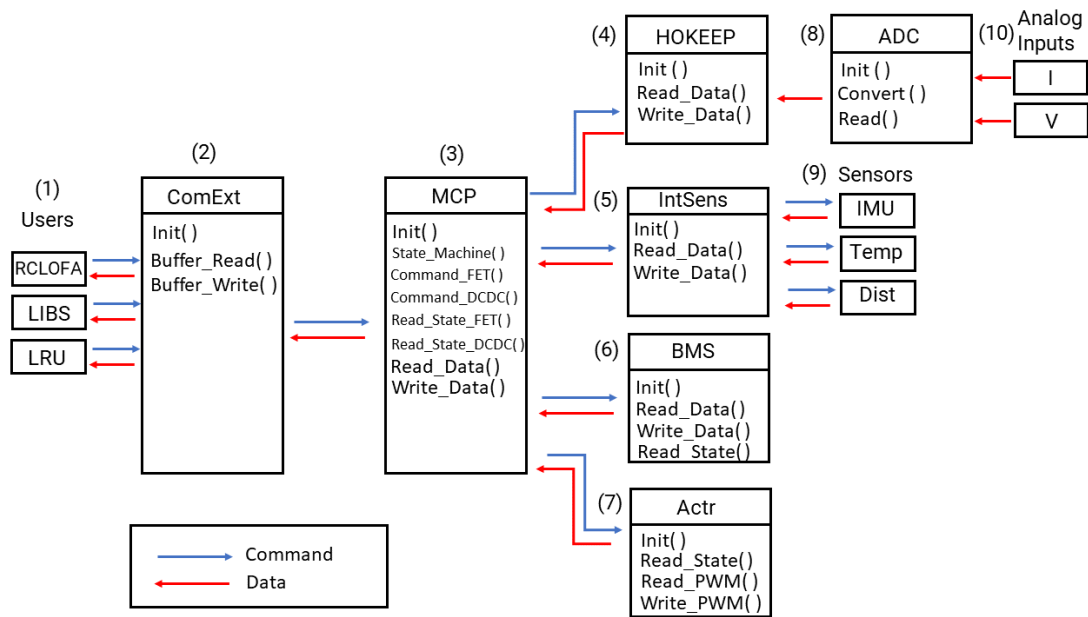


Figure 63 – Functional Block Diagram for the Basic Software

As can be observed, the external users (1) of the PBIMS Basic Software are the RCLOFA, the LIBS and the LRU. They can both send commands or read data from the system. The communication between the Users and the PBIMS can be carried out through USB, UART RS-485, Ethernet, Wi-Fi, or Bluetooth. Specific source files are designed for each of these communication options. At Communication with External Devices (ComExt) (2) commands coming from the Users and data coming from the system are consolidated in a Buffer which will temporarily store them during the transferring and receiving process. At Master Control Program (MCP) (3), there is a state machine which can execute an action based on the states of some parts of the system. Such actions can be switching off power buses or power supplies in case of overvoltage occurrence. The MCP can also read and write data from the entire system as well as control the GPIOs connected to FETs and DC-DC converters. The Housekeeping (HOKEEP) (4) consolidates bus voltages, currents, system temperature, timestamp, bus-state, actuator-state and BMS-state. This is essential information that is valuable to the Users. The Internal Sensors (IntSens) (5) can read and write data from/to the IMU, the Temperature sensor, and the Distance sensor (9). The communication is performed through I2C or SPI with specific source files for each of these alternatives. The Battery Management System (BMS) (6) can read/write data from/to the BMS circuit attached to each battery pack and get the BMS circuit's state which will help to understand if the batteries are operating accordingly. The Actuator (Actr) (7) can send commands to activate the servomotor which will deploy the RCLOFA antenna and read the state of the activation. The Analog-to-Digital Conversion (ADC) (8) can convert and read the data coming from the analog inputs (10). Finally, the Sensors (9) will have their specific source files for setting themselves up and to enable communication to the MCU.

## **4.4 Payload Modules and Tools**

This section presents several types of payload carriers and tools designed to be used in the ARCHES demo mission. The diverse payload modules are the Radio Communication and Low Frequency Array (RCLOFA) payload box, the Laser Induced Breakdown Spectroscopy (LIBS) Spectrometer payload box, the Power Supply (PS) payload box, the Sample Payload Box and the Wi-Fi Repeater Box. While the tools are the Karlsruhe Institute of Technology (KIT) Hand Tool, the Shovel and the Segregation Tool. They are important elements in the robotic network because they can extend the capabilities of the robotic platforms. In ARCHES project, LRU-2 is the robot which will dock to these toolsets. However, in the future, other robot units can also benefit from them if they have standardized electromechanical docking interfaces incorporated into their bodies. These elements will be introduced in the following subsections.

#### 4.4.1 Radio Communication and Low Frequency Array (RCLOFA) Payload Box

The RCLOFA payload module is responsible for two main tasks: It localizes itself and the other RCLOFA boxes in the network, and acts as a simplified radio telescope operating in low frequency (LF). While the former helps the robots to localize the RCLOFA modules infrastructure on the terrain, the latter can identify LF radio waves (20 MHz) such as emissions from Jupiter and the Sun. The ARCHES robots rely on their cameras and optical systems to be able to identify the payload carriers in the field. This adds several errors in their traverses and limits their capability of accurately recognizing the boxes when they are far. The radio communication feature ensures that the robots can 'see' the payload modules even when they are out of the camera's field of view. For the future, it is expected that this attribute will also support the navigation of the LRUs and Ardea.

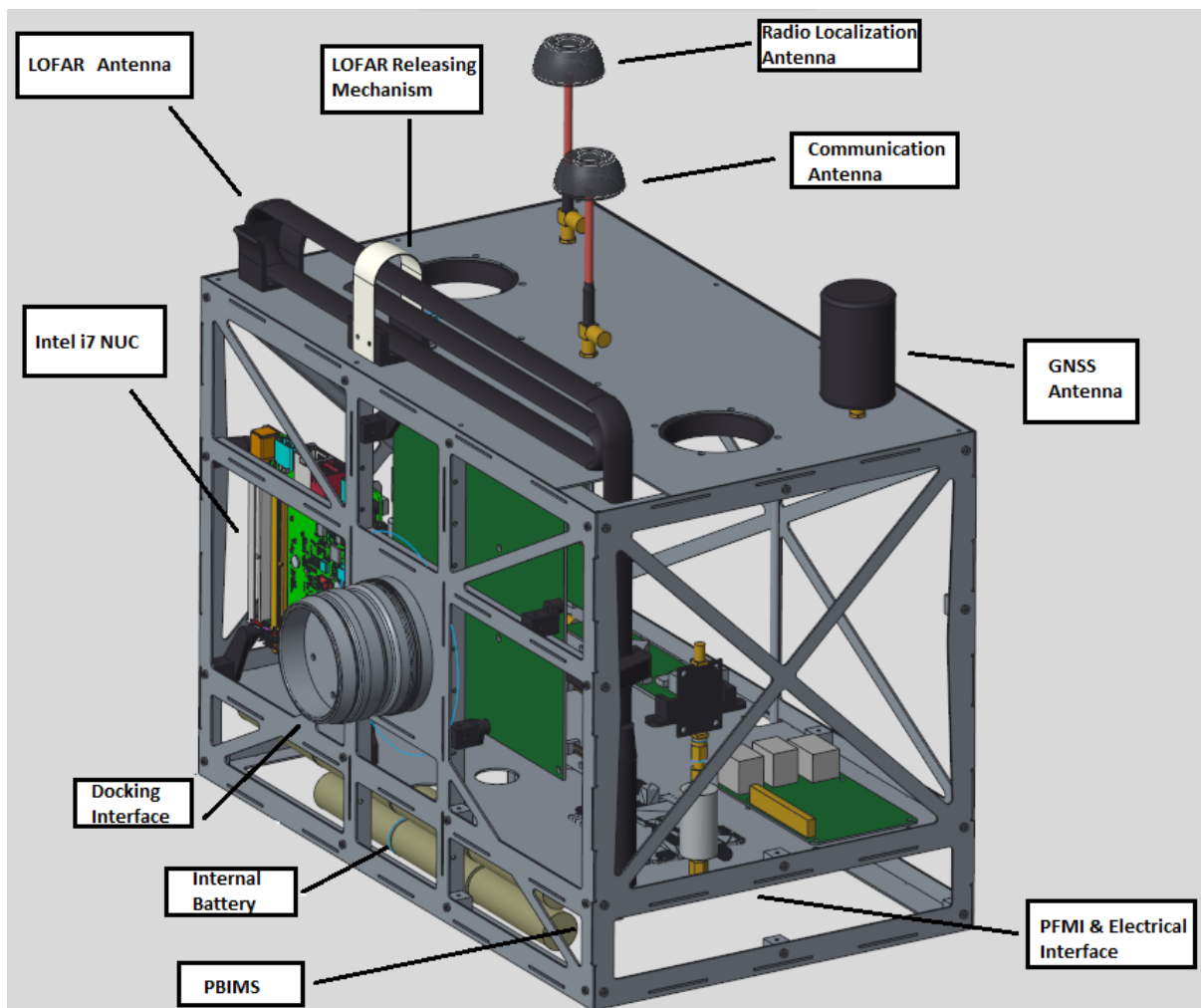


Figure 64 - RCLOFA payload module 3D-Model

The main components of the RCLOFA payload carrier are: The RCLOFA scientific system, the PBIMS, internal batteries, mechanical and electrical interfaces, the LOFAR antenna releasing mechanism, and the mechanical structure of the payload carrier. The diagram that specifies the elements of the RCLOFA scientific system is shown as follows:

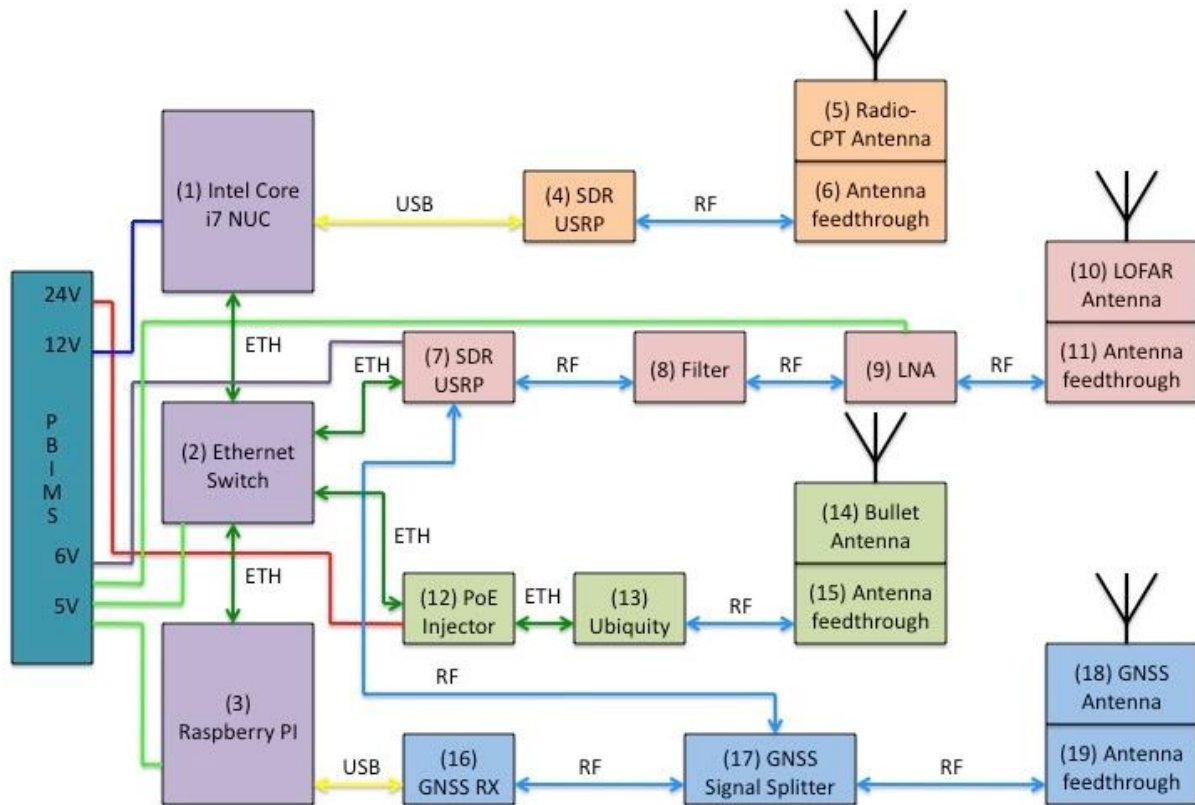


Figure 65 - RCLOFA scientific system diagram.

In the diagram presented, it is possible to see several components interconnected. The intel Core i7 NUC (1) is responsible for pre-processing the data from Radio CPT Antenna and the LOFAR Antenna. The Raspberry PI (2) is responsible for the system housekeeping. The first branch (orange), which is composed of the Software-defined Radio (SDR) (4), the Antenna feedthrough (5) and the Radio-CPT Antenna (6), is responsible for the radio localization of the RCLOFA boxes, and in the future will support the navigation of the ARCHES robot network. The second branch (pink), which encompasses the SDR (7), the Filter (8), the Low Noise Amplifier (LNA) (9), the Antenna feedthrough (10) and the LOFAR Antenna (11), has the function of LF radio wave measurement. The third branch (green), which has the Power over Ethernet (PoE) injector (12), the Ubiquity (13), the Antenna feedthrough (14) and the Bullet Antenna (15), is in charge of the communication to the Lander and to the Control Center in Catania. Finally, the fourth branch (blue), which includes the Global Navigation Satellite System (GNSS) RX (16), the GNSS Signal Splitter (17), the Antenna feedthrough (18) and the GNSS Antenna (19), has the purpose of providing ground truth to the RCLOFA modules.

It is important to highlight the versatility of the payload module structure and the electronics in its interior. Their features offer the possibility of future changes or incorporation of new technologies. For instance, if different antennas, more powerful electronics or actuators need to be included, the payload carrier structure and the PBIMS will be compatible if the constraints of power, weight and volume are respected.

Considering the V-shaped model methodology, it is possible to point out the main stakeholders, the requirements, the model and the implementation of the RCLOFA payload model.

The main stakeholders are: KN institute, which is the owner and designer of the RCLOFA scientific system, RM Manipulation Team, which will deploy the RCLOFA payload modules on the terrain, RM Navigation Team, which will use the localization information from the RCLOFA PB, and ESA-DLR astronomers and planetary scientists, which will use the data from the RCLOFA PB after they are deployed.

The requirements for the RCLOFA PB are: power and data requirements specified on section 4.2, payload module able to accommodate scientific payload with 1kg weight, payload module with top part able to incorporate four different antennas, and mechanism to release the LOFAR dipole antenna.

The model of the RCLOFA payload carrier was carried out with the CAD tool PTC CREO 3.0. The structural analysis of the loads and stresses that the box would face in the real operation were simulated with CREO Simulate. The application of extreme loads (20 to 60 N) on the box created maximum stress of 2797 MPa. With the Carbon Fiber Tensile strength between 3000 to 5000 MPa, damages are not expected if the forces applied are within the simulated limit.

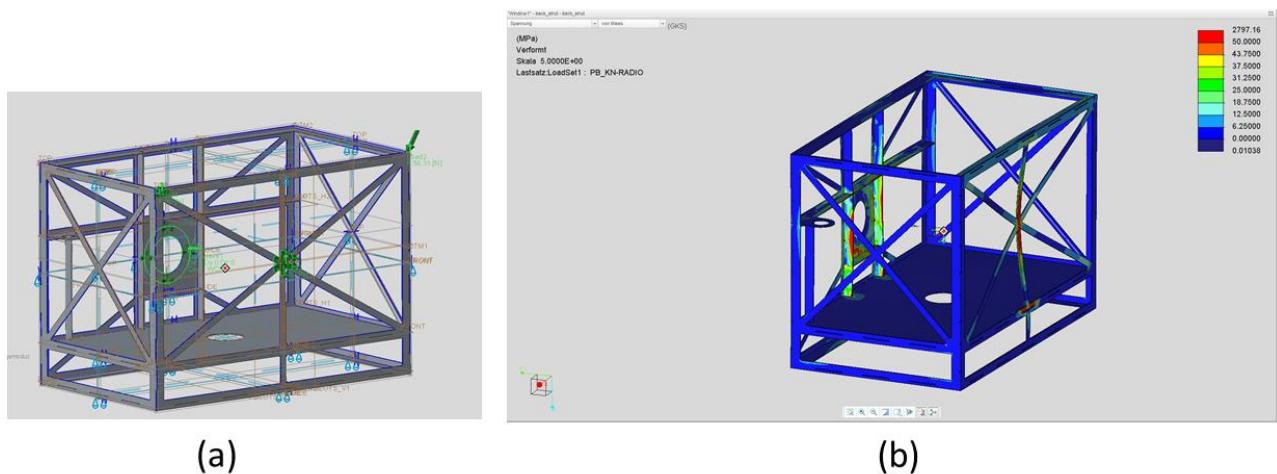


Figure 66 - Standard Payload Box Structural Analysis. (a) Loads from 20 to 60 N applied in specific parts of the box; (b) Stresses in MPa after simulation.

Finally, the implementation of the RCLOFA payload box occurred in the RM mechanical workshop with the assembling of parts and electronic components.

#### 4.4.2 LIBS Spectrometer Payload Box

The main function of the LIBS spectrometer Payload box is to identify and analyze the mineral elements of rocks. This module works with the shooting of a laser source to a target which will have part of it converted into ionized plasma. The light wavelengths emitted in this process are captured by the optical system and then analyzed by the spectrometer.

The main parts of the LIBS payload module are the LIBS spectrometer scientific system, the PBIMS, internal batteries, mechanical and electrical interfaces, and the mechanical structure of the payload carrier. Figure X presents the LIBS payload module 3D-model:

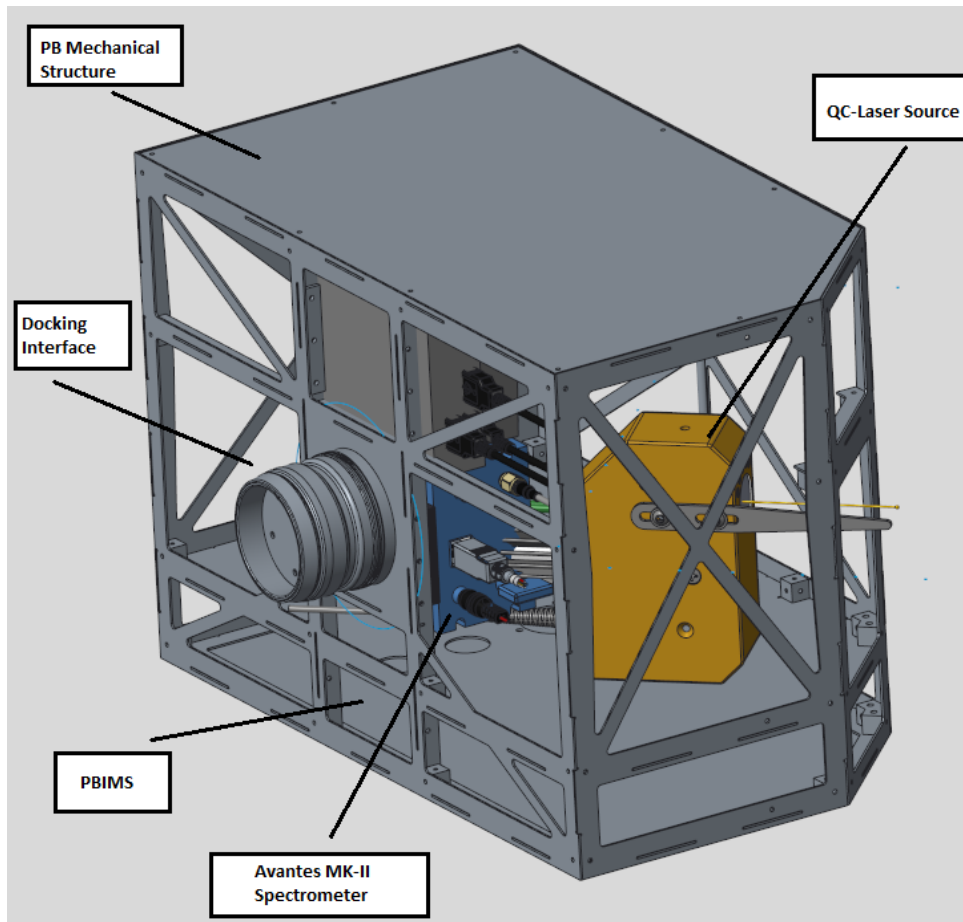


Figure 67 - LIBS payload module 3D-model

It is possible to observe the LIBS scientific system diagram as follows:

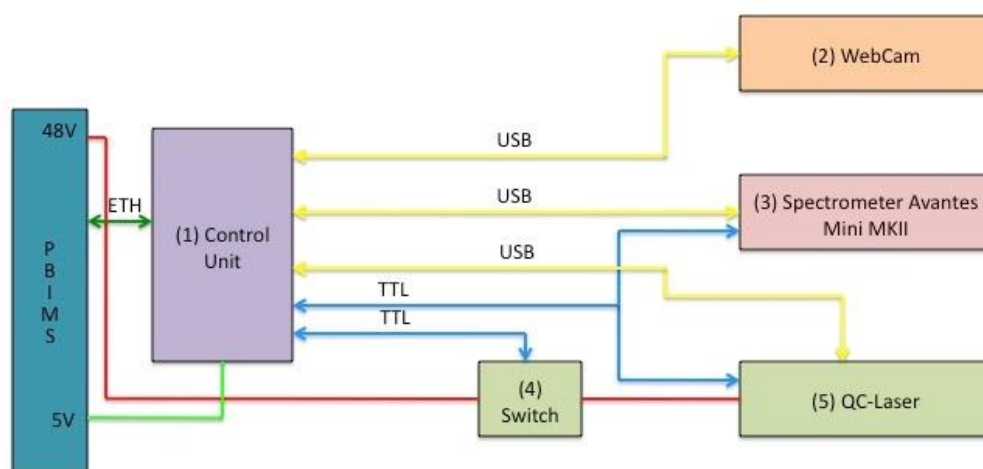


Figure 68 - LIBS scientific system diagram.

Considering the V-shaped model methodology, it is possible to highlight the principal stakeholders, the requirements, the model and the implementation of the LIBS payload model.

The main stakeholders are: OS institute, which is the owner and designer of the LIBS scientific system, RM Manipulation Team, which will manipulate the LIBS payload modules during the LIBS geological task, and ESA-DLR geologists and planetary scientists, which will use the data from the LIBS payload carrier after they measurements are taken.

The requirements for the LIBS payload module are: power and data requirements specified on section 4.2, payload module able to accommodate scientific payload with 1kg weight, payload module with one of its edges chamfered.

The model of the LIBS payload carrier was carried out with the CAD tool PTC CREO 3.0. The structural analysis of the loads and stresses that the box would face in the real operation were simulated with CREO Simulate.

Finally, the implementation of the LIBS payload box occurred in the RM mechanical workshop with the assembling of parts and electronic components.

#### 4.4.3 Power Supply (PS) Payload Box

The purpose of the PS payload module is to provide extra power to the other payload carriers to be deployed in the field. This ensures that the autonomy of these devices is extended to several additional hours. Its battery pack capacity is 200 Wh which will add up four extra hours for a 50 W nominal consumption. The connection to other payload modules is performed with the stacking of the scientific payload carrier on top of the PS payload box. In case it is necessary to increase the power autonomy of the scientific modules, two or more PS boxes can be stacked on top of each other. The only constraint is the height limitation of 1 m that the LRU-2 robotic arm can reach.

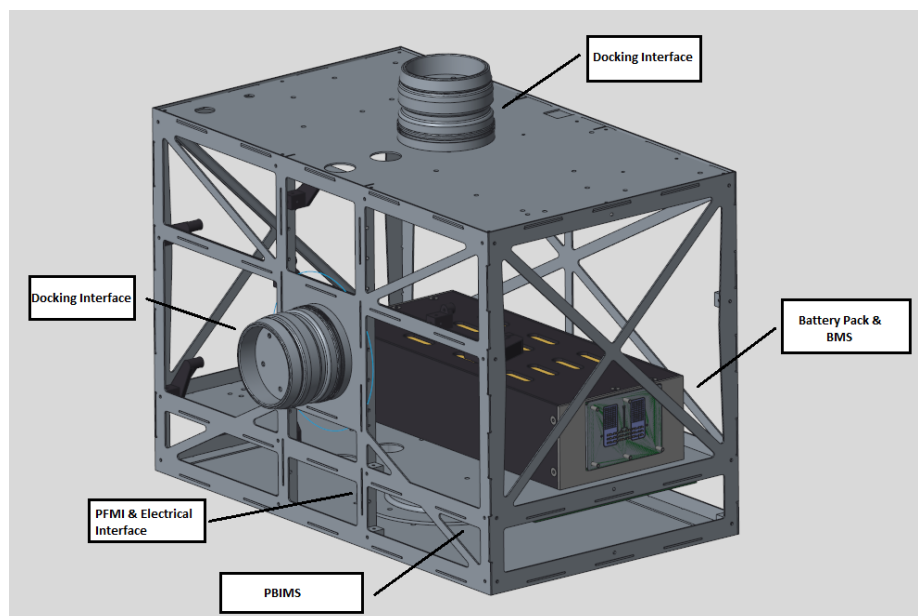


Figure 69 - PS payload box 3D-model.

The main components of the PS payload module are: The Li-ion battery pack, the PBIMS, the electrical and mechanical interfaces, and the payload module mechanical structure.

Regarding the V-shaped model methodology, it is possible to highlight the main stakeholders, the requirements, the model and the implementation of the PS payload model.

The main stakeholders are: KN institute, which will have their RCLOFA payload module stacked on top of the PS module and the RM Manipulation Team, which will deploy the PS payload modules on the terrain.

The requirements for the PS payload module are: power requirements specified on section 4.2, payload module able to accommodate battery pack with 1.8kg weight, mechanical and electrical interfaces on the top, side and bottom of the boxes.

The model of the PS payload carrier was carried out with the CAD tool PTC CREO 3.0. The structural analysis of the loads and stresses that the box would face in the real operation were simulated with CREO Simulate.

Finally, the implementation of the PS payload box occurred in the RM Electronics Laboratory with the assembling of parts and electronic components.

#### 4.4.4 Sample Payload Box

The Sample Payload Box is an open container designed for the storage of soil samples and rocks collected by the LRU-2 during the geological task. Standard size, weight and mechanical interfaces are used in its construction. Although this payload module has no electronics on it, it can be upgraded in the future with the PBIMS and actuators with the purpose of sealing and isolating each sample.

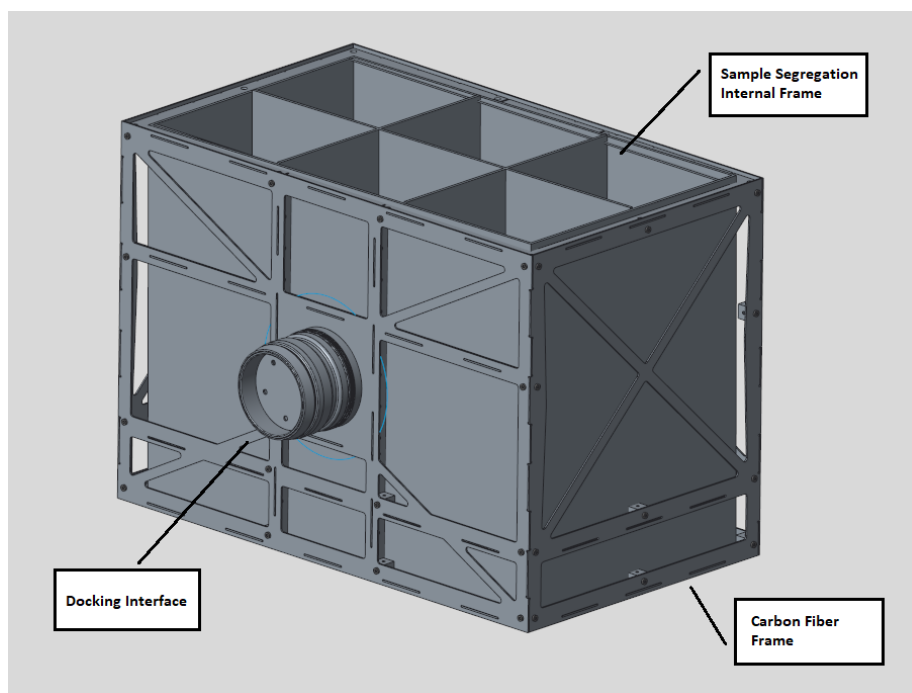


Figure 70 - Sample Payload Box 3D-Model

The main stakeholders are: RM Manipulation Team, which will operate the arm during the sampling task, KIT Team, which will operate the hand and store the collected rocks in the container, and the ESA-DLR geologists and planetary scientists, which will receive the samples for further analysis.

The specifications defined by the parts involved are maximum weight (1 kg), dimensions of the six openings in the container (105 mm x 82 mm x 236 mm), and standardized mechanical interfaces.

The model of the Sample payload module was carried out with the CAD tool PTC CREO 3.0. The structural analysis of the loads and stresses that the box would face in the real operation were simulated with CREO Simulate.

The implementation of the Sample payload box occurred in the RM Mechanical Workshop with the assembling of parts.

#### 4.4.5 Wi-Fi Repeater Box

The Wi-Fi Repeater Payload box is an essential element in the multi-robotic network because it extends the WLAN network. Both LRUs, Ardea and the Lander have a Wi-Fi router which are limited to 200 m. The use of Wi-Fi repeaters distributed in the field can provide continuous communication between the components of the network in the enhanced range of 250-300 m.

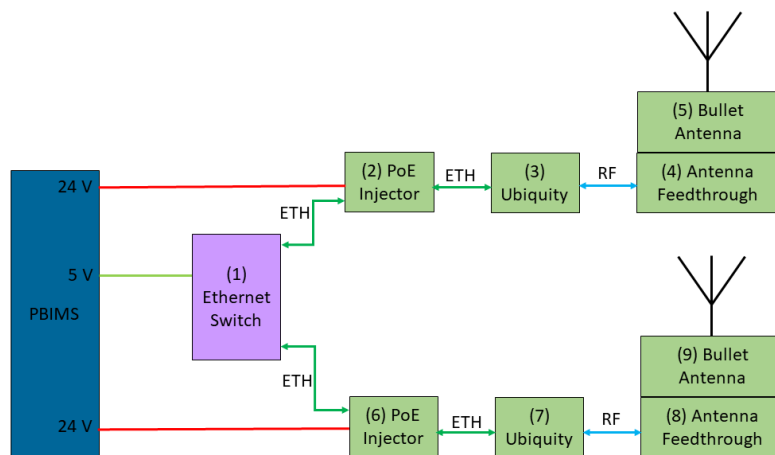


Figure 71 – Wi-Fi Repeater system diagram.

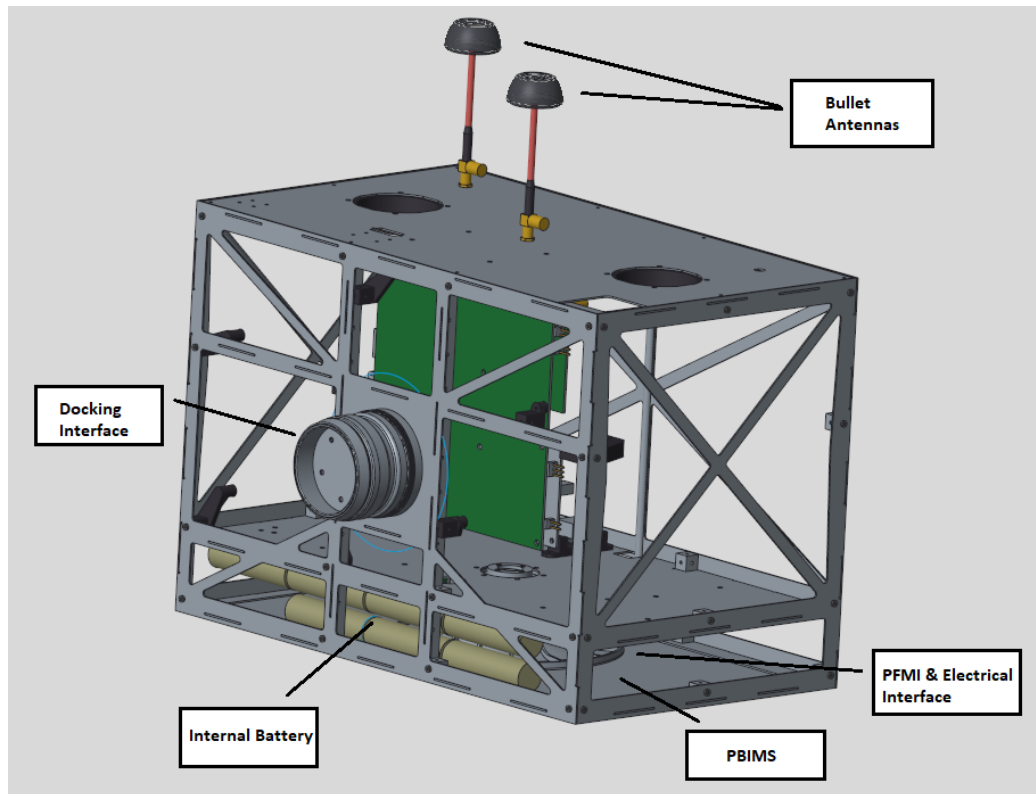


Figure 72 – Wi-Fi Repeater Payload Box 3D-Model.

#### 4.4.6 KIT Hand Tool

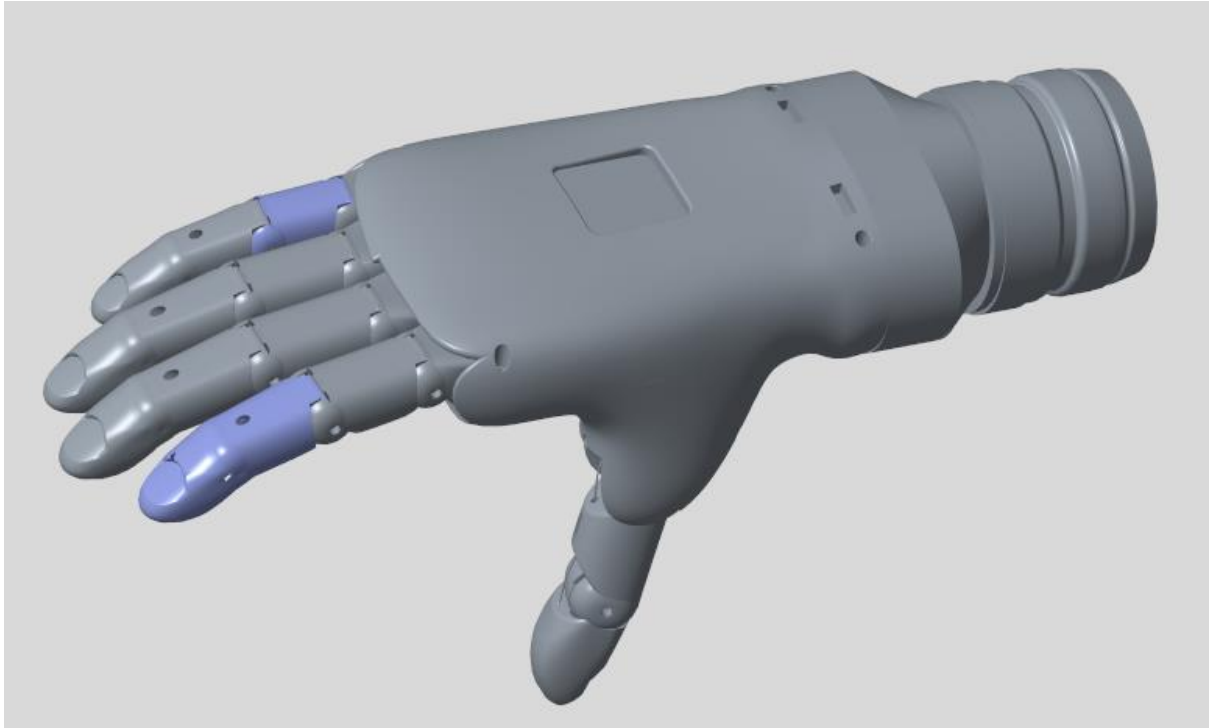
The Karlsruhe Institute of Technology (KIT) Hand tool is a robotic hand designed for grasping different sizes of rocks on the terrain. After the identification of the rocks with the LRU-1 cameras and separation with the Segregation tool, the KIT Hand, which is docked to the LRU-2 manipulator end-effector, will collect the rocks and place them in the Sample payload box.

The main elements of the KIT Hand Tool are: the KIT hand, a mechanical adaptor, a DC-DC converter board, and the electromechanical docking interface.

The KIT hand is a prosthetic five-fingered hand with two motors actuating ten degrees of freedom developed by KIT. It has a cylindrical grasp force of 24.2 N, hook grasp of 120 N and hand closing time of 1.3 s [95].

The DC-DC converter board is a buck converter to lower down the 24 V supplied by the robotic arm to 12 V which is necessary for powering ON the KIT hand tool. Because of space limitation in the interior of the adaptor and presence of a single power requirement, the PBIMS obviously could not be utilized in this device.

The KIT hand Adaptor was built with the purpose of integrating the KIT Hand to the passive docking interface. It was designed long enough to accommodate the DC-DC converter board, but not so long that would create some momentum to the robotic arm.



*Figure 73 - KIT Hand tool 3D-Model*

Considering the aspects of the V-shaped model descending branch, stakeholders, requirements, model and implementation are presented.

The main stakeholders are: the RM Manipulation Team, which will operate the LRU-2 robotic arm, the KIT Team, which will operate the hand, and the, ESA-DLR geologists and planetary scientists, which will use the data from the geological task performed with the KIT Hand tool.

The requirements specified from the parts involved were: electrical and mechanical interface to integrate the KIT hand to the LRU-2 robotic arm, supply voltage of 12 V, and interface geometry adequate to the manipulability of the robotic arm.

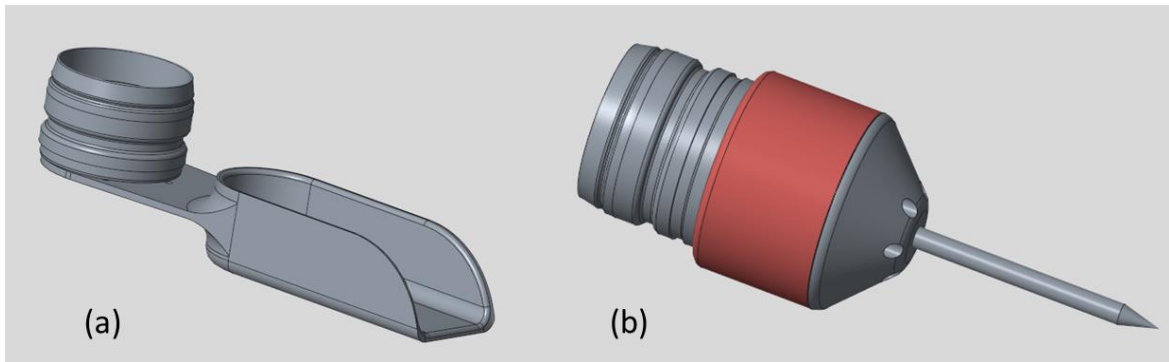
The model of the KIT Hand tool was carried out with the CAD tool PTC CREO 3.0. The structural analysis of the loads and stresses that the tool would face in the real operation were simulated with CREO Simulate.

Finally, the implementation of the KIT Hand tool occurred in the RM Electronics Laboratory with the assembling of parts and electronic components.

#### **4.4.7 Shovel and Segregation Tool**

The Shovel and the Segregation Tool are essential tools for the geological tasks the LRUs will perform in the terrain. The shovel is used to collect soil samples and place them in the Sample payload box. The segregation tool is utilized for separating one rock from each other when they are aggregated in a pile with the purpose of facilitating the task of the KIT hand tool that will grasp rock samples. Although these tools are fully mechanical and have only the Passive Male

Mechanical Interface (PMMI) as part of the MI, they were included in this thesis to demonstrate the versatility of the MI with the implementation of multi-function tools and instruments to the robotic team.



*Figure 74 – (a) Shovel; (b) Segregation Tool 3D-Model.*

## **4.5 Electromechanical Docking Interface**

The electromechanical Docking Interface encompasses several elements which allow the robotic arm to connect to the payload modules or to special purpose tools, and payload modules to stack to each other. These main elements are the Electrical Interface Connector, the Passive Female Mechanical Interface (PFMI), the Passive Male Mechanical Interface (PMMI), and the Active Female Interface (AFI). They are described in this section.

### **4.5.1 Electrical Interface Connector (EIC)**

The electromechanical Docking Interface was not equipped with an electrical interface for power and data transferring. For this reason, the electrical interface connector (EIC) was developed. Two counterparts were designed so they could mate during the docking process. With the intention of having an accurate mating, the male-female designation was chosen. This type of connector has proven to be reliable in the subsea industry (Marine and Oil & Gas), where it is heavily used.

The main components of the EIC are: the Polyoxymethylene (POM) casing, the copper-beryllium electrical contacts, and the 18 AWG copper wires. With its modular assembling process, the EIC can have three or four electrical contacts. Each contact can handle current of 2.5 A and data transfer of 10 MBps. Figure X presents the male and female electrical connector as follows:

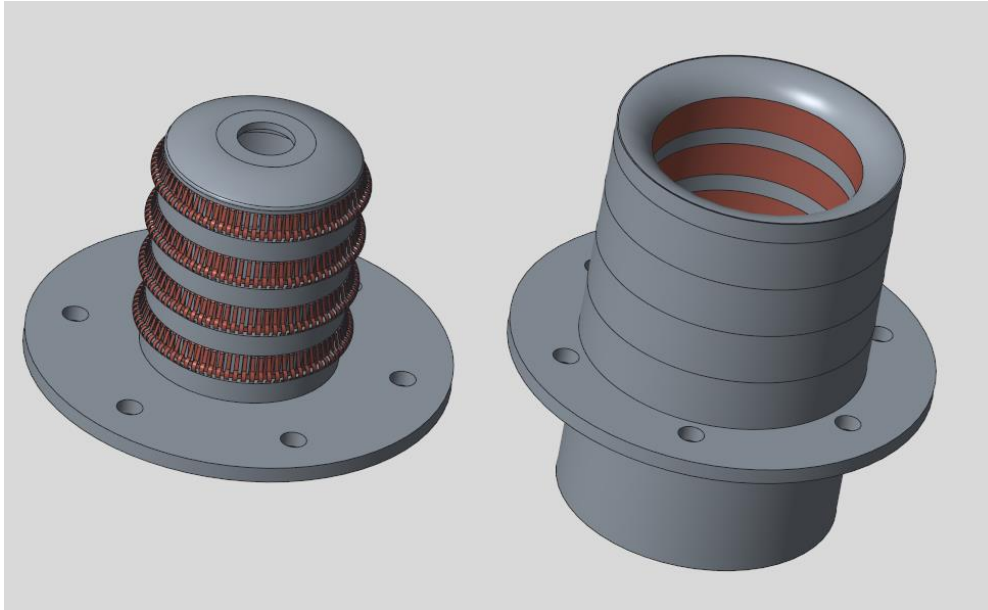


Figure 75 - Electrical Interface Connector (EIC) 3-D Model.

Creo Simulate was used for the docking simulation in a hypothetical situation of misalignment between the connectors (worst case). The force normally observed in this task is (-6.5, -1.2, 9) N, but for simulation purposes it was multiplied by four. It is possible to notice that even in this extreme situation the maximum stress on the base of the connector is 6 MPa (N/mm<sup>2</sup>) and the maximum displacement is 0.0237 mm. The stress necessary for starting the deformation of the POM is about 65 MPa [96] which is much higher than the simulated stress. The following figure show the results of the simulation:

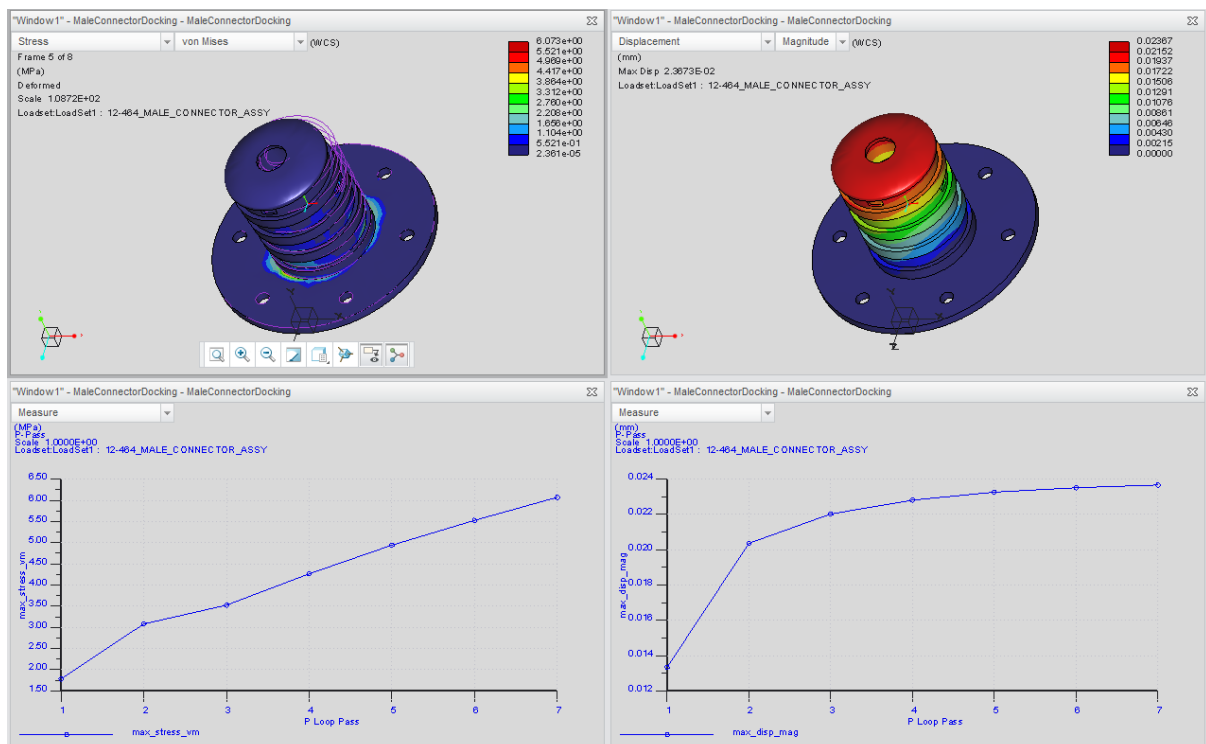


Figure 76 - Structure Analysis Male Electrical Interface Connector with CREO simulate.

Looking to the V-shaped model descending part, stakeholders, requirements, model and implementation are identified.

The main stakeholder is the RM Manipulation Team which will operate the robotic arm during the stacking of the RCLOFA box on top of the PS module.

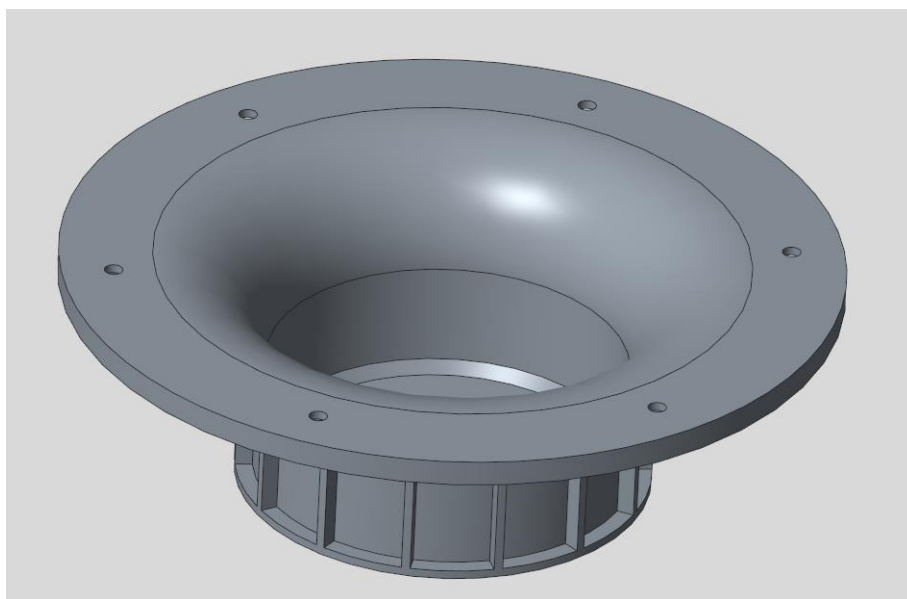
The design criteria is: geometry to adapt to existing docking interface (active and passive), enough clearance and favorable shape to account for the inaccuracies of the robotic arm, electrical contacts able to supply power of 24 V at 2.5 A and transfer data at the rate of 10 Mbps.

The model of the EIC was done with the CAD tool PTC CREO 3.0. The structural analysis of the loads and stresses that the connector would face in the real operation were simulated with CREO Simulate.

Finally, the implementation of the EIC happened in the RM Electronics Laboratory with the assembling of mechanical parts and electronic components.

#### **4.5.2 Passive Female Mechanical Interface (PFMI)**

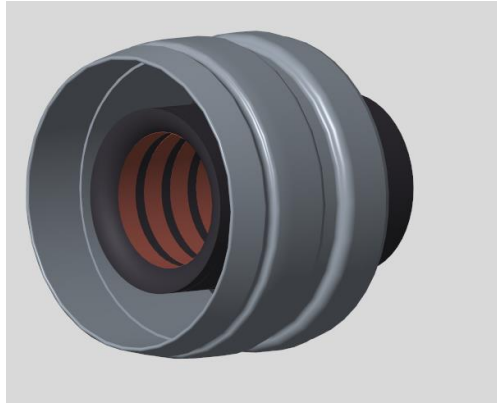
Although the mechanical docking interfaces for the robotic arm end-effector (active) and for the lateral surface of the payload boxes were already developed, there was a necessity of building a new passive docking mechanism to allow two payload modules to be docked to each other. Therefore, the Passive Female Mechanical Interface (PFMI) was created to be added to the bottom part of the payload carrier. Considering the inaccuracies of the robotic arm, it has a rounded edge of 30 mm and clearance of 2 mm. This funnel shape ensures that the counterpart connector can be properly mated even when it is not precisely centered. The following figure shows the PFMI:



*Figure 77 - Passive Female Mechanical Interface (PFMI) 3-D Model.*

### 4.5.3 Passive Male Mechanical Interface (PMMI)

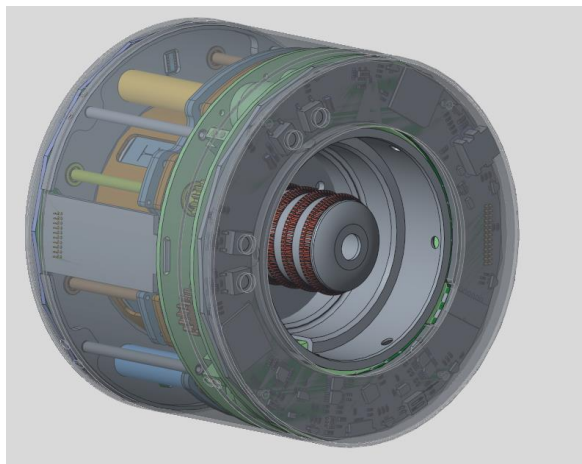
The Passive Male Mechanical Interface (PMMI) is a mechanical part which allows payload modules and tools to be docked to the LRU-2 arm. Its geometry facilitates the latching and locking process during the docking. The female EIC is connected to its interior with the purpose of enabling power and data transfer.



*Figure 78 – Passive Male Mechanical Interface (PMMI) 3-D Model.*

### 4.5.4 Active Female Interface (AFI)

The Active Female Interface (AFI) is an essential part of the docking interface. It is the end-effector of the LRU-2 robotic arm and with a spring-loaded system can actively latch the PMMI which is connected to payload boxes and tools. With this, the LRU-2 robotic arm can manipulate objects or deploy instruments on the terrain. The male EIC is connected to its interior with the purpose of enabling the power and data transfer between the LRU-2 and the tool or payload module connected to it.



*Figure 79 – Active Female Interface (AFI) 3-D Model.*

## 5 Testing and Evaluation

This chapter aims to demonstrate the ascending branch of the V-shaped Model through the execution of tests in the component and system level which allowed the integration of the whole mechatronics infrastructure (MI) to the ARCHES robotic network. This process had the stakeholders involved in each stage with the purpose of having the appropriate verification and validation of the MI. The results of each phase are presented in each section.

### 5.1 Hardware Testing

This section presents the tests executed at the component level with the focus on the hardware elements. They were carried out with the intention of checking the functionality of each component without considering the entire system. The procedure and results are described as follows.

#### 5.1.1 Docking interfaces

For the Hardware test of the docking interfaces the focus was on the Electrical Interface Connectors (EICs). Resistance, current and temperature values were measured as follows.

##### Electrical and Temperature values

The resistance values for the male and female EICs are presented in the following table:

*Table 9 – Resistance values for EIC*

Electrical Interface Connector	Stack1 Resistance ( $\Omega$ )	Stack2 Resistance ( $\Omega$ )	Stack3 Resistance ( $\Omega$ )
Male Connector	0.37	0.67	0.44
Female Connector	0.44	0.42	0.59

Considering the geometry of the contacts with about 10 cm of 18 AWG copper wire and a copper beryllium ring of 30 mm diameter, 4 mm height and 1 mm thickness, the resistance about 0.5  $\Omega$  is as expected.

For checking the temperature on the contacts of the connectors, one stack of both female and male EICs were connected to a variable load which was set up to 2 A/ 50 W. The temperature measured was 23.7° C. The test run for three hours and no significant variations were observed. Figure X illustrates this test.

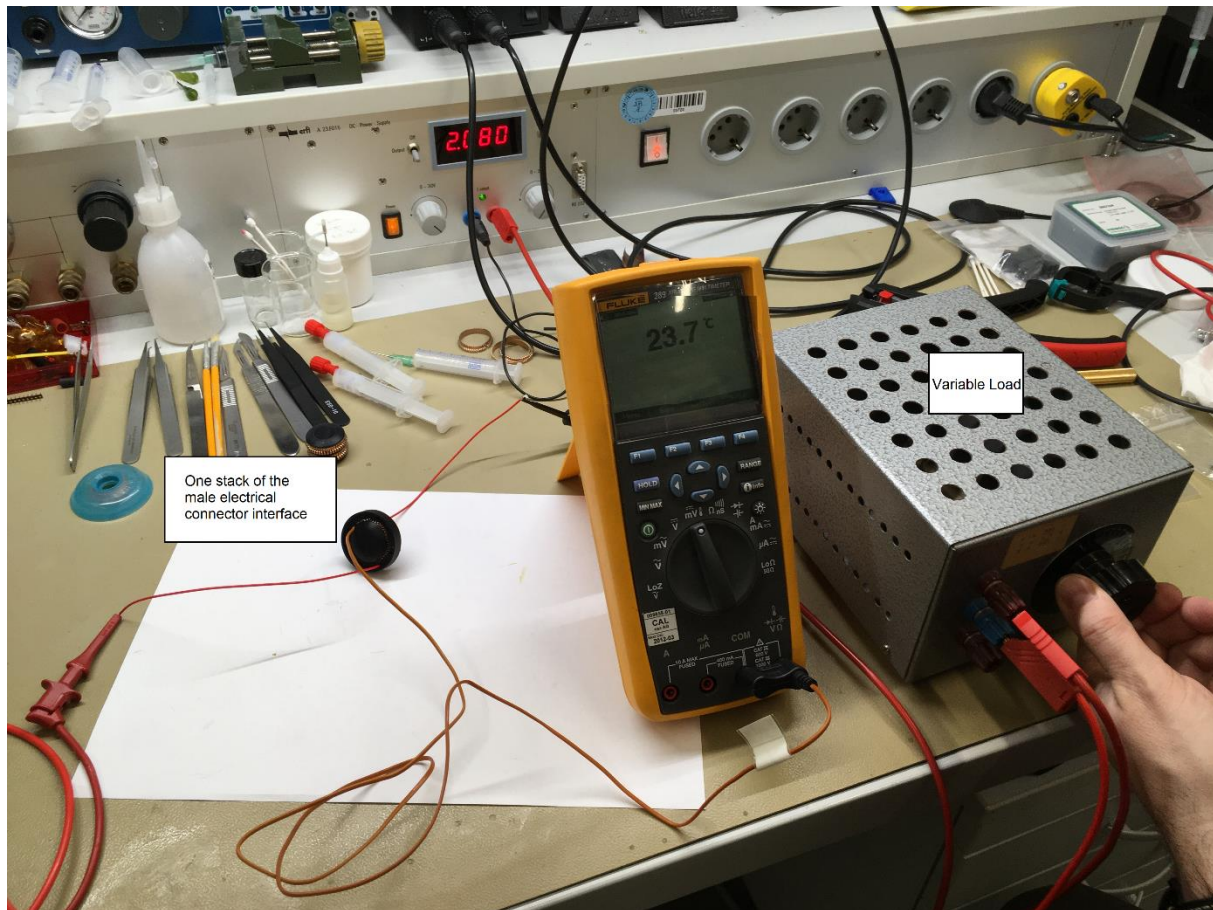


Figure 80 – Electrical Interface Connector (EIC) Temperature and Current test

### 5.1.2 PBIMS

#### DC-DC conversion

The test to check the accurate DC-DC conversion was carried out in four buck converters and one boost converter. The output voltage levels, and the ripple voltage were measured. The test was carried out for 3 hours and the levels showed stable values. Figure 81 presents the results of the buck converters for 5 V (a), 6 V (b), 12 V (c) and 24 V (d). In quadrant (a) the input voltage is 28.44 V, the output voltage is 5.06 V, and the voltage ripple is 30.22 mVpp. In quadrant (b) the input voltage is 28.30 V, the output voltage is 6.15 V, and the voltage ripple is 25.39 mVpp. In quadrant (c) the input voltage is 28.28 V, the output voltage is 12.69 V, and the voltage ripple is 37.22 mVpp. In quadrant (d) the input voltage is 28.29 V, the output voltage is 23.94 V, and the voltage ripple is 23.33 mVpp. All the conversions happened within the 5% tolerance, the 97% efficiency and the voltage ripple limit (40 mVpp) of the TDK i3a series buck converter.

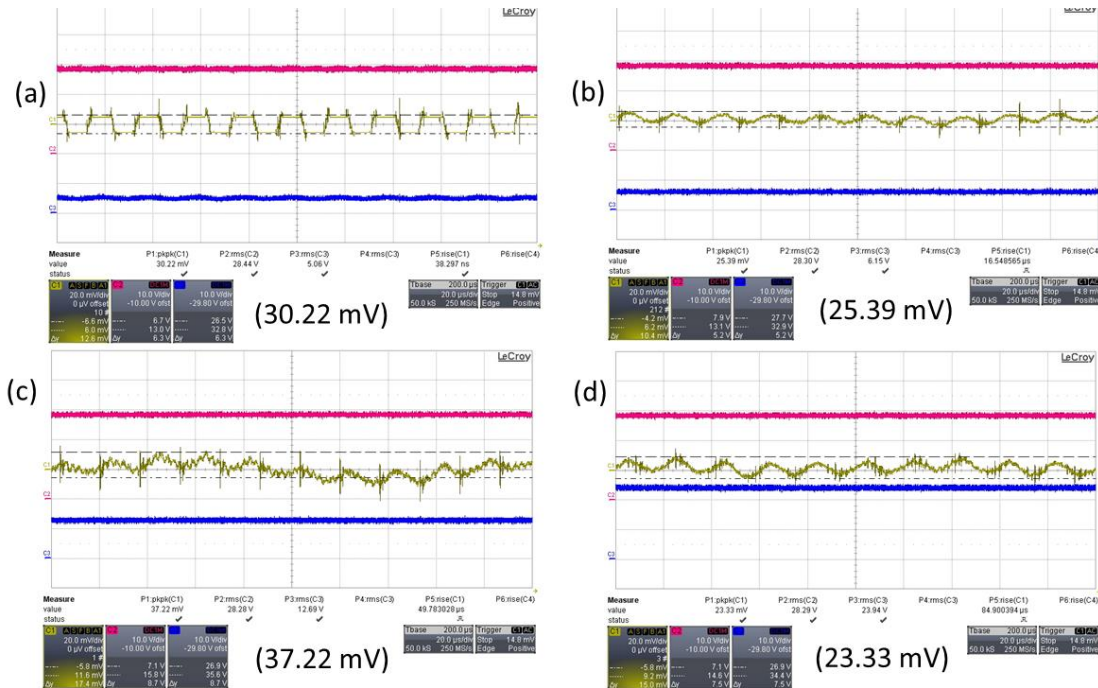


Figure 81 – (a) Buck converter 28 V to 5 V with ripple 30.22 mVpp; (b) Buck converter 28 V to 6 V with ripple 25.39 mVpp; (c) Buck converter 28 V to 12 V with ripple 37.22 mVpp; (d) Buck converter 28 V to 24 V with ripple 23.33 mVpp.

Figure 82 shows the results of the boost converter for 48 V. The input voltage is 28.6 V and the output voltage is 50.8 V. The voltage ripple is 425 mVpp, which is within the specification of the Vicor DCM2322 Boost regulator (474 mVpp).

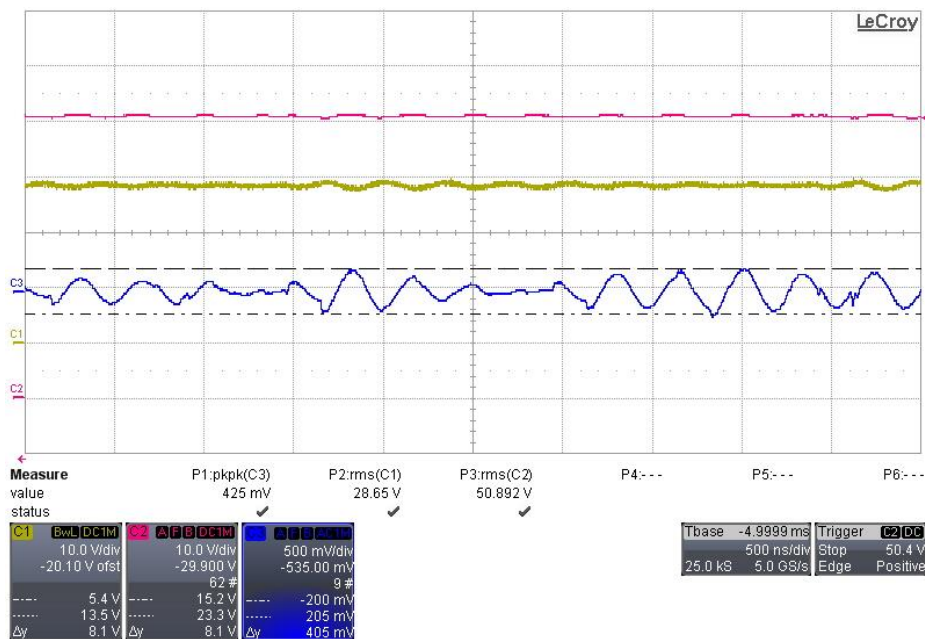


Figure 82 – Boost Converter 48 V with ripple 425 mVpp.

## PPC

Three tests were carried out to check the PPC functionality:

- Measurement of the UV/OV window for each voltage source
- Verification of correct switching among prioritized power sources
- Measurement of switching time between power sources

For the UV/OV window measurement, the calculated UV/OV range (23 V to 28 V) in the subsection 4.2.1 was used as reference. Then, the values were measured with the use of an oscilloscope. One probe was attached to the output voltage (yellow - C1) and another to the power supply (pink - C2). First, the lower threshold was measured, and the value is 23.64 V as observed on figure 83:

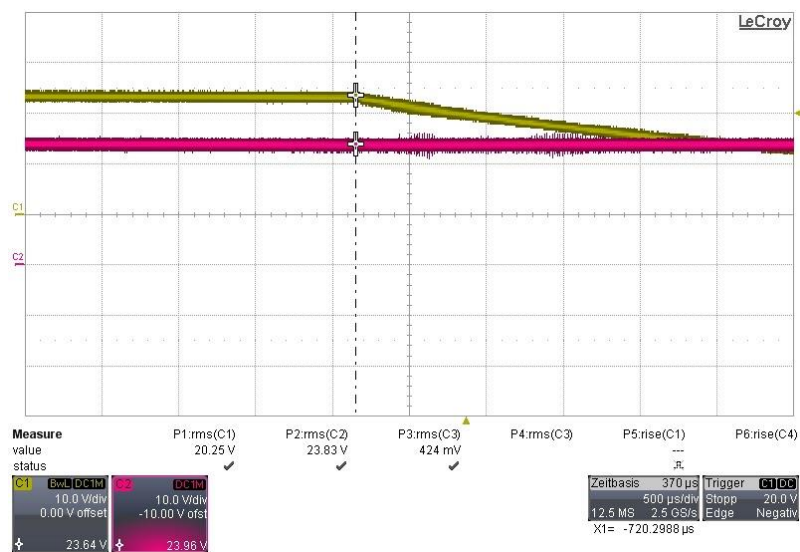


Figure 83 - Oscilloscope with lower threshold of the UV/OV window.

Then, the upper limit was measured, and the value is 28.82 V as shown on figure 84:

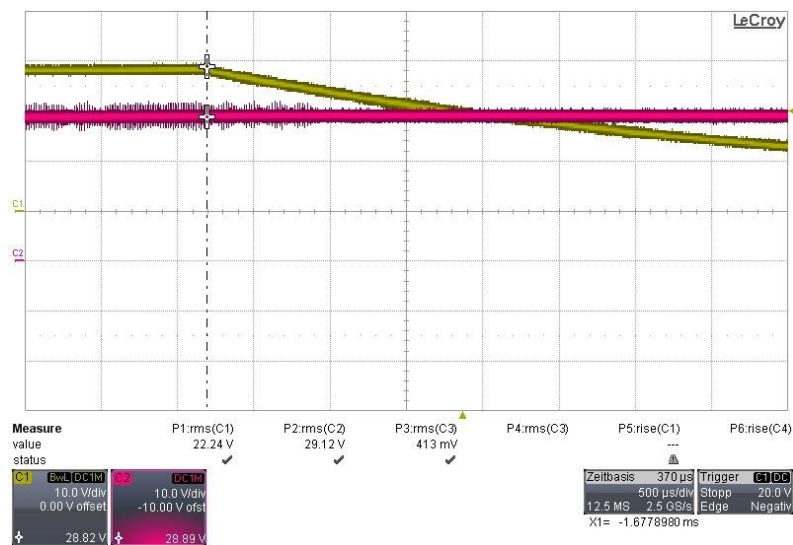


Figure 84 - Oscilloscope with upper threshold of the UV/OV window.

For the evaluation of the correct switching among power supplies, the probes were connected to V1 (C2 - pink - set as 28.5 V), V2 (C3 - blue - set as 24.5 V), V3 (C4 - green - set as 27 V) and Vout (C1 - yellow). Initially, Vout value is 28.5 V as V1(highest priority). Then, V1 is increased to 29 V (outside the window). Vout value drops to 24.5 V as V2 (second highest priority) (1). V2 voltage is lowered to 23.6 V and this leads to the Vout switching to V3 (last priority) with 27 V (2). Finally, after V3 is lowered to 22 V, Vout goes to zero (3). These results are shown as follows:

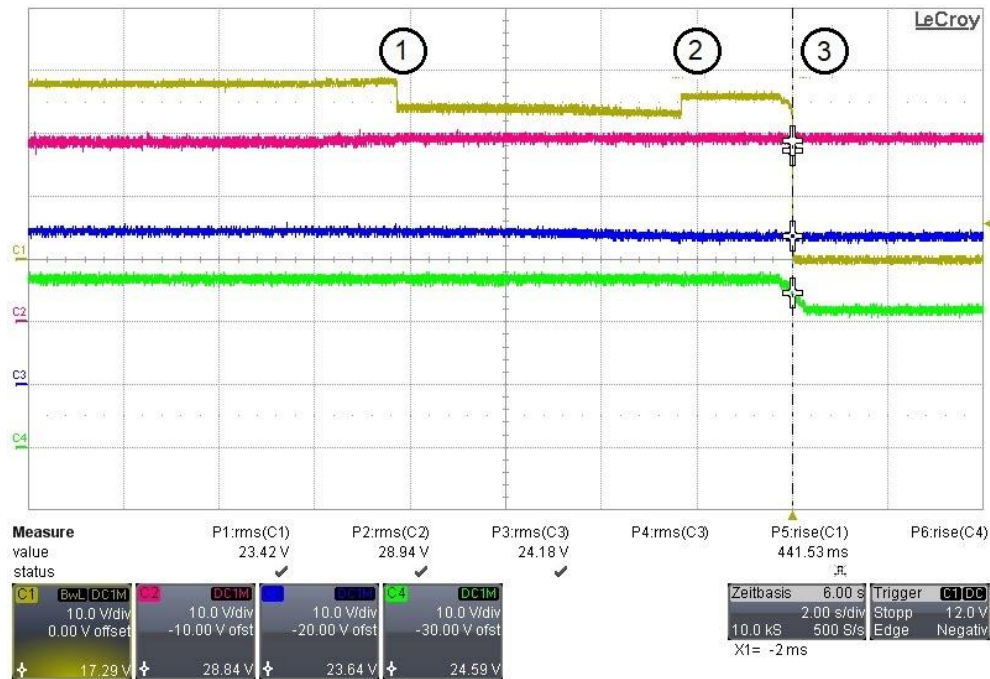


Figure 85 - Accurate switching among prioritized power sources.

For the measurement of switching time between power sources an ideal and a non-ideal switch were used. The non-ideal switch represents the imperfect connection between the robotic arm and the payload box or between two payload modules. This connection does not happen immediately because of the mechanical parts and the alignment of the electrical contacts. In figure 86, it is possible to observe the output voltage channel (C1-yellow) changing from a power source with less priority (C3-blue) to a high priority power source (C2-pink) when the latter is activated by a switch. In (a), with the ideal switch, the voltage switching occurred from 25.81 V to 28.8 V, and the switching time is 1.96  $\mu$ s. While in (b), with the non-ideal switch, the voltage switching occurred from 25.63 V to 28.9 V, and the switching time is 2.01  $\mu$ s. There is no relevant difference between the two different switches. The transition happens smoothly in both situations. The damped oscillation in the high priority source (C2-pink) occurs because of the unbalanced capacity between the DC Power Supply Unit and the PBIMS.

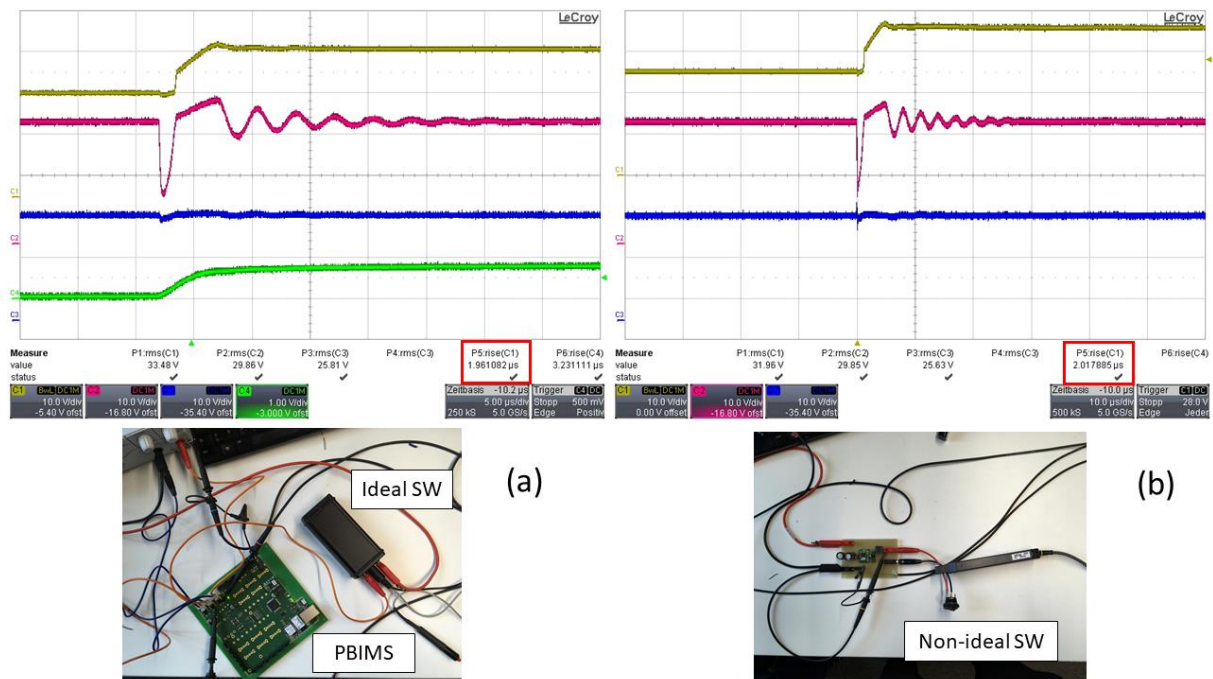


Figure 86 – (a) Switching time Ideal switch ( $1.96 \mu\text{s}$ ); (b) Switching time Non-ideal switch ( $2.01 \mu\text{s}$ ).

## Temperature

To check the temperature of the system and its components, the PBIMS was encapsulated inside an isolated box with the purpose of stressing the temperature limits. The PBIMS was in operation with a 28 V supply power during 3 hours in this condition. There were no interruptions due to overheating during the test. The temperatures measured on the components of the PBIMS immediately after the box was opened were: Boost converter ( $84^\circ\text{C}$ ), Buck converters 5 V and 12 V ( $73^\circ\text{C}$ ), Buck converters 6 V and 24 V ( $67^\circ\text{C}$ ), MCU ( $53^\circ\text{C}$ ), Inner board ( $63^\circ\text{C}$ ), and Outer board ( $37^\circ\text{C}$ ). All the temperatures were within the range of operation of each component.

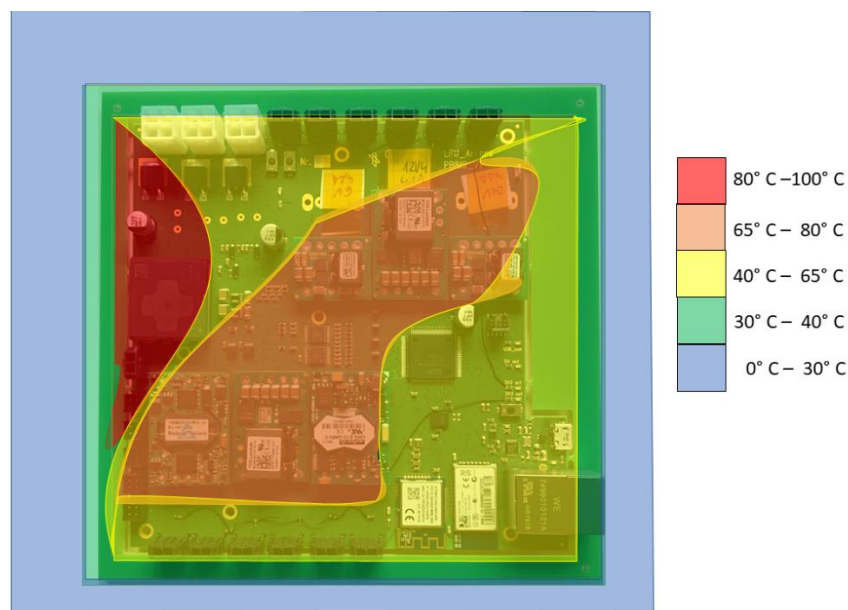
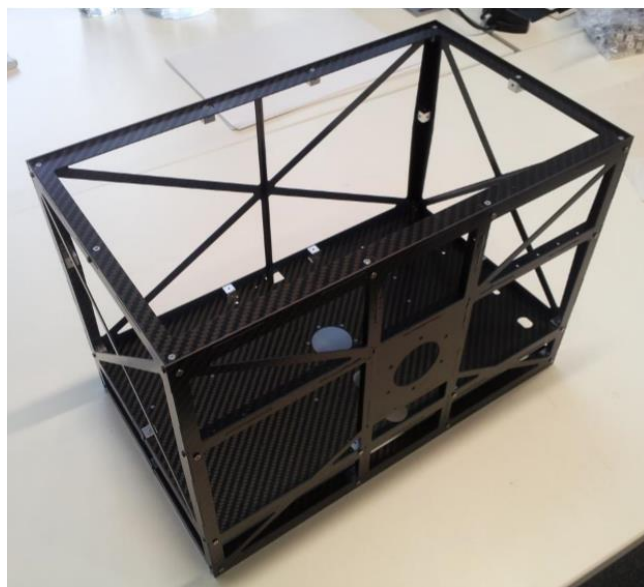


Figure 87– Temperature Diagram over the PBIMS.

### 5.1.3 Payload Modules

The standard payload module manufactured in carbon fiber had a quality check for dimensions, weight and volume. Afterwards, a drop test was performed to understand how robust the box is considering situations that could happen during the demonstration mission on Mount Etna.



*Figure 88 – Standard Payload Module Frame.*

#### Dimensions, Weight and Volume

The payload box had the following measurements presented on Table 10:

*Table 10 – Payload Module Frame Dimensions, Weight and Volume*

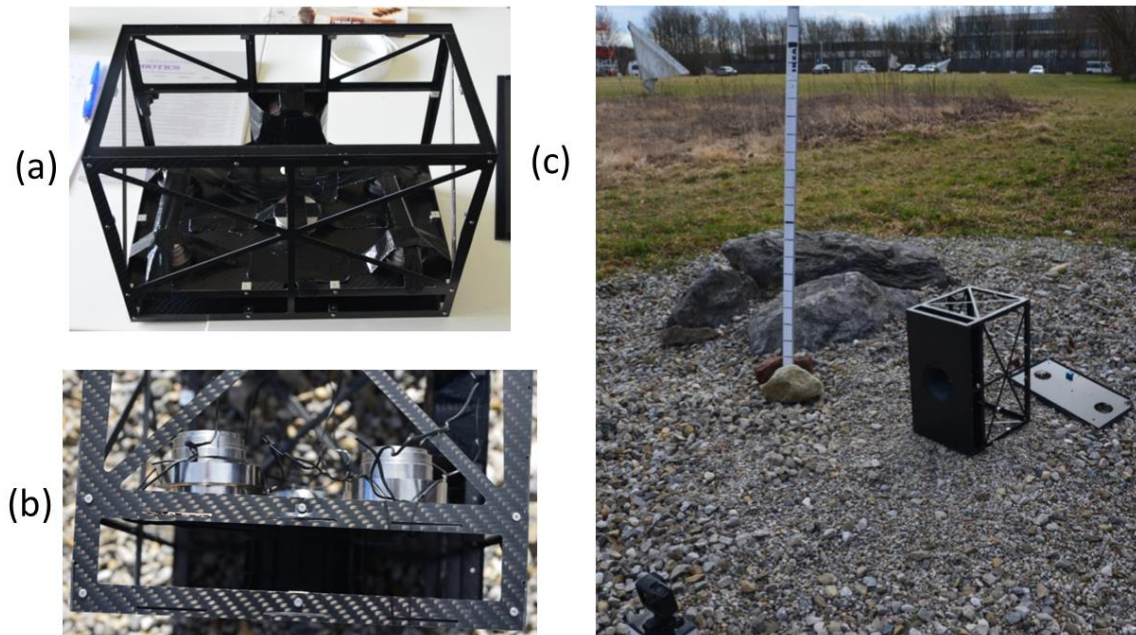
	Dimensions (mm x mm x mm)	Weight (kg)	Volume ( $dm^3$ )
Payload Module Frame	340 x 200 x 237	0.54	16.1

The dimensions consider a tolerance of 0.5 mm. The weight allows for 2.4 kg of scientific payload, batteries, electronics and connectors. The total volume is 16.1  $dm^3$ , of which 3  $dm^3$  are dedicated to electronics and internal battery and 13.1  $dm^3$  to scientific instruments or basic infrastructure components.

#### Drop Test

The drop test was carried out four times with heights of 0.5 m and 1.0 m. This considers the height limitation which the LRU-2 arm can reach and the height of the Mockup Lander where the

payload modules will be placed. To represent the scientific instruments, batteries and electronics inside the box, a load of 2.4 Kg was attached to the parts of the payload module.



*Figure 89 – Payload Module Drop Test. (a) 2.4 kg Load attached to the box; (b) Minor damages after four drops; (c) Field with medium grain gravel where the test was performed.*

After the test, it was observed minor damages on the box which do not compromise the whole structure. Therefore, it passed in the mechanical resistance test.

## 5.2 Software Testing

This section introduces the tests performed at the component level with the focus on the software architecture. They were carried out with the intention of checking the functionality of each component without considering the entire system. The procedure and results are described next.

### 5.2.1 Power Buses and Switches Activation Test

This test had the purpose of checking the accurate activation of the power buses and the FET switches. The C code was developed in NXP MCUXpresso environment and after debugging, it is possible to see the activation of BUS1\_EN and the Switches 1 and 2 (BUS1\_SW1 and BUS1\_SW2) as illustrated in the following figures:

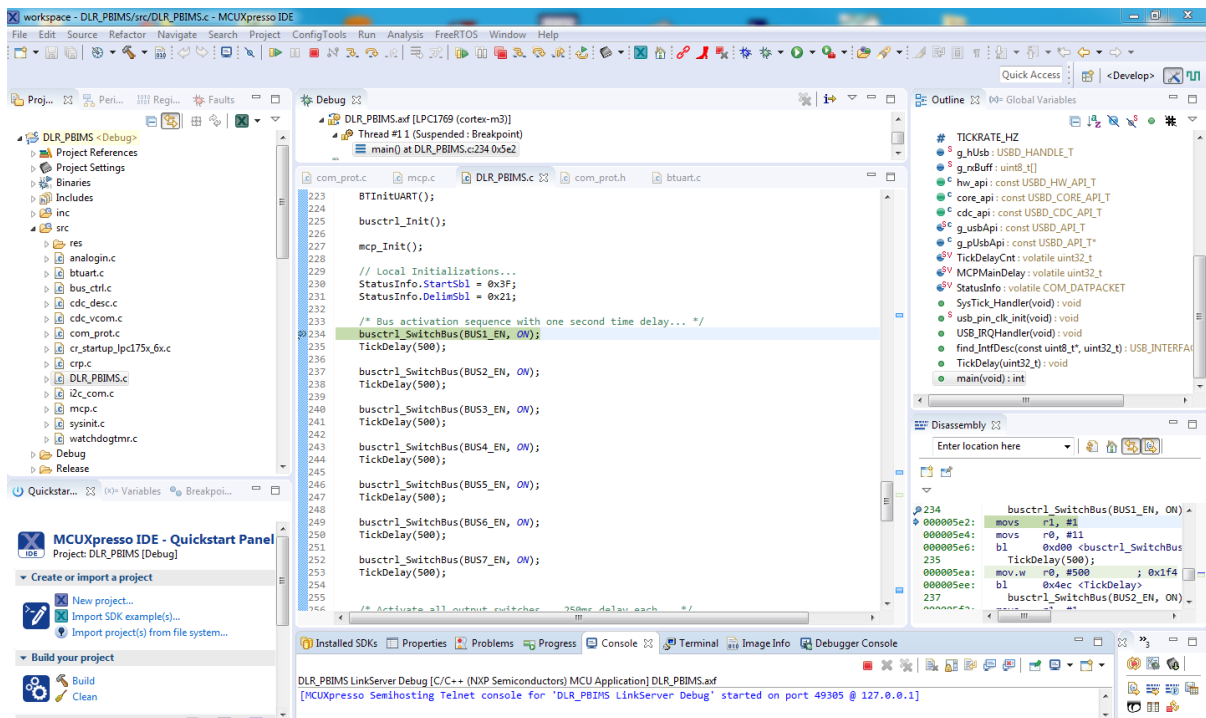


Figure 90 – NXP MCUXpresso BUS1\_EN enabling

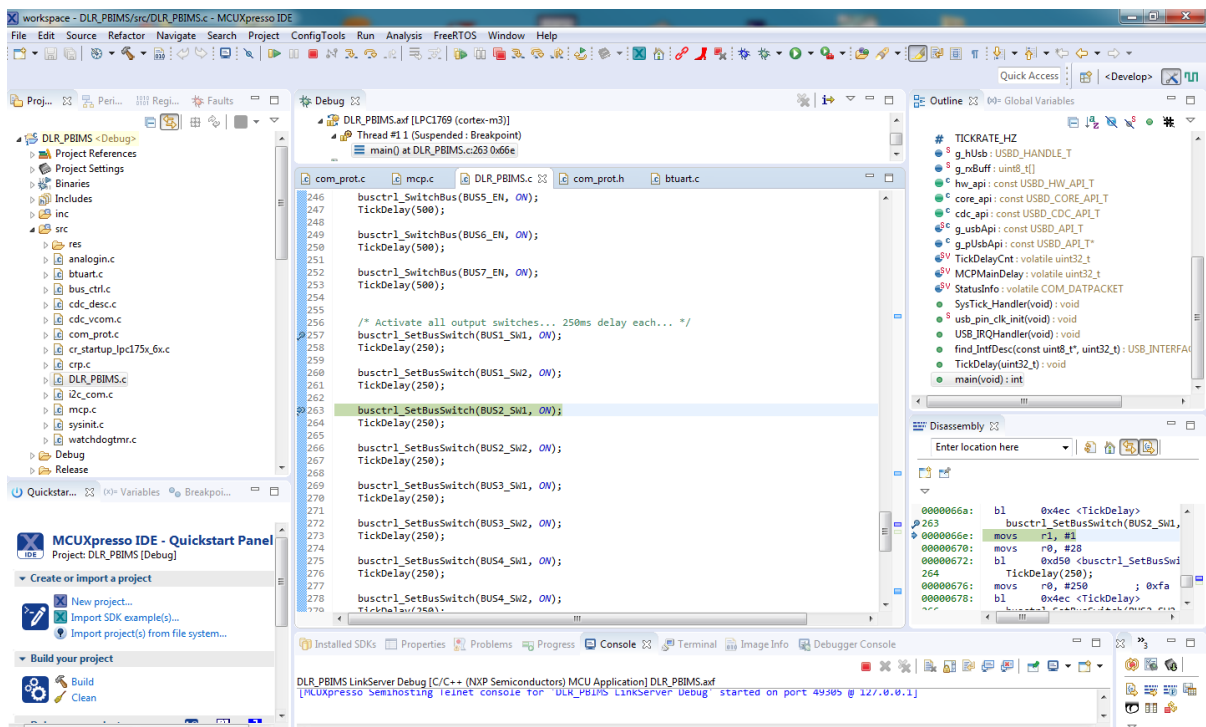


Figure 91 – NXP MCUXpresso BUS1\_SW1 and BUS1\_SW2 enabling

With the connection of the PBIMS to an oscilloscope it is possible to observe in figure 92 the voltage level increasing from 0 V to 24 V for BUS1 (channel 1 – yellow). In figure 93, the FET switches 1 (channel 1 – yellow) and 2 (channel 2 – blue) are activated with approximately 250 ms delay.

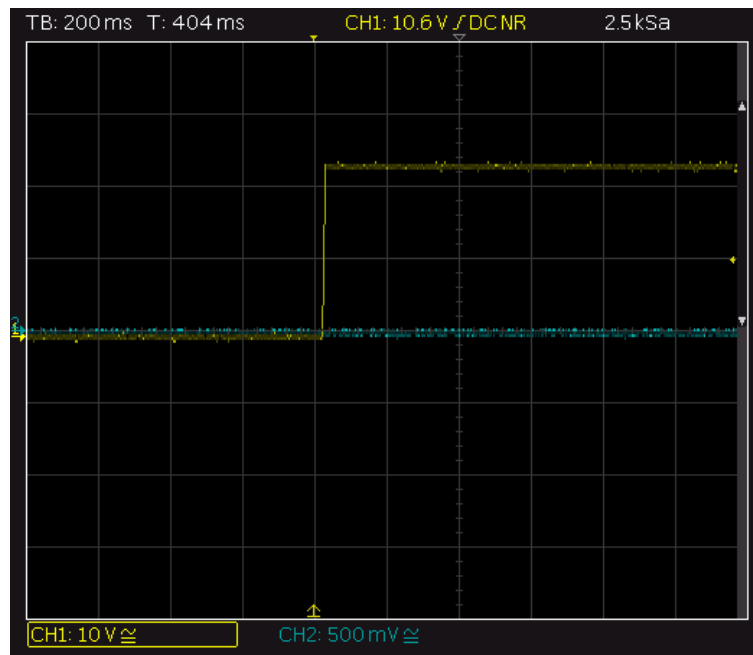


Figure 92 – Oscilloscope measurement after BUS1 (24V) is activated.

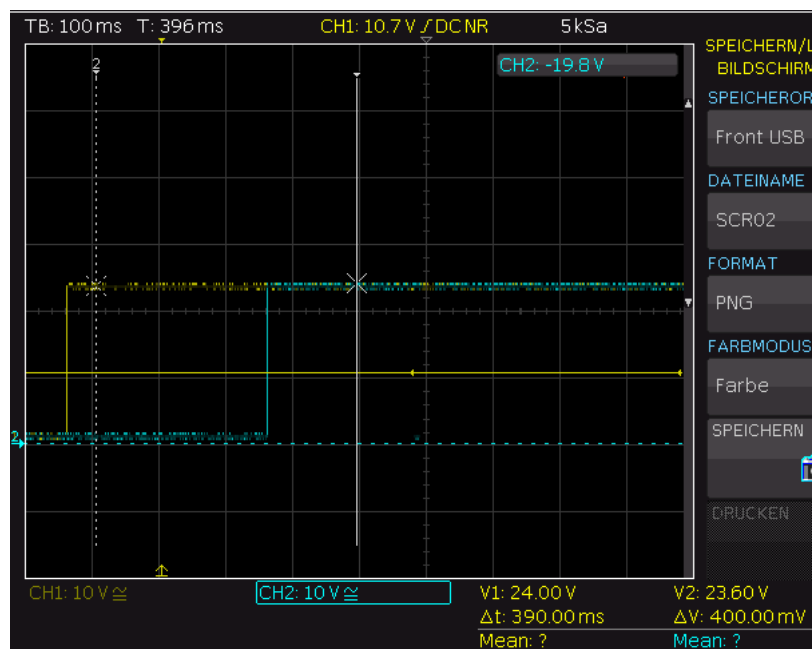


Figure 93 – Oscilloscope measurement after BUS1\_SW1 and BUS1SW2 are activated with 300 ms delay.

In conclusion, the functions `busctrl_SwitchBus()` and `busctrl_SetBusSwitch()` are working as expected. The seven power buses and the fourteen FET switches can be enabled and disabled through the activation of GPIOs in the MCU.

## 5.2.2 Communication Network Test

The Communication Network Test was carried out implementing the C Code from the NXP MCUXpresso in the MCU on the PBIMS. As explained in the subsection 4.3, the data from the MCU will be gathered in a buffer before it is transmitted or received through the communication

network (Bluetooth, Wi-fi, Ethernet, USB). For this, the source file *com\_prot.c* will handle the data in a First-In-First-Out (FIFO) fashion. The maximum capacity of the buffer is 512 messages of 16 bits. The input command handler function inside the source file of the communication network will call the command handler function of the *com\_prot.c* and send the data if it is available via the communication network. In figure 94, it is possible to see how it is set for the Bluetooth communication.

```

144 //
145 // void BTCommHndlr(void)
146 //
147 // @brief Bluetooth UART input command handler
148 //
149 void BTCommHndlr(void)
150 {
151
152     cpvt_CommHndlr(&rxring, &BtMsgBuf);           // Call com_prot-handler with BT-data...
153     cpvt_SendMsgBuff(&BtMsgBuf, PORT_BTCOM, LPC_UART1); // Send via BT if data are available
154
155 }
156

```

Figure 94 – Bluetooth input command handler calling the *com\_prot* handler.

For checking the communication, the open source software HTerm 0.8.1beta was used to simulate the external user. Following the activation of the GPIOs to control the power buses and FET switches, with this test the user can send the commands and get a feedback of the status of each power bus via Bluetooth. This process is shown in the following figure:

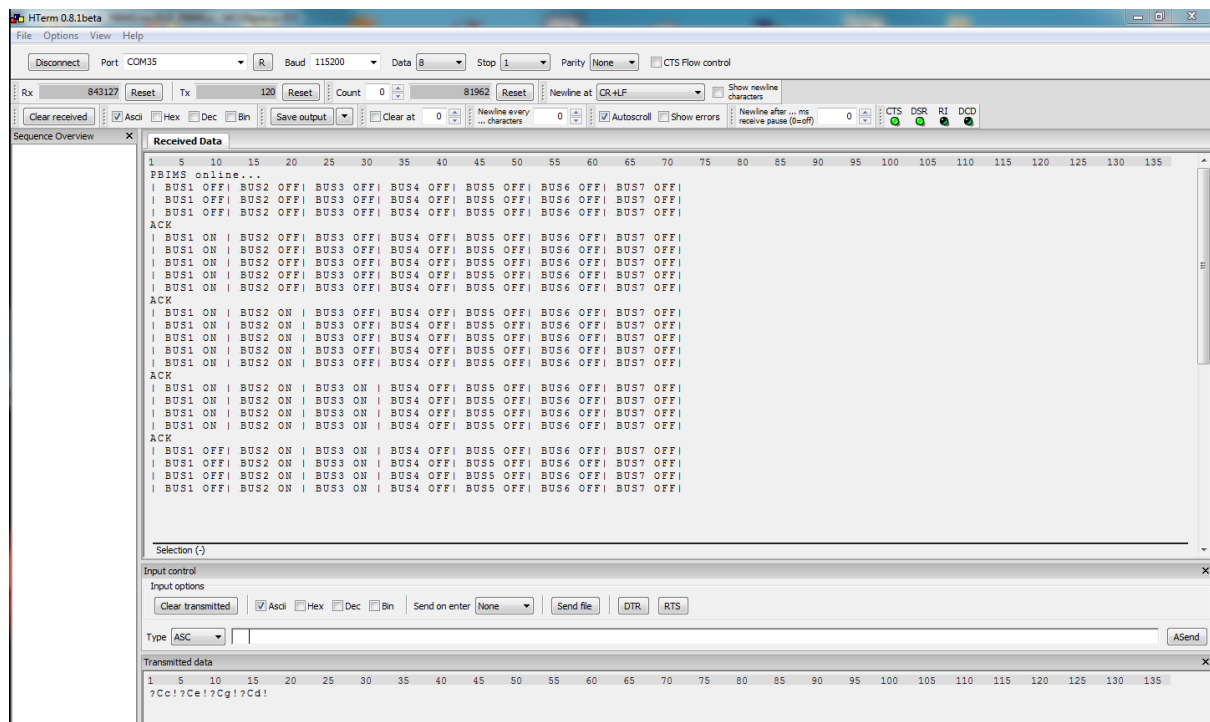


Figure 95 – HTerm window with transmission of commands and reception of status via Bluetooth communication.

It can be observed that in the command *Input control* and *Transmitted data* window the commands “?Cc!”, “?Ce!”, and “?Cg!” turned BUS1, BUS2 and BUS3 on. Then, command “?Cd!” turned BUS1 off. The feedback of the operation is seen in the *Received Data* window. The commands sent were defined in the header file *com\_prot.h* and can be seen in the figure 96.

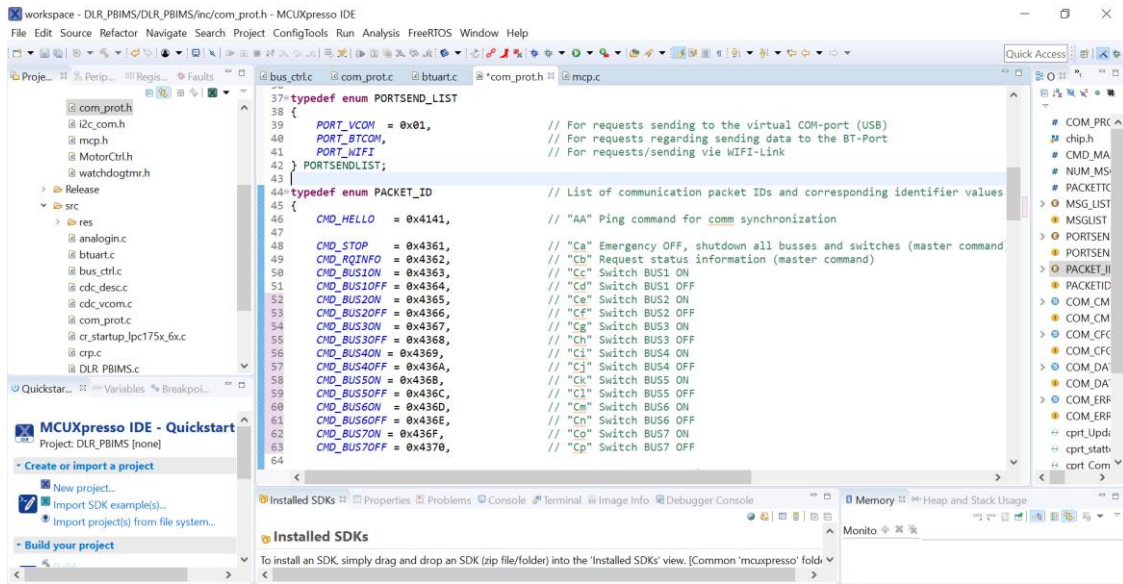


Figure 96 – Header file *com\_prot.h* with the definitions of commands.

The command includes a start symbol "?", the PACKETID, parameters, and the end symbol "!" as illustrated in the following figure.

```
103=typedef struct COM_CMDPACKET           // The command packet is defined to be of fixed size, containing an identifier
104 {
105     char StartSbl;                       // Packet start symbol, defined as "?"
106     uint16_t PacketID;                   // Packet ID contains PACKETIDS-value
107     uint16_t Param;                      // Parameters, 2x 16bit
108     char DelimSbl;                       // Packet end symbol, defined as "!"
109 } COM_CMDPACKET;
```

Figure 97 – The structure of the command packet.

The result of the activation and deactivation of the power buses can be confirmed with the oscilloscope measurements of the BUS1(24 V), BUS2 (12 V) and BUS3 (5 V) as follows:

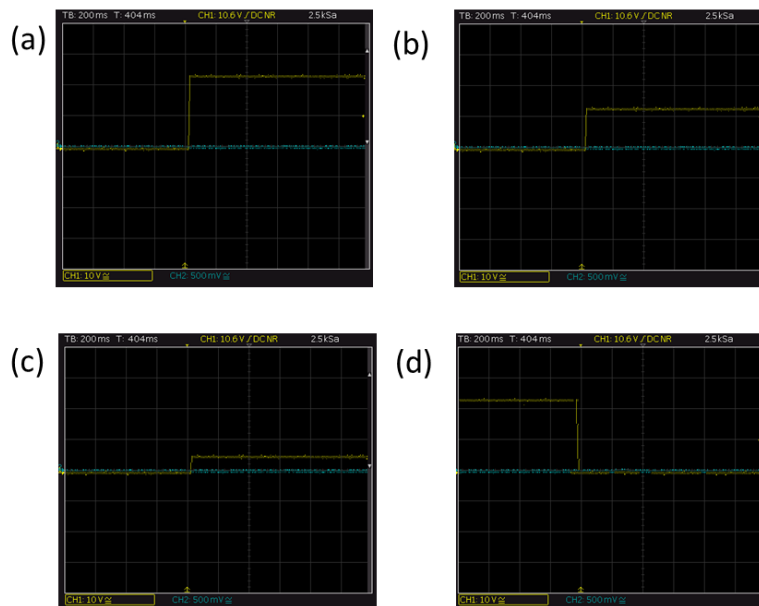


Figure 98 – Oscilloscope measurements of BUS1, BUS2 and BUS3. (a) BUS1 (24 V) is ON; (b) BUS2 (12 V) is ON; (c) BUS3 (5 V) is ON; (d) BUS1(24 V) is OFF.

In conclusion, this test demonstrated the accurate working of the data handling using the buffer and the communication network. Commands can be sent by the user and then the status of the buses can be verified.

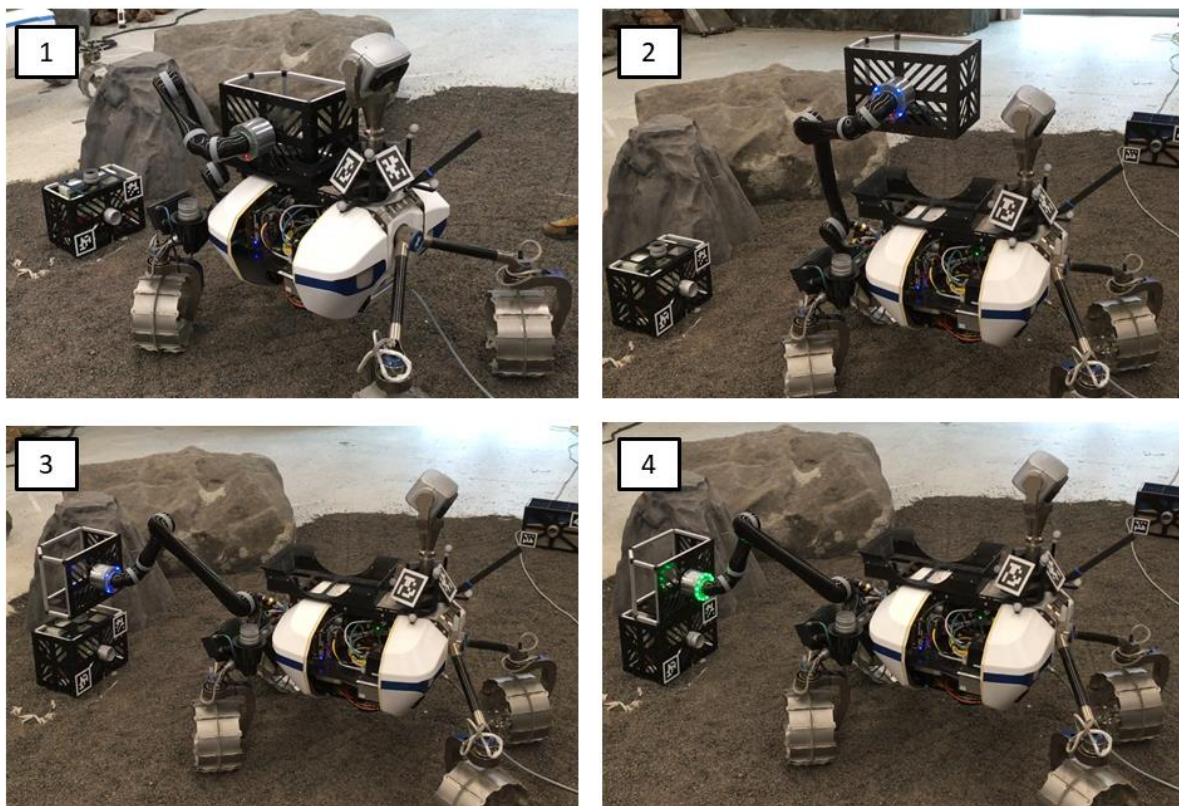
### 5.3 System Integration and Testing

This section shows the tests performed at the system level for both hardware and software elements. This is one step forward in the V-shaped model and aims for the functionality across the components of the MI. Ultimately, this has the purpose of validating the integration of all parts of the MI as a system. The procedure and results are explained as follows.

#### 5.3.1 Electrical and Mechanical Interface Test between Payload Modules

As explained previously, payload modules can be stacked on top of each other through the presence of docking interfaces on their top and bottom surfaces. This process is done with the use of the robotic arm which has inaccuracies in its Tool Center Point (TCP). This imprecision of the arm can lead to an offset of up to 20 mm.

The docking sequence occurs with the LRU-2 using its robotic arm to reach the payload box located on the storage platform (1), taking it (2, 3) until the top of the module placed on the ground, and stacking upper and lower boxes (4).



*Figure 99 - Docking sequence with LRU-2, robotic arm, and payload boxes.*

For the Mechanical test, two parameters were tested: the offset distance from the center of alignment of the docking interfaces and the angle between them. The purpose was to find the limit values for these two parameters in which the docking occurs with reliability.

For the distance offset, a millimeter grid was used on the ground and the lower box was shifted in the x-axis and in the y-axis. The docking was carried out 10 times in each position and the results are presented as follows:

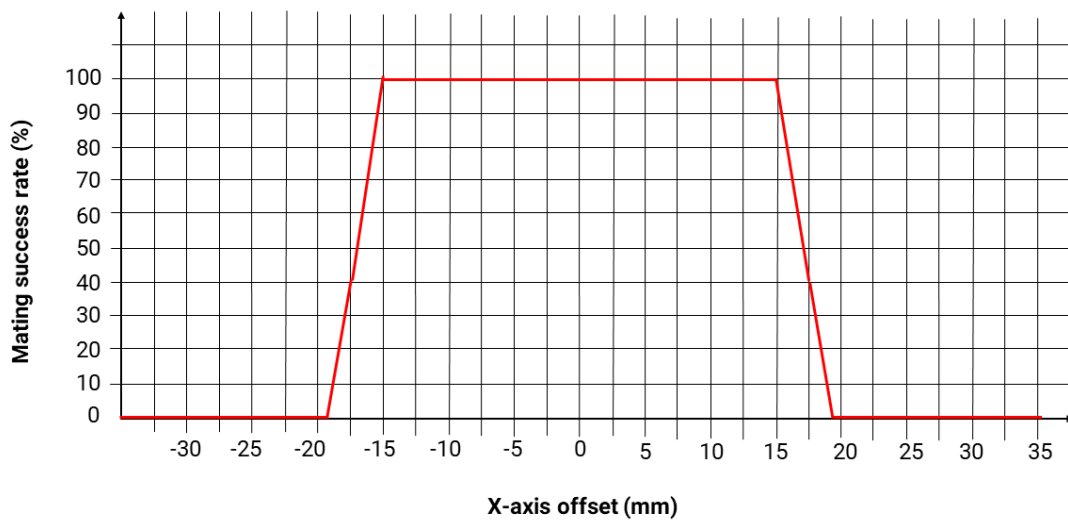


Figure 100 - Mating success rate (%) with the offset distance (mm) in the x-axis.

As observed, the mating was successful 100 % of the time with 15 mm. Therefore, this is considered a reliable threshold. With distances beyond this limit, the reliability drops to 40 % at 17.5 mm and 0 % at 19 mm.

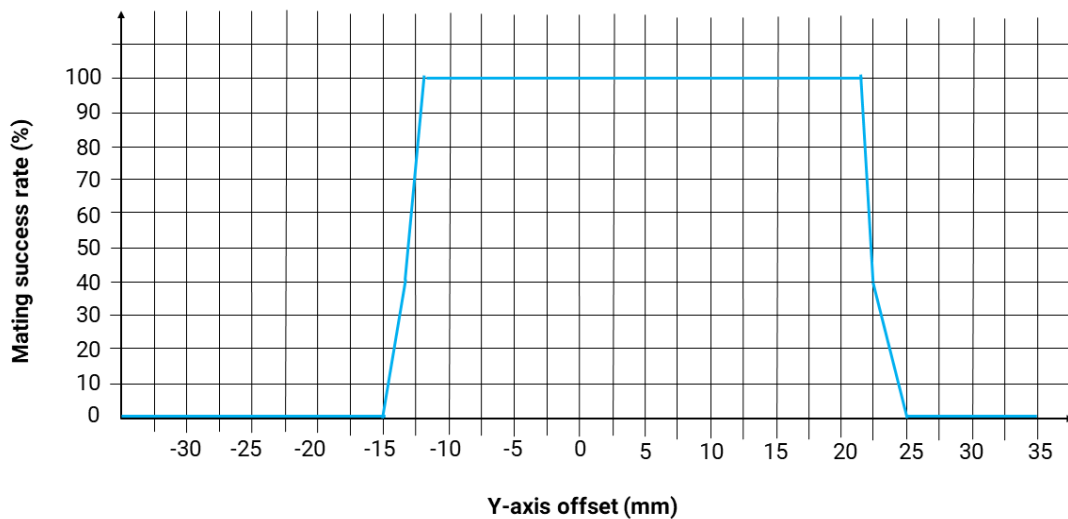
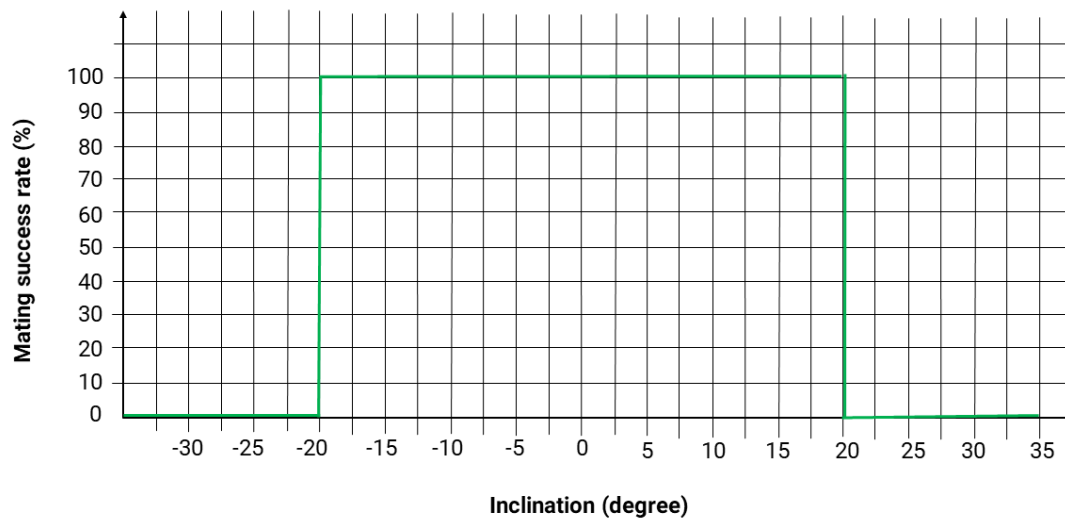


Figure 101 - Mating success rate (%) with the offset distance in the y-axis.

As shown, the mating was successful 100 % of the time with -12 mm and +22 mm. This difference occurs because of the presence of the docking interface in this axis. While on the positive side the forces applied by the robotic arm create a momentum which helps the mating process, on the negative side the momentum is not enough to do the same. These measured values are considered the reliable thresholds. With distances beyond these limits, the reliability decreases to 40 % at -13 mm and + 22.5 mm, and 0 % at -15mm and + 25 mm.

For the angle between docking interfaces, a digital inclinometer was attached on the top box and simulated angles from 0 to 20 degrees were set. The docking was carried out 10 times in each inclination and the result is as follows:



*Figure 102 - Mating success rate (%) with inclination of top box in relation to the ground (degree).*

As it is possible to see, the reliable limit is 20 degrees. Also, it was noticed that beyond these values the edge of the upper box touches the edge of the lower box before the connectors meet each other. Therefore, the effect of the geometry of the connector is lost. Higher inclination values are not considered a concern during the operation because the LRU has a driving limitation for 10 degrees slopes which implies that the situation with angles higher than 20 degrees might not occur.

For the Electrical test, the parameters tested were resistance, current and voltage levels. The resistance measured for each contact was as follows:

Table 11 – Resistance values for EIC during Integration.

EIC	Stack1 Resist. ( $\Omega$ )	Stack2 Resist. ( $\Omega$ )	Stack3 Resist. ( $\Omega$ )	Stack4 Resist. ( $\Omega$ )
Male Connector	0.35	0.59	0.40	0.45
Female Connector	0.39	0.43	0.57	0.49

In this situation with two payload modules to be docked to each other, the EIC has four stacks. The resistance values around 0.5  $\Omega$  is consistent with the measurements already presented in the subsection 5.1.1.

With a battery pack in the lower payload box and the PBIMS in the upper box, the current and voltage levels were measured in the no-load and load condition as listed in the following table:

Table 12 – Voltage and Current levels during stacking of payload modules.

Component	Condition	Power (W)	Voltage (V)	Current (A)
Battery Box 1	No-load	0.3	29.3	0.01
EIC	No-load	0.3	29.1	0.01
Input PBIMS	No-load	0.6	29.1	0.02
Output PBIMS 1	No-load	0.2	23.94	0.01
Output PBIMS 2	No-load	0.05	5.05	0.01
Output PBIMS 1	Load	47.6	23.80	2.00
Output PBIMS 2	Load	3.8	5.03	0.75

### 5.3.2 Electrical and Mechanical Interface Test between Robotic End-Effector and Payload Modules

For this test, two situations were considered: the docking of the robotic end-effector to the LIBS payload box and the connection of the end-effector to the KIT hand tool.

#### Robotic end-effector to LIBS

Concerning the integration between the LIBS payload box and the robotic end-effector, the Active Female Interface (AFI), the male and female Electrical Interface Connector (EIC), and the LIBS payload module were utilized. The male EIC was integrated to the AFI while the female EIC was incorporated to the PMMI on payload box. The mechanical integration occurred with no issues and the payload box was connected to the robotic end-effector accurately. The electrical test was performed through the interfaces with the PBIMS and a load inside the LIBS payload box. The results of the electrical measurements are presented on Table 13:

Table 13 – Electrical Measurements LIBS payload box integration with robotic end-effector.

Component	Condition	Power (W)	Voltage (V)	Current (A)
LRU-2 End-Effector	No-load	0.3	28.2	0.01
EIC	No-load	0.3	28.15	0.01
Input PBIMS	No-load	0.6	28.15	0.02
Output PBIMS 1	No-load	0.5	50.2	0.01
Output PBIMS 2	No-load	0.05	5.05	0.01
Output PBIMS 1	Load	72.5	48.3	1.5
Output PBIMS 2	Load	3.8	5.03	0.75

The results show that the values in each interface are as expected after the tests of the PBIMS were performed in the subsection 5.1.2.

The sequence of the docking demonstrating how the LIBS payload box will be utilized in the field is shown as follows:

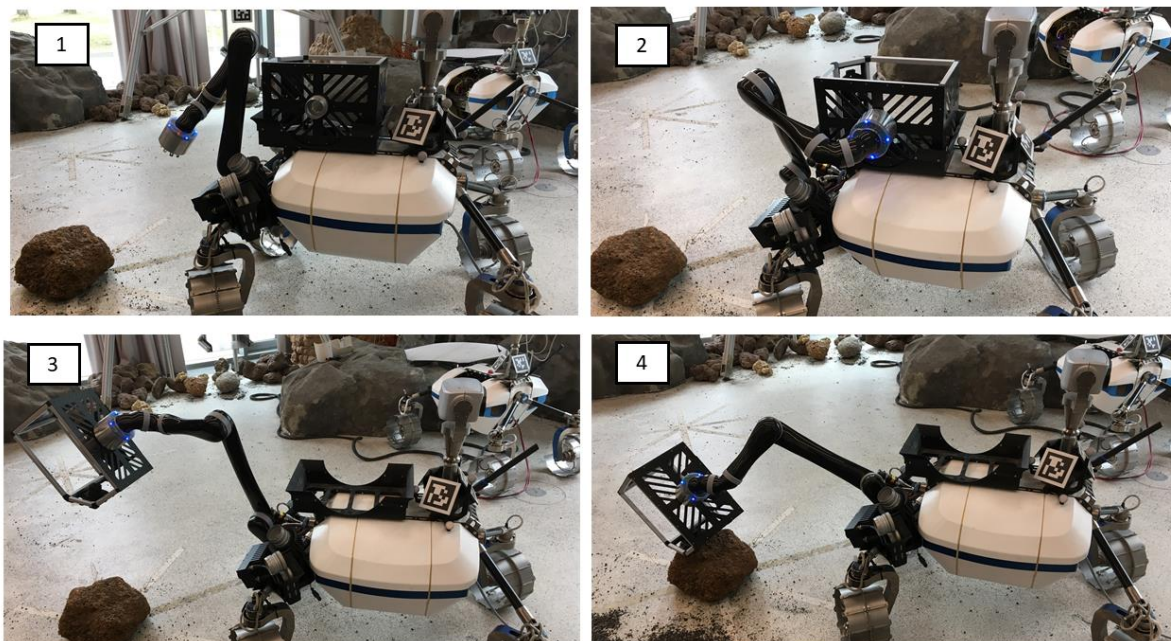


Figure 103 – LIBS payload box integrated to the robotic docking interface.

### Robotic end-effector to KIT Hand tool

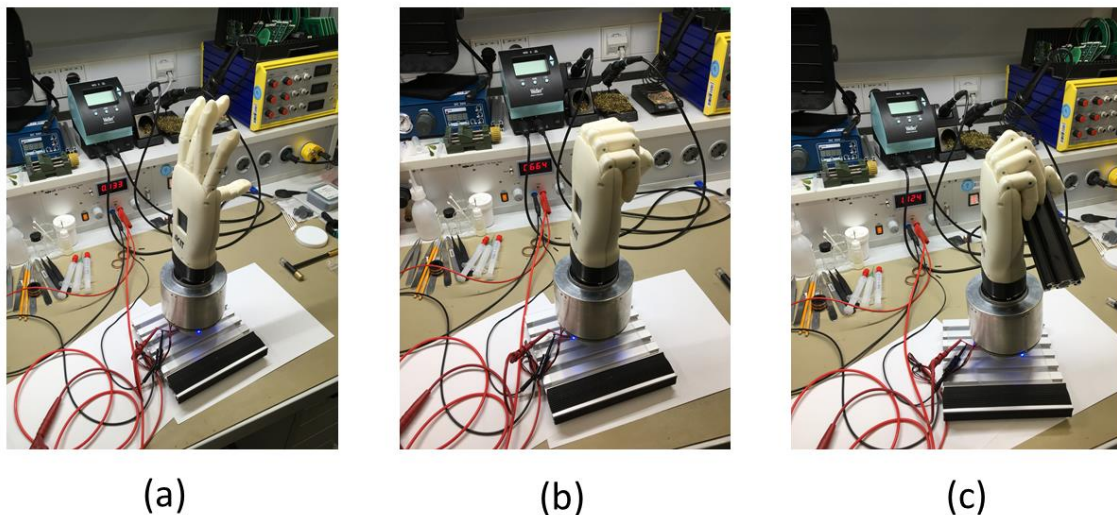
This integration test involves the Active Female Interface (AFI), the male and female Electrical Interface Connector (EIC), and the KIT Hand tool. The male EIC was integrated to the AFI while the female EIC was incorporated to the PMMI on the KIT Hand tool. The mechanical integration test was performed to check if the AFI could dock with the KIT Hand tool and this operation occurred flawless. The following test was to carry out the electrical measurements to see if the

KIT Hand would power ON and to measure the current while the hand was in operation. The KIT Hand was powered ON accurately, which means the DC-DC conversion (24 V to 12 V) occurred as expected. The results for the current values in mA with different configurations are presented on Table 14.

*Table 14 – Current Measurement for the KIT Hand Tool in operation.*

Configuration	Current Level (mA)
AFI	60
AFI docked to KIT Hand Tool	133
System with hand open	133
System with hand closed	664
System with hand grasping an object	1124

As can be observed, the maximum current measured when the KIT Hand has its motors providing a high torque for the grasping movement is 1.13 A which is below the limit of 2.5 A for the EIC with only three contacts. The temperature of the contacts was measured after the operation and it was around 24° C which cannot cause any problem to the plastic manufactured parts. The communication to operate the hand with Bluetooth was executed with simple ASCII commands. The sequence of the operation of the KIT hand tool docked is illustrated as follows:



*Figure 104 – KIT Hand Tool integrated to the robotic docking interface. (a) Hand open; (b) Hand closed; (c) Hand grasping object.*

As presented, it is possible to see that the power conversion occurred as expected and the stability of the current and voltage levels are adequate.

### 5.3.3 PBIMS with Scientific Instruments

For this integration test, the parameters tested were voltage and current levels to each specific load, and the activation and deactivation of the power buses.

#### Integration PBIMS to RCLOFA

The test was set up on a bench with all the hardware components connected to each other accordingly. Figure 105 shows this configuration:

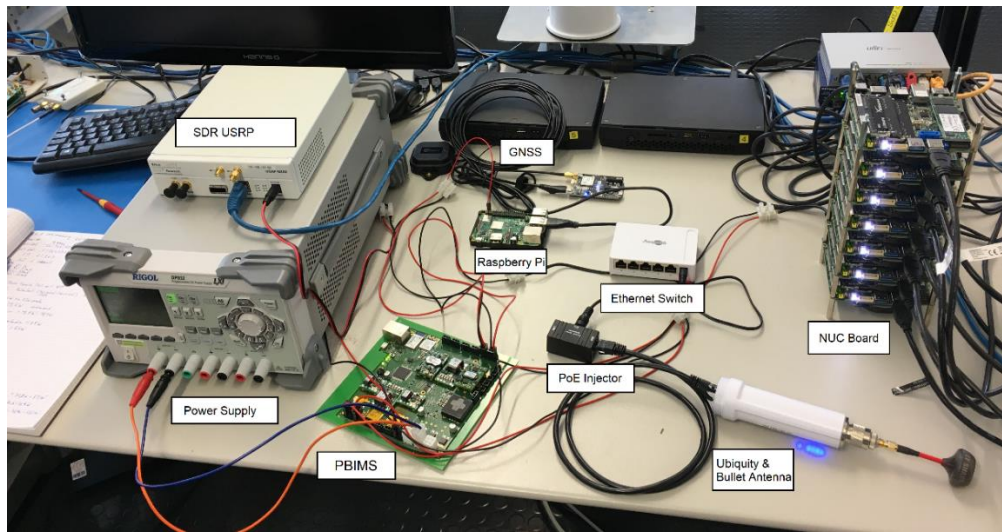


Figure 105 - Setup of the integration of the PBIMS to the RCLOFA payload box.

Table 15 – Electrical Values with RCLOFA and PBIMS setup.

Component	Power (W)	Voltage (V)	Current (A)
Only PBIMS	6	28	0.21
SDR LOFAR	16	6.11	2.61
Raspberry Pi	1.5	5.05	0.30
GNSS	0.4	5.04	0.08
Bullet Antenna	2.2	23.95	0.09
ETH Switch	0.6	5.06	0.12
ETH Cables	0.2	5.06	0.04
12 V NUC (booting)	8	12.5	0.64
12 V NUC (power saving)	5.5	12.5	0.44
12 V NUC (processing)	38	12.6	3.00
12 V NUC (idle)	8	12.5	0.64
24 V NUC (booting)	8	23.95	0.33
24 V NUC (power saving)	5.5	23.90	0.23
24 V NUC (processing)	38	24.05	1.58
24 V NUC (idle)	8	23.95	0.33

As it can be observed the total power measured was 64.9 W in the situation when the NUC is processing. Because the NUC operates between 12 - 30 V, the test was performed with both 12 V and 24 V. With 12 V the total current reaches 6.45 A while with 24 V it reaches 5 A. To keep the value close to 5 A, which is the expected operational value of the system, it was decided that the power supply channel for the NUC would be the 24 V.

Finally, similar tests to those performed in section 5.2 were performed to accurately switch ON/OFF the power buses used by the RCLOFA. Using the Bluetooth communication and HTerm 0.8.1beta in an external computer, the power buses of 5 V, 6 V, 12 V and 24 V were activated and deactivated as expected.

### Integration PBIMS to LIBS

The test was set up on a bench with all the hardware components connected to each other accordingly. Figure 106 shows this configuration:

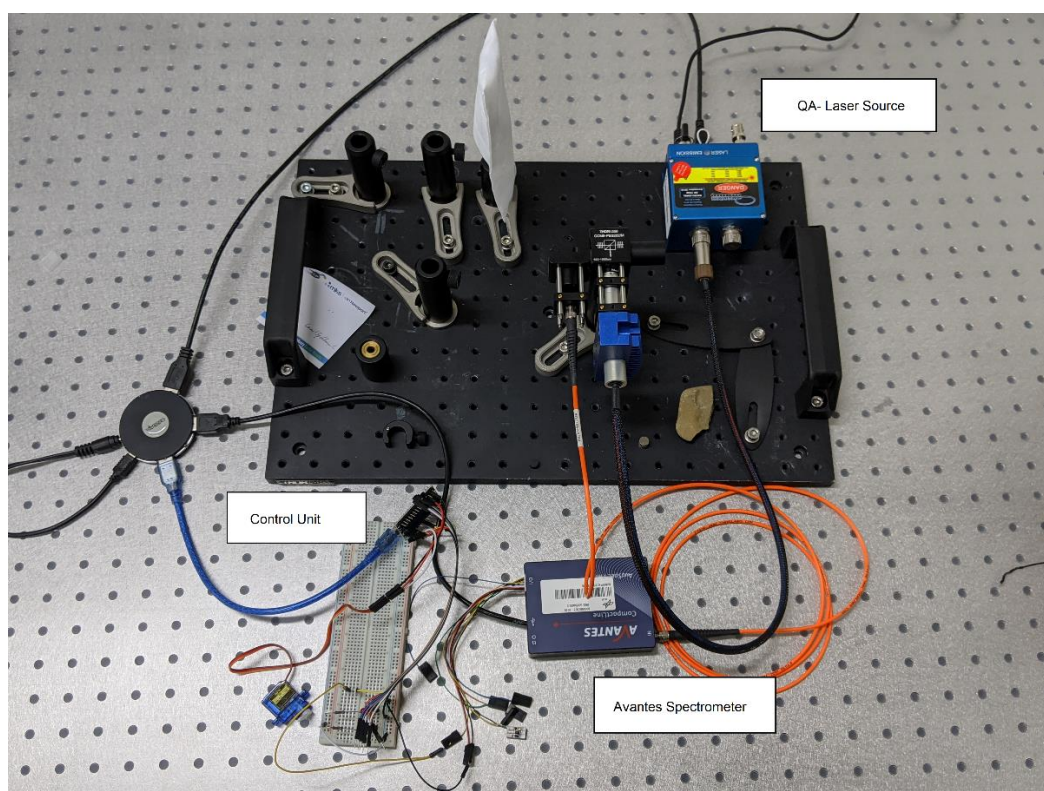


Figure 106 - Setup of the integration of the PBIMS to the LIBS payload box

Table 16 – Electrical Values with LIBS and PBIMS setup

Component	Power (W)	Voltage (V)	Current (A)
QA-Laser	70.2	48.40	1.45
Control Unit	3	5.05	0.59
Avantes Spectrometer	2.8	5.10	0.55
WebCam	2.7	5.05	0.53

As it can be seen the total power measured is 78.7 W when the QA-Laser is operating. Because the laser shooting is an operation which takes about 2 seconds, this power value will not be seen very often. However, the system is designed to withstand this threshold. The total current is 3.12 A in this limit situation.

One of the requirements of the OS Institute was to design a circuit that could support current peaks of 1.3 A in the frequency of 10 Hz when the laser source is shooting (a). This situation was simulated with a switch in the frequency of 9.5 Hz and with maximum peaks of 1.5 A (b). This is represented in the figure X, where it is possible to notice that in a sequence of 10 peaks (C3 – blue), the output voltage drops (C1 – yellow) by 2V (from 50 V to 48 V), which is less than the 5% tolerance acceptable.

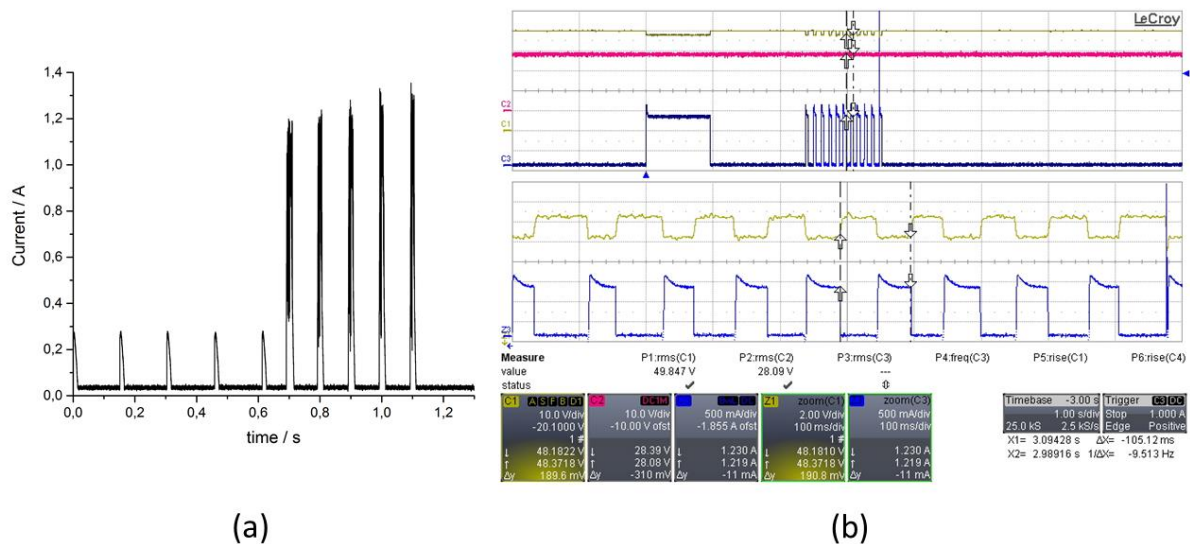


Figure 107 – Simulated series of current peaks. (a) OS laser real shooting; (b) Oscilloscope screen of simulated laser shooting at 9.5 Hz frequency.

Finally, similar tests to those performed in section 5.2 were also performed to accurately switch ON/OFF the power buses used by the LIBS system. Using the Bluetooth communication and HTerm 0.8.1beta in an external computer, the power buses of 5 V and 48 V were activated and deactivated without the presence of nonconformities.

### 5.3.4 PBIMS with Power Sources

For this interface test, the following parameters were tested: Voltage levels, current levels, and priority according to the availability of different power sources.

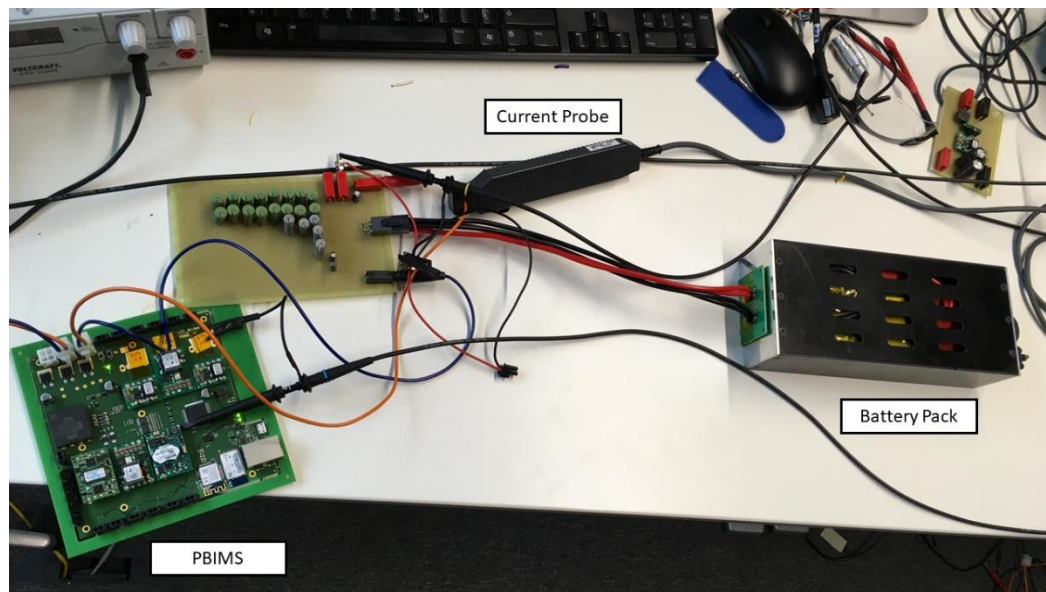


Figure 108 – Setup PBIMS with Battery Pack and DC Power Supply Unit.

First, the PBIMS was connected to each power source individually in no-load condition. The voltage and current levels were measured and recorded as shown on table 17:

Table 17 – Electrical Values with Power Sources and PBIMS setup

Power Sources	Voltage Level (V)	Current Level (A)
DC Power Supply Unit (V1)	26.5	0.005
Battery Pack (V2)	29.6	0.5

Then, the PBIMS was tested when more than one power source was available. In this case, the power sources were the DC power supply unit represented by C3 (blue) and the battery pack by C2 (pink). The output voltage (C1 – yellow signal), initially indicates 26.5 V which was the value

of the highest priority power source (V1- DC power supply). Then, when the value of V1 is lowered to 23.31 V (outside UV/OV window), the battery pack (V2) takes the priority and the value of the output voltage measured is 29.6 V. The transition between the two different power sources happens flawlessly and the functionality of the PPC was checked in a system context. The results of this test are presented as follows:

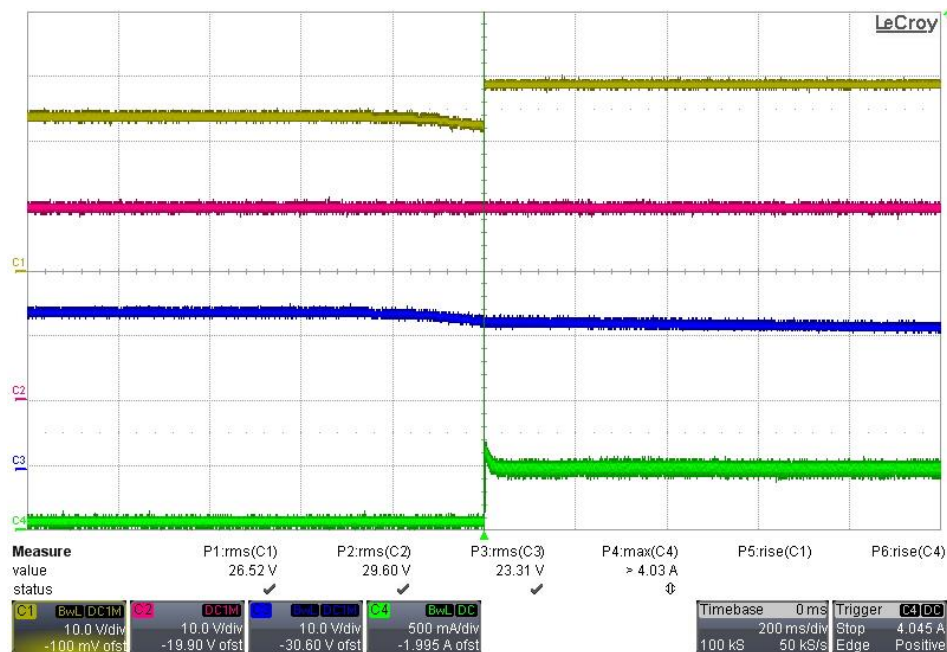


Figure 109 – Switching power between Power Supply and Battery Pack.

Besides that, the Battery Pack was connected and disconnected with the purpose of measuring the inrush current. The value measured over the FET was 32.4 A as shown in the figure 110. This was already simulated with LTspice in section 4.2.1 with a value in the same magnitude of the real measurement. C1(yellow) is the output voltage and C4 (green) is the current value.

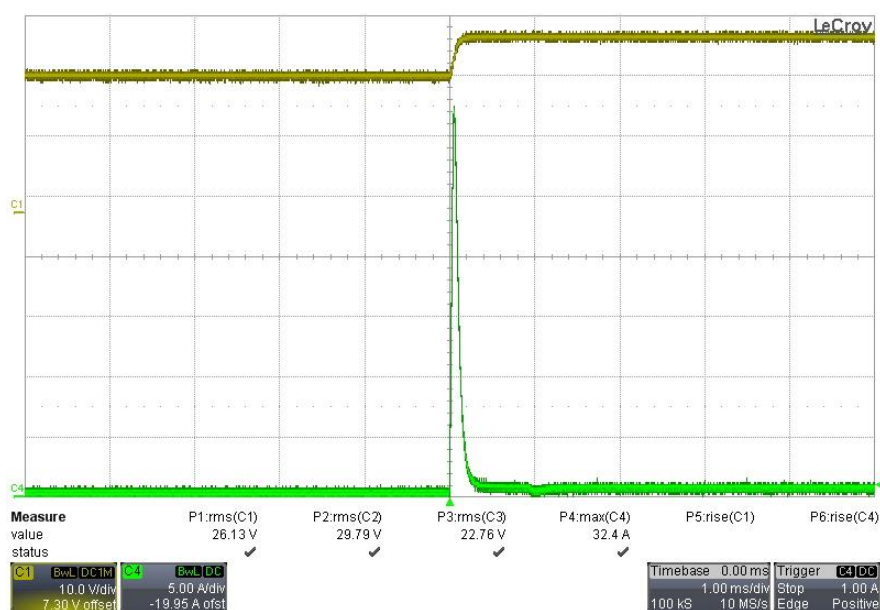


Figure 110 – Inrush current when plugging the battery pack.

## 5.4 Experimental Results

The results were presented in each section and subsection of this chapter. It was possible to see that either in the component level or the system level the measured values were within the specifications and requirements. The following table summarizes the evaluation of the entire system:

*Table 18 – Summary of Test Results*

Test	Electrical	Mechanical	Software
EIC	Pass	Pass	N/A
PBIMS	Pass	N/A	Pass
Payload Module	Pass	Pass	N/A
Software	N/A	N/A	Pass
Integration between payload boxes	Pass	Pass	N/A
Integration between arm and payload boxes	Pass	Pass	Pass
PBIMS with scientific instruments	Pass	N/A	Pass
PBIMS with power sources	Pass	N/A	Pass

The results are considered as PASS for the electrical, mechanical, software aspects for each of the tests performed. With the use of the V-Shaped Model, some adjustments were carried out during the development process, such as increasing the limits of the PPC's UV/OV window to 23.4 V – 31V or the change of the voltage for the NUC in the RCLOFA system from 12 V to 24 V. These corrections allowed the system to keep its robustness and to be more flexible to incorporate more power sources available.

It is important to remember, that all the parameters tested will be rechecked and validated during the ARCHES demonstration mission on Mount Etna in July. This will be an opportunity to get feedbacks about the system operating in the field and to have its subsystems stressed out by the extreme conditions of the volcanic environment.

## 6 Discussion and Lessons Learned

This chapter brings the analysis of the results presented in the previous chapter and the lessons learned obtained during the hardware and software development process.

### 6.1 Discussion of Results

The results obtained in Chapter 5 can be divided into three categories: Hardware Test, Software Test and System Integration and Testing. They are described as follows:

#### Hardware Test

- The Electrical Interface Connectors (EICs) had their contacts resistance measured and they were in accordance to their geometry and dimensions. They were tested with loads up to 2 A and the temperature was measured during three continuous hours. There were no occurrences of temperature rising which would melt the POM structure or damage additional parts connected to the EIC.
- The PBIMS was tested to check its main functionalities. The DC-DC conversions with all the planned power buses (5 V, 6 V, 12 V, 24 V, and 48 V) were successfully tested and both the voltage ripple and the output voltage measured were within their reference limits. The Power Path Control (PPC) was first tested to check the accuracy of the UV/OV window. Both upper and lower limit values were as calculated and simulated in LTspice. The correct switching among the three different power sources was then tested. The output voltage measure in the oscilloscope showed the switching respecting the priority of each power source and the UV/OV window. The third test for the PPC was the measurement of switching time between the power sources and for that an ideal switch and a non-ideal switch were used. In both situations, the time of about 2  $\mu$ s was measured. This is particularly interesting because during the demonstration mission the LRU-2 will connect and disconnect its end-effector to the payload modules several times. Even with the mechanical inaccuracies of the docking process, the time to have one power source replaced by the other is fast enough to guarantee a continuous power supply to the scientific instruments. The data transferring test of the PBIMS to other components occurred flawlessly and as planned. Finally, the temperature test of the PBIMS was carried out during three uninterrupted hours with the PCB on an enclosed case, and the maximum temperature observed was in the boost converter (73° C). All the DC-DC converters can work within a temperature of 125° C and the MCU can operate in a maximum temperature of 85° C.
- The standard Payload module, after manufactured in Carbon Fiber plates, had its dimensions and weights measured. The dimensions were within the 0.5 mm reference tolerance and the total weight of the frame was as planned. The drop test was carried out with heights of 0.5 m to 1 m, respecting the limitations of the LRU-2 arm and the height of the compartments of the lander mockup. The four drops did not cause major damages in the frame, which shows that the carbon fiber mechanical resistance and the geometry of the box structure are adequate.

## Software Test

- The activation test for power buses and switches was performed with the purpose of enabling and disabling the seven power buses and fourteen FET switches present on the PBIMS. The functions *busctrl\_SwitchBus()* and *busctrl\_SetBusSwitch()* were able to activate the GPIOs in the MCU with a delay between them. The change from LOW to HIGH condition in the pin was showed with the measurements in the oscilloscope. The internal Resistance-Capacitance (RC) oscillator of the MCU creates a slight difference in delay between the C code (250 ms) and the electrical measurements (300 ms). The test demonstrated that the function of activating and deactivating dedicated pins was implemented correctly.
- The test of the communication network using a buffer for the data handling had good performance. The external computer representing the User could send commands to activate the power buses and receive the status of each of them via the Bluetooth serial communication. During the test three buses (BUS1, BUS2, and BUS3) were checked and their adequate enabling and disabling via the communication network were observed. Oscilloscope measurements were done to double check that the action was really carried out in the PBIMS. Additionally, it is important to highlight that the accurate functioning of the buffer receiving and transmitting data allows that several communication network types can be added to the infrastructure.

## System Integration Testing

- The mechanical test of the interface between payload boxes demonstrated that the docking process can occur with reliability even in the situation of linear and angular misalignment. The 15mm (linear) and 20 degrees (angular) limits show that the geometry of the connectors is adequate to the docking operation. If compared with the much more complex docking system of the ISS which has 20mm (linear) and 5 degrees (angular) tolerances [97], these results are even more satisfactory.
- The electrical test of the interface between payload carriers were in accordance with the defined requirements for the PBIMS to deliver to the RCLOFA system. The battery pack on the lower box provided 29 V via the EIC and the PBIMS converted it to 5 V and 24 V with the buck regulators. No relevant voltage drop was observed with during the load condition of 2 A. The 140-mV drop is minimal and within the 5 % tolerance accepted.
- The electrical and mechanical interface test between the robotic end-effector and the LIBS payload showed that the mechanical tolerances of the interfaces allowed a perfect connection between the parts during the operation of approaching the target rock. Also, the electrical measurements of current and voltage levels were in accordance with what the PBIMS should deliver to the LIBS scientific instrument. The LRU-2 arm delivered 28 V through the EIC and the PBIMS could converted it to 48 V with the boost and 5 V with the buck converter. With a load of 1.5 A the voltage drop for the boost power bus was about 2 V which is within the 5 % tolerance accepted.

- The electrical and mechanical interface test between the robotic end-effector and the KIT Hand tool was performed without nonconformities. The mechanical integration of the KIT Hand, the EIC, the PMMI, and the AFI occurred within the mechanical tolerances of the parts. The docking process was carried out ten times and no glitches were present. The DC-DC conversion from 24 V to 12 V was accurate, and the current measured in each step of the operation of the hand reached a maximum of 1.3 A. This current seen during the operation is very safe because the maximum current as per requirement is 2.5 A. Also, the temperature was measure during the operation of the hand and it did not achieve values higher than 24° C, which is very low to be able to melt or damage the POM structure of the connector.
- The tests performed in the integration between the PBIMS and the RCLOFA system showed accurate functional performance. With all the RCLOFA components connected and the NUC processing the data from the LOFAR antenna, the maximum power observed was 65 W, which is less than the expected consumption of 80 W. The PBIMS system was design for withstanding consumptions of 80-100 W, which gives some tolerance in case some components might have higher consumption than those presented during the test. Although the NUC processing will happen for a maximum of 30 minutes in the demo mission, the test at maximum power consumption ran for three hours and no shutdowns of the system were observed. The NUC was tested with the power bus of 12 V and 24 V. After the measurements were taken, it was decided to keep the NUC operating at 24 V, so the current is lower. With this configuration, the total current of the system stays around 5 A which is the required value as per design requirements. The activation and deactivation of the power buses (5V, 6V, 12 V and 24 V) and FET switches occurred flawless as it was expected after the software was tested in the subsection 5.2.2.
- The tests performed in the integration between the PBIMS and the LIBS system demonstrated good performance. The maximum power consumption with all the LIBS components attached to the setup was 79 W. The total current measured was 3 A. These values are within the range of operation the PBIMS system. Additionally, for understanding the impact of the laser shooting to the PBMIS, a simulated series of peaks of 1.5 A at 10 Hz were performed and the maximum voltage drop in the 48 V power bus was 2 V, which is below the 5% tolerance accepted by the LIBS instrumentation. The enabling and disabling of the power buses (48 V and 5 V) and FET switches occurred with no issues.
- The tests carried out in the integration between the PBIMS and the power sources were satisfactory. The battery packs, which are present in the interior of the LRU-2, the PS payload box and in the interior of each payload module, are an essential part of the system. The use of a battery pack identified the need of setting a wider UV/OV range for the PPC. With the resistors to set the range replaced, the switching between power sources performed accurately. One concern was the impact of the inrush current over the FETs when connecting/disconnecting to/from the power sources (batteries). This was tested and the value measured was 32 A, which is in the same magnitude of the simulated value in subsection 4.2.1 (37 A).

Finally, after having the entire development of the MI, the Modularity Qualitative Assessment, which was introduced in the subsection 2.1.6, can be applied to ARCHES. Considering the same criteria as the other robotics systems evaluated, the MI and the power management and data handling (PMDH) board were assessed as follows:

- For the ARCHES MI, all the attributes had high scores because of its very versatile features. It is highly multi-functional with five different payload carriers and three individual tools. The modularity levels go from the payload modules, to the docking interface and the internal electronics. Its docking process has high angular and linear tolerances. The power and data handling electronics board are flexible to provide several requested power buses and data communication networks.
- For the ARCHES PMDH, named PBIMS, the attributes were evaluated as high specially because of versatility and integration capability. It provides modularity in the DC-DC converters that can be easily incorporated or removed from the PCB. The power buses alternatives are 5 V, 6 V, 12 V, 15 V, 24 V and 48 V. It also offers a wide variety of data communication buses (RS-485, USB, Ethernet, Wi-Fi, Bluetooth). Actuators can be incorporated to the payload modules and controlled by the PBIMS. The software can be integrated to the external network which includes the rovers and Mission Control. In summary, the PBIMS architecture offers a versatile range of services for any scientific instrument or infrastructure component to be included to the payload carriers.

## 6.2 Lessons Learned

This study presented a roadmap in the Hardware and Software development process with the application of the Model Based Engineering (MBE) method for an autonomous multi-robot planetary exploration project. As expected, adjustments were performed during the development to adhere the result to the end goal. This led to some lessons learned listed as follows:

- The implementation of an MBE method in a research center needs to be adapted to a format that does not cease the experimental approach and creativity. In this regard, this thesis presented some flexibility in the application of the V-shaped model. When moving from one stage to another the use of low cost and agile methods contributed to the definition of few requirements during the process instead of having them all specified a priori. Few examples were prototyping with additive manufacturing for mechanical parts and use of COTS for electronic circuits.
- Not all the battery packs were available and checked in the beginning of the development. Then, during the test phase, some of the recent arrived battery packs presented output voltage of 29-30 V. This led to the change of the PPC's UV/OV window from 24-28 V to 24 -31 V. Even with all the simulations and pre-test with COTS electronics performed with the initial range, the modification was carried out quickly with the change of the resistors which set the UV/OV window. This situation could have been avoided improving the communication with the battery manufacturer.

## 7 Conclusion and Future Work

This chapter concludes the work and briefly discusses about future developments, how the system can be enhanced and how the systems can be implemented in real space applications.

### 7.1 Conclusion

In this thesis, it was presented the design, implementation, test and integration of the mechatronics infrastructure (MI) in an autonomous robotic network as part of the German Aerospace Center (DLR) ARCHES project. The hardware and software development method used was the Model-based Engineering (MBE), specifically the V-Shaped model, which ensured that all the stages of the process were always validated and tested.

In Chapter 2, existing modular robotics systems were introduced and qualitatively evaluated with the purpose of identifying potential points of improvement in their modular systems. This was crucial for the development of ARCHES MI which was designed with the intention of exploring the versatility and integration capability aspects. Additionally, some examples of modularity in small satellites were presented. Their modular internal subsystems are related to the PBIMS architecture. Then, important concepts of power system, communication system and scientific instruments were described.

In Chapter 3, the ARCHES project was presented. The robotic units were introduced, the demomission scenario explained, and its goals listed. This led to the relation of these goals and the requirements for this thesis. In an operation where manipulation and docking are key, the creation of a MI with standardized interfaces and versatile mechatronics elements collaborates to the achievement of the ARCHES objectives.

In Chapter 4, the MI design was described with focus on the descending branch of the V-shaped model. The PBIMS, the Software Architecture, the Payload Modules and Tools, and the Electromechanical Docking Interface were described. Their main components were presented with requirements, stakeholders, modeling and simulation. This contributed to the detailed design and final implementation.

In Chapter 5, the Testing and Evaluation of the MI elements were carried out. This represented the ascending branch of the V-shaped model. From hardware and software testing to system integration, the tests performed demonstrated good results. The implemented and tested modular MI paved a track for future robotic devices that can benefit from modularity.

Finally, in Chapter 6, the discussion of the results and lessons learned were presented. The results of the Hardware, Software and Integration test showed that the MI performs within the specifications of its components and according to the requirements defined by the stakeholders in the beginning and during the development. A couple of lessons learned were presented specially considering the experimental nature of the DLR Robotics and Mechatronics research center which made the V-shaped model sometimes flexible and accepted adaptations during the MI development process.

In conclusion, this work demonstrated the entire development of a modular MI and the importance of using a model-based methodology to ensure the quality of standardization and versatility of the system. With the future sustainable planetary exploration missions, long-term architectures will be built, maintained and integrated with new technologies along the time. The MI, as essential part of the modular approach, will guarantee the achievement of these visionary goals and provide access to new actors in space exploration.

## 7.2 Future Work

There are additional challenges which lie beyond the work presented in this thesis. However, it is expected that improvements and extensions may happen during the ARCHES program which goes until December 2020 or in future space robotic projects. Some of the possible future works are listed as follows:

- Implementation of the data transferring through the electrical docking interface. Although the connector has the two channels for this purpose, there is additional work with the cabling in the LRU-2 robotic arm and the configuration of the FPGA for processing the information and extend it to the ROS network.
- Incorporation of docking interfaces on the other robotic units with the purpose that they can also benefit from the MI. In particular, the Power Supply (PS) payload module that could extend their autonomy. For instance, Ardea can only fly for ten minutes before it is running out of power. If the PS payload modules are spread out on the terrain, the upgraded version of Ardea could be recharged on intermediary points without the necessity of returning to the lander. Additionally, both LRUs could extend the time they can operate, if they were equipped with a docking interface on their back and could carry an extra PS module with them. This integration would also generate modifications on the design of the robots.
- Integration of new scientific instruments in the payload carriers and to the PBIMS. This would continue to validate the versatility of the MI and create the opportunity to generate data for the development time evaluation. With additional data, more precise analysis on the impact of standardization of interfaces and modular structures could be done.
- Development of the Solar Panel Supply box. This payload module was considered in the conceptual phase of this project but left outside because of the volume of hardware to be manufactured. This box would be used to recharge the PS payload modules. This would extend the operation time of the scientific instruments and the robots.
- Automatization of the payload modules. Upgraded versions of the boxes could incorporate actuators and small motors which could release more antennas, move sensors and scientific instruments on the surroundings of the payload carrier, deploy solar panels, and even provide some mobility to the payload boxes.

- Implement the CAN hardware and software in the PBIMS. With the current scientific payloads present in ARCHES, the CAN bus was not requested. Therefore, its implementation was not carried out. However, because the PBIMS modular design allows new technologies incorporation, further development which includes the CAN implementation is planned.
- Incorporate additional sensors to the PBIMS. The PBIMS developed in this thesis has three basic sensors (IMU, Distance sensor and Temperature sensor) which were considered essential for the operation planned for the demonstration mission on Mt. Etna in July 2020. However, there might be additional sensors that could be relevant for equivalent analogue missions using new scientific instruments. The versatility of the PBIMS allows the easy integration of these new sensors.
- Upgrade the DC-DC converters for software control of duty cycle. The DC-DC converters used in the PBIMS adjust their duty cycle with the change of resistors in the circuit. This directly affects the output voltage. As there is no need for changing output voltages during the mission, the hardware implementation was considered sufficient. However, the duty cycle software control could be beneficial for future applications.
- Keep the implementation of additional Communication network. With the development of the Data Handling Buffer, the first implementation was performed with Bluetooth communication. Until the demonstration mission on Mount Etna in July, further development in the software implementation of the Wi-Fi, Ethernet and USB will be carried out.
- Expand the software architecture for the external network. The current software architecture has limited connection with the external network. It basically communicates with the scientific instruments and the LRU-2. Further development could include the additional robot units, the lander and other payload boxes. With this upgrade, all the elements of the ARCHES system could form a unique and large network.

## References

- [1] Ellery, A., *Planetary Rovers: Robotic Exploration of the Solar System*, Springer, 2016, pp. 1-2.
- [2] ISECG, *Global Exploration Roadmap*, Technical report, International Space Exploration Coordination Group, 2018.
- [3] de Concini, A. and Toth, J., *The Future of European Space Sector: How to Leverage Europe's Technological Leadership and Boost Investments for Space Ventures*, European Investment Bank, 2019.
- [4] BHO Legal, Spacetec, German Federal Ministry of Economy and Energy, *New Business Models at the Interface of the Space Industry and Digital Economy: Opportunities for Germany in a Connected World*, Executive Summary, Spacetec, 2016.
- [5] Kring, D. A., *Lunar Mobility Review*, Lunar Exploration Initiative, 2006. [pdf]. Available at: <[https://www.lpi.usra.edu/science/kring/lunar\\_exploration/briefings/lunar\\_mobility\\_review.pdf](https://www.lpi.usra.edu/science/kring/lunar_exploration/briefings/lunar_mobility_review.pdf)>. [accessed October 2019].
- [6] NASA, *Mars Curiosity Rover*, NASA Science, Mars Exploration Group, 2019. [pdf]. Available at: <<https://mars.jpl.nasa.gov/msl/spacecraft/rover/summary/>>. [accessed October 2019].
- [7] Fukuda, T. and Kawauchi, Y., *Cellular Robotic System (CEBOT) as one of the realizations of the self-organizing intelligent universal manipulator*, 1990. In: Proceedings of the 1990 IEEE International Conference on Robotic and Automation. IEEE Xplore. Vol.1, pp.662-667
- [8] Brandt, D., Christensen, D. J., and Lund, H. H., *ATRON robots: Versatility from self-reconfigurable modules*. In: International Conference on Mechatronics and Automation, IEEE, 2007. pp. 26-32. IEEE. <https://doi.org/10.1109/ICMA.2007.4303511>
- [9] Christensen, D. J., Schultz, U. P., and Stoy, K., *A distributed and morphology-independent strategy for adaptative locomotion in self reconfigurable modular robots*. Robotics and Autonomous Systems. Elsevier, 2013. p. 5.
- [10] Wilcox, B. H., Litwin, T., Biesiadecki, J., Matthews, J., Heverly, M., Morrison, J., Townsend, J., Ahmad, M., Sirota, A., and Cooper, B., *ATHLETE: a Cargo Handling and Manipulation Robot for the Moon*, Journal of Field Robotics, 2007. [pdf]. Available at: < [https://www-robotics.jpl.nasa.gov/publications/Todd\\_Litwin/athlete-jfr-2007.pdf](https://www-robotics.jpl.nasa.gov/publications/Todd_Litwin/athlete-jfr-2007.pdf) >. [accessed October 2019].
- [11] Wettergreen, D., Jonack, D., Kohanbash, D., Moreland, S., Spiker, S., Tesa, J., and Whittaker, W., *Design and Experimentation of a Rover Concept for Lunar Crater Resource Survey*, Carnegie Mellon University, 2009. [pdf]. Available at: < [https://www.ri.cmu.edu/pub\\_files/2009/1/09aiaa.scarab.pdf](https://www.ri.cmu.edu/pub_files/2009/1/09aiaa.scarab.pdf) >. [accessed October 2019].

- [12] Roehr, T. M., Cordes, F., Kirchner, F., *Reconfigurable Integrated Multi-Robot Exploration System (RIMRES): Heterogeneous Modular Reconfigurable Robots for Space Exploration*. In: Journal of Field Robotics 31, 2014, Nr. 1, pp. 3–34.
- [13] Dorsey, J. T., Collins, T. J., Moe, R. V., and Doggett, W. R., *Framework for Defining and Assessing Benefits of a Modular Assembly Design Approach for Exploration Systems*, NASA Langley Research Center and NASA Goddard Spaceflight Center, 2006. [pdf]. Available at: <<https://ntrs.nasa.gov/archive/nasa/casi.ntrs.nasa.gov/20060008661.pdf>>.[accessed October 2019].
- [14] Fukuda, T. and Nakagawa, S., *Method of Autonomous Approach, Docking and Detaching Between Cells for Dynamically Reconfigurable Robotic System CEBOT*. JSME International Journal, 1990. Vol.33, pp.263-268. [pdf]. Available at: <[https://www.jstage.jst.go.jp/article/jsmec1988/33/2/33\\_2\\_263/pdf/-char/ja](https://www.jstage.jst.go.jp/article/jsmec1988/33/2/33_2_263/pdf/-char/ja)>.[accessed October 2019].
- [15] Joergensen, M. W., Oestergaard, E. H., and Lund, H. H., *Modular ATRON: Modules for Self-Configurable Robot*, 2004. In: Proceedings of the 2004 IEEE/RSJ International Conference on Intelligent Robots and Systems. September 28 – October 2, 2004, Sendai, Japan. Vol.1, pp.2068-2073.
- [16] Stoy, K., Christensen, D. J., Brandt, D., Bordignon, M., and Schultz, U. P., *Exploit Morphology to Simplify Docking of Self-Reconfigurable Robots*, 2009. In: Asama H., Kurokawa H., Ota J., Sekiyama K. (eds) Distributed Autonomous Robotic Systems 8. Springer, Berlin, Heidelberg, pp.441-452.
- [17] Sanders, G. B., Larson, W. E., Quinn, J. W., Colaprete, A., Picard, M., and Boucher, D., *RESOLVE for Lunar Polar Ice/ Volatile Characterization Mission*, NASA Ames Research Center, NASA Johnson Space Center, and Canadian Space Agency, 2011. European Planetary Science Congress, Nantes, France, October 2011. [pdf]. Available at: <<https://ntrs.nasa.gov/archive/nasa/casi.ntrs.nasa.gov/20110014548.pdf>>.[accessed October 2019].
- [18] Brinkmann, W., Roehr, T. M., Natarajan, S., Cordes, F., Sonsalla, R. U., Szczuka, R., Bartsch, S., and Kirchner, F., *Design and Evaluation of an End-Effector for a Reconfigurable Multi-robot System for Future Planetary Missions*. DFKI-RIC, 2019. [pdf]. Available at: <[https://www.dfki.de/fileadmin/user\\_upload/import/9383\\_2019Design\\_and\\_evaluation\\_of\\_an\\_end-effector.pdf](https://www.dfki.de/fileadmin/user_upload/import/9383_2019Design_and_evaluation_of_an_end-effector.pdf)>.[accessed October 2019].
- [19] Wang, Z., Cordes, F., Dettmann, A., and Szczuka, R. *Evaluation of a Power Management System for Heterogeneous Modules in Self-Reconfigurable Multi-Module Systems*. DFKI, 2011. In: Proceedings of the 2011 IEEE/RSJ International Conference on Intelligent Robots and Systems. 25-30 September 2011. San Francisco, United States. [pdf]. Available at: <[https://www.dfki.de/fileadmin/user\\_upload/import/5524\\_110718\\_Evaluation\\_of\\_a\\_Power\\_Management\\_System\\_for\\_Heterogeneous\\_Modules\\_in\\_Self-Reconfigurable\\_Multi-Module\\_Systems\\_IROS\\_WHang.pdf](https://www.dfki.de/fileadmin/user_upload/import/5524_110718_Evaluation_of_a_Power_Management_System_for_Heterogeneous_Modules_in_Self-Reconfigurable_Multi-Module_Systems_IROS_WHang.pdf)>.[accessed October 2019].

- [20] ESA, *Technology CubeSats*, European Space Agency, 2019. [online]. Available at: <[https://www.esa.int/Enabling\\_Support/Space\\_Engineering\\_Technology/Technology\\_CubeSats](https://www.esa.int/Enabling_Support/Space_Engineering_Technology/Technology_CubeSats)>. [accessed October 2019].
- [21] Klesh, A. T. and Krajewski, J., *MarCO: CubeSats to Mars in 2016*, in: 29th Annual AIAA/USU Conference on Small Satellites, Logan, Utah, Aug 8-13, 2015.
- [22] JPL, *MarCO CubeSats*, Jet Propulsion Laboratory/NASA, 2019. [online] Available at: <[https://www.jpl.nasa.gov/news/press\\_kits/insight/assets/images/appendix/appendix\\_marco\\_02-full.jpg](https://www.jpl.nasa.gov/news/press_kits/insight/assets/images/appendix/appendix_marco_02-full.jpg)>. [accessed October 2019].
- [23] Rinaldi, R. and Cuollo, M., *CubeSat Trade-Off: The Argomoon Case*, in: iCubeSat 2018 Paris, France, Argotec, 2018. [pdf]. Available at: <<https://icubesat.files.wordpress.com/2018/05/b-1-5-201805300740-rinaldi.pdf>>. [accessed October 2019].
- [24] IRS, *Flying Laptop*, Small Satellites Program, Institute of Space Systems (IRS), University of Stuttgart. [online]. Available at: <<https://www.irs.uni-stuttgart.de/en/research/satellitetechnology-and-instruments/smallsatelliteprogram/flying-laptop/>>. [accessed October 2019].
- [25] Eickhoff, J., *A Combined Data and Power Management Infrastructure*, J. Eickhoff, Ed. Stuttgart, Germany: Springer-Verlag Berlin Heidelberg, 2013, pp. 1-25.
- [26] Eickhoff, J., *ibidem*, pp. 27-41.
- [27] Eickhoff, J., *ibidem*, pp. 151-167.
- [28] Wilson, P., and Mantooth, H. A., *Model-Based Engineering for Complex Electronic Systems: Techniques, Methods and Applications*, Oxford, United Kingdom: Elsevier Science & Technology, 2013, pp. 3-4.
- [29] Benington, H. D., *Production of Large Computer Programs*. In: Proceedings of ONR Symposium on Advanced Programming Methods for Digital Computer, June 1956, pp-15-27.
- [30] Royce, W. W., *Managing the Development of Large Software Systems*. In: Proceedings of IEEE Wescon, August 1970, pp 1-9.
- [31] Boehm, B. W., *A Spiral Model of Software Development and Enhancement*, Los Calamitos, United States: IEEE Computer, 1988, Vol.21, pp. 61–72.
- [32] Forsberg, K. and Mooz, H. The Relationship of System Engineering to the Project Cycle. 1991. In: Proceedings of the National Council on Systems Engineering (NCOSE) Conference. Chattanooga, TN. pp. 57-65.
- [33] Forsberg, K.; Mooz, H. System Engineering for Faster, Cheaper, Better. In INCOSE International Symposium; Wiley Online Library: Brighton, UK, 1999; Volume 9, pp. 924–932.
- [34] Weillkiens, T., Lamm, J., Roth, S., and Walker, M., *Model-based System Architecture*. West Sussex, England: John Wiley & Sons, 2015. pp. 343-351.

- [35] Farr, R. A., Christensen D. L. and Keith, E. L., *The Business Case for Spiral Development for Heavy-Lift Launch Vehicle Systems*, 2005, 41st AIAA/ASME/SAE/ASEE Joint Propulsion Conference & Exhibit, 10-13 July 2005 Tucson Arizona.
- [36] NASA, *Manned Space Flight: Projects Mercury and Gemini*, NASA NF- 9/VOL. II. NO. 8, 1967, pp. 9–12.
- [37] NASA, *Soyuz 5*, Nasa Space Science Data Coordinated Archive, 2019. [online]. Available at:<<https://nssdc.gsfc.nasa.gov/nmc/spacecraft/display.action?id=1969-005A>>. [ accessed October 2019].
- [38] Godwin, R. (ed.), *Rocket and Space Corporation Energia*, Ontario, Canada: Apogee Books, 2001, pp. 124.
- [39] NASA, *Skylab: America's First Space Station*, Nasa History, 2019. [online]. Available at:<<https://www.nasa.gov/feature/skylab-america-s-first-space-station>>. [accessed October 2019].
- [40] Swan, W., *The Apollo–Soyuz Test Project Docking System*, 10th Aerospace Mechanism Symposium, NASA TM 33-777, Pasadena, CA., 1976, pp. 29-36.
- [41] NASA, *Mir Space Station*, Shuttle-Mir, Nasa History, 2019. [online]. Available at:<<https://history.nasa.gov/SP-4225/mir/mir.htm>>. [accessed October 2019].
- [42] Yan, X. T., Brinkmann, W., Palazzetti, R., Melville, C., Li, Y., Bartsch, S., and Kirchner, F., *Integrated Mechanical, Thermal, Data, and Power Transfer Interfaces for Future Space Robotics*, in: Frontiers Robotics and AI, 2018. vol.5, Article 64.
- [43] Cruijssen, H., Ellenbroek, M., Henderson, M., Petersen, H., Verzijden, P., and Visser, M. The European Robotic Arm: A High-Performance Mechanism Finally on its Way to Space. Technical Report NASA, 2014.
- [44] DLR, *iBoss Modular Satellite*. DLR, TU Berlin, RWTH Aachen, FZI Karlsruhe, 2019. [online]. Available at: <[https://www.dlr.de/content/de/artikel/news/2017/20170823\\_dlr-beim-tag-der-offenen-tuer-der-bundesministerien\\_23812.html](https://www.dlr.de/content/de/artikel/news/2017/20170823_dlr-beim-tag-der-offenen-tuer-der-bundesministerien_23812.html)>. [accessed October 2019].
- [45] Tatnall, A. R. L. et al., *Spacecraft Systems Engineering*, 4th ed., Fortescue, P., Stark, J., and Swinerd, G., Eds. Chichester, West Sussex, England: John Wiley & Sons, 2011. pp.327-350.
- [46] Lempereur, V. *Electrical Power Systems*. Thales Alenia Space, Belgium, 2017. [pdf]. Available at: < [http://www.s3l.be/usr/files/di/fi/2/2017\\_EPS\\_Lempereur\\_201811271527.pdf](http://www.s3l.be/usr/files/di/fi/2/2017_EPS_Lempereur_201811271527.pdf) >. [accessed October 2019].
- [47] Renesas, *Battery Management System Tutorial White Paper*, 2018. [pdf]. Available at: <<https://www.renesas.com/eu/en/doc/whitepapers/battery-management/battery-management-system-tutorial.pdf>>. [accessed October 2019]

- [48] ANALOG, *Prioritized PPC LTC4417 Datasheet*, 2019. [pdf]. Available at: <<https://www.analog.com/media/en/technical-documentation/data-sheets/4417f.pdf>>. [accessed October 2019].
- [49] ELECTRONICS, *MOSFET as a Switch*, 2019. [online]. Available at: <[https://www.electronics-tutorials.ws/transistor/tran\\_7.html](https://www.electronics-tutorials.ws/transistor/tran_7.html)>. [accessed October 2019].
- [50] Texas Instruments, *Switching Regulator Fundamentals*, 2019. [pdf]. Available at: <<http://www.ti.com/lit/an/snva559c/snva559c.pdf>>. [accessed October 2019].
- [51] ELECTRONICS, *Pulse Width Modulation*, 2019. [online]. Available at: <<https://www.electronics-tutorials.ws/blog/pulse-width-modulation.html>>. [accessed October 2019].
- [52] MECHATRONICS, *Arduino DC Motor Control Tutorial*, 2019. [online]. Available at: <<https://howtomechatronics.com/tutorials/arduino/arduino-dc-motor-control-tutorial-l298n-pwm-h-bridge/>>. [accessed October 2019].
- [53] Irazabal, J. M., and Blozis, S., *AN10216-01: I2C Manual*, Phillips Semiconductors, 2003.
- [54] Afzal, S., *What is I2C?*, Analog Devices, 2019. [online]. Available at: <<https://www.analog.com/en/technical-articles/i2c-primer-what-is-i2c-part-1.html#>>. [accessed October 2019].
- [55] Dhaker, P., *Introduction to SPI Interface*, Analog Dialogue 52, 2018. [pdf]. Available at: <<https://www.analog.com/media/en/analog-dialogue/volume-52/number-3/introduction-to-spi-interface.pdf>>. [accessed October 2019].
- [56] Heath, S., *Embedded Systems Design*, 2nd ed., Oxford, United Kingdom: Newnes, 2003. pp.142-193.
- [57] All about Circuits, *Back to Basics: The Universal Asynchronous Receiver Transmitter UART*, 2019. [online]. Available at: <<https://www.allaboutcircuits.com/technical-articles/back-to-basics-the-universal-asynchronous-receiver-transmitter-uart/>>. [accessed October 2019].
- [58] Pfeiffer, O., Ayre, A., and Keydel, C., *Embedded Networking with CAN and CANopen*, San Clemente, United States: Copperhill Technologies Corporation, 2003. pp.203-240.
- [59] Mishra, S., Singh, N. J., and Rousseau, V., *System on Chip Interfaces for Low Power Design*, Burlington, United States: Morgan Kaufmann Publishers, 2015. pp.331-344.
- [60] Spurgeon, C., and Zimmerman, J., *Ethernet: The Definitive Guide - Designing and Managing Local Area Networks*, 2nd Ed., Surrey, United Kingdom: O'Reilly Media, 2014.
- [61] Olonewa, J., *Guide to Wireless Communications*. 3rd Ed., Boston, United States: Course Technology, 2014.
- [62] Maufer, T., *A Field Guide to Wireless LANs: For Administrators and Power Users*. Upper Saddle River, United States: Pearson Education, 2004. pp. 290-293.

- [63] Lakdawalla, E., *The Design and Engineering of Curiosity: How the Mars Rover Performs its Job*, Chichester, United Kingdom: Praxis Publishing & Springer International Publishing, 2018. pp.294-307.
- [64] NASA, *Example of a Spectrum from Curiosity's ChemCam Instrument*, 2019. [online]. Available at: <[https://www.nasa.gov/mission\\_pages/msl/multimedia/pia15104.html](https://www.nasa.gov/mission_pages/msl/multimedia/pia15104.html)>. [accessed October 2019].
- [65] Anderson, R. C., Jandura, L., Okon, A. B., Sunshine, D., Roumeliotis, C., Beegle, L. W., Hurowitz, J., Kennedy, B., Limonadi, D., McCloskey, S., Robinson, M., Seybold, C., and Brown, K. *Collecting Samples in Gale Crater, Mars; an Overview of the Mars Science Laboratory Sample Acquisition, Sample Processing, and Handling System*, Jet Propulsion Laboratory, Pasadena United States: Springer International Publishing, 2012. p.63.
- [66] University of Texas, *NASA Viking Lander Soil Sampler*, 2019. [online]. Available at: <<http://www.tsgc.utexas.edu/spacecraft/viking/sample1.html>>. [accessed October 2019].
- [67] NRAO, *What are Radio Telescopes?*, National Radio Astronomy Observatory, 2019. [online]. Available at: <<https://public.nrao.edu/telescopes/radio-telescopes/>>. [accessed October 2019].
- [68] University of Oregon, *Radio Telescope Diagram*, 2019. [online]. Available at: <[http://abyss.uoregon.edu/~js/glossary/radio\\_telescope.html](http://abyss.uoregon.edu/~js/glossary/radio_telescope.html)>. [accessed October 2019].
- [69] NASA, *ZOND-3*, Nasa Space Science Data Coordinated Archive, 2019. [online]. Available at: <<https://nssdc.gsfc.nasa.gov/nmc/spacecraft/display.action?id=1965-056A>>. [accessed October 2019].
- [70] NASA, *RAE-1*, Nasa Space Science Data Coordinated Archive, 2019. [online]. Available at: <<https://nssdc.gsfc.nasa.gov/nmc/spacecraft/display.action?id=1968-055A>>. [accessed October 2019].
- [71] Alexander, J. K., Kaiser, M. L., Novaco, J. C., Grena, F. R., and Weber, R. R., *Scientific Instrumentation of the Radio-Astronomy-Explorer-2 Satellite*, NASA Goddard Space Flight Center, in: *Astronomy and Astrophysics Journal*, vol.40, no.4, May 1975, pp.365-371.
- [72] JAXA, *HALCA*, Institute of Space and Astronautical Science, Japanese Space Agency, 2019. [online]. Available at: <<http://www.isas.jaxa.jp/en/missions/spacecraft/past/halca.html>>. [accessed October 2019].
- [73] RadioAstron, *Spektr-R*, RadioAstron Project, Russia, 2019. [online]. Available at: <<http://www.asc.rssi.ru/radioastron/index.html>>. [accessed October 2019].
- [74] ISIS, *NCLE: The Netherlands Chine Low Frequency Explorer*, 2019. [online]. Available at: <<https://www.isispace.nl/projects/ncle-the-netherlands-china-low-frequency-explorer/>>. [accessed October 2019].
- [75] van Haarlem, M.P., et al., *LOFAR: The Low-Frequency Array*, in: *Journal Astronomy & Astrophysics*, 2013. Vol.556, A2, pp.1-53.

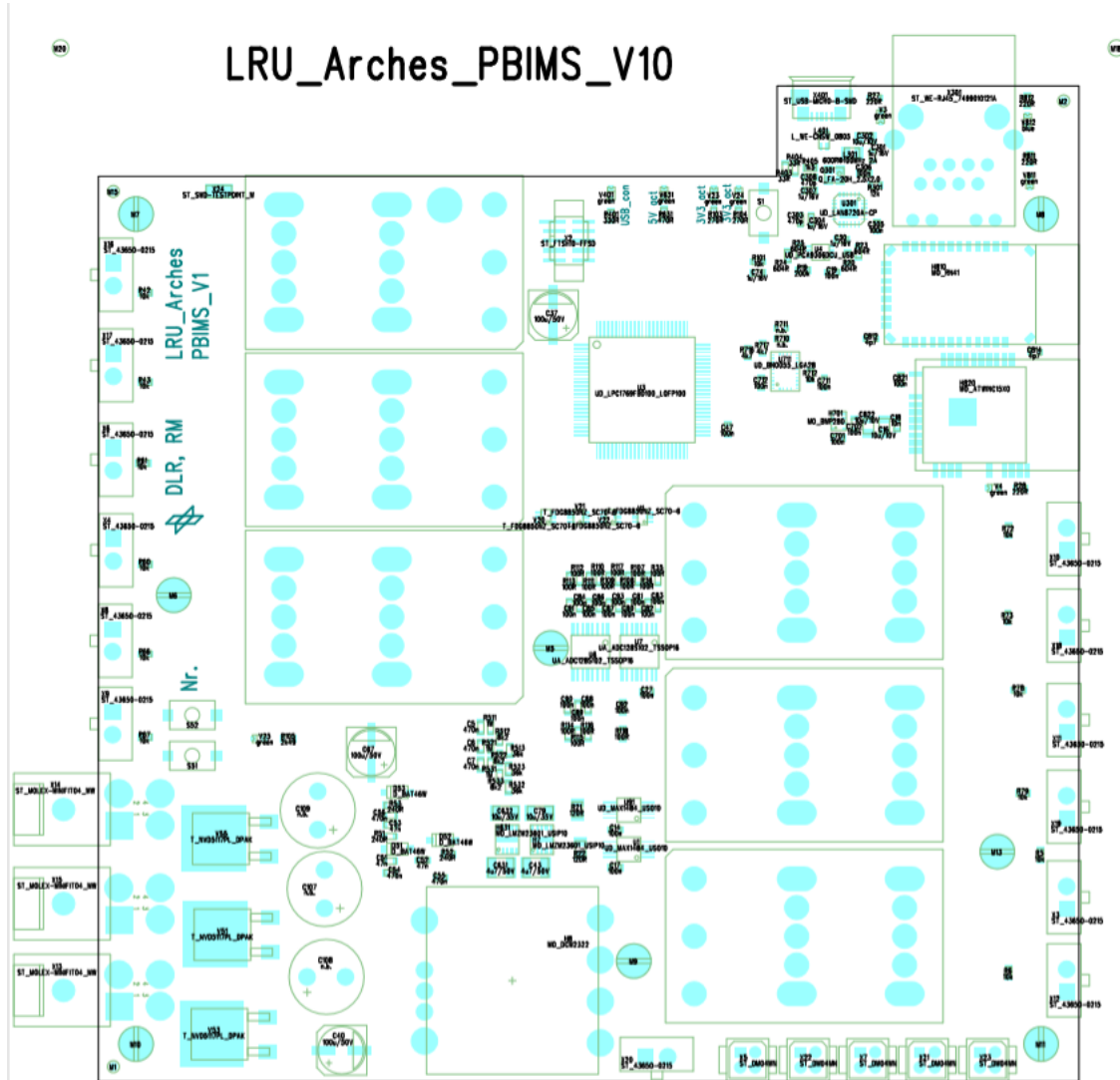
- [76] Bentum, M. J., Verma, M. K., Rajan, R. T., Boonstra, A. J., Verhoeven, C. J. M., Gill, E. K. A., van der Veen, A. J., Falcke, H., Wolt, M. K., Monna, B., Engelen, S., Rotteveel, J., and Gurvitis, L. I., *A Roadmap Towards a Space-based Radio Telescope for Ultra-Low Frequency Radio Astronomy*, Advances in Space Research, 2019. [pdf]. Available at: <<https://arxiv.org/pdf/1909.08951.pdf>>. [accessed October 2019].
- [77] Technical University of Delft, *OLFAR Network*, 2019. [online]. Available at: <<http://elca.tudelft.nl/Research/project.php?id=124>>. [accessed October 2019].
- [78] DLR, *Ardea: the Micro Aerial Vehicle (MAV)*, 2019. [online]. Available at: <<https://www.dlr.de/rm/en/desktopdefault.aspx/tabid-11715/#gallery/29283>>. [accessed October 2019].
- [79] Schuster, M. J., *Collaborative Localization and Mapping for Autonomous Planetary Exploration*, PhD thesis, University of Bremen & German Aerospace Center (DLR), 2019.
- [80] Wedler, A., Wilde, M., Reill, J., Schuster, M. J., Vayugundla, M., Brunner, S. G., Bussmann, K., Dömel, A., Drauschke, M., Gmeiner, H., Lehner, H., Lehner, P., Müller, M. G., Stürzl, W., Triebel, R., Vodermaier, B., Börner, A., Krenn, R., Dammann, A., Fiebig, U.-C., Staudinger, E., Wenzköfer, F., Flögel, S., Sommer, S., Asfour, T., Flad, M., Hohmann, S., Brandauer, M., and Albu-Schäffer, A. O., *From single autonomous robots toward cooperative robotic interactions for future planetary exploration missions*. In: 69th International Astronautical Congress (IAC), Bremen, Germany, Oct. 2018.
- [81] DLR, *Lightweight Rover Unit (LRU)*, 2019. [online]. Available at: <<https://www.dlr.de/rm/en/desktopdefault.aspx/tabid-11431/#gallery/32387>>. [accessed October 2019].
- [82] Bussmann, K., Meyer, L., Steidle, F., and Wedler, A., *Slip Modeling and Estimation for a Planetary Exploration Rover: Experimental Results from Mt. Etna*. In: IEEE/RSJ International Conference on Intelligent Robots and Systems (IROS). IEEE, 2018. doi: 10.1109/IROS.2018.8594294.
- [83] DLR, *Docking Interface ENVICON Docking Sequence*, 2016. ROBEX Design Team Docking & Interfaces. ROBEX Community Workshop, 12<sup>th</sup> October 2016. Kaiserslautern, Germany.
- [84] DLR, *MASCOT: An asteroid scout with a sense of direction*, 2019. [online]. Available at: <<https://www.dlr.de/irs/en/desktopdefault.aspx/tabid-11302/#gallery/28470>>. [accessed October 2019].
- [85] TDK, *Buck Converter i3a series Datasheet*, 2019. [PDF]. Available at: <[https://www.us.tdk-lambda.com/ftp/specs/i3a\\_full\\_datasheet.pdf](https://www.us.tdk-lambda.com/ftp/specs/i3a_full_datasheet.pdf)>. [accessed October 2019].
- [86] Vicor, *Boost Converter DCM2322 Datasheet*, 2019. [PDF]. Available at: <[http://www.vicorpower.com/documents/datasheets/DCM2322x50T5360y6z\\_ds.pdf](http://www.vicorpower.com/documents/datasheets/DCM2322x50T5360y6z_ds.pdf)>. [accessed October 2019].

- [87] NXP, *Microcontroller LPC1769FDB100*, 2019. [online]. Available at: <<https://www.nxp.com/products/processors-and-microcontrollers/arm-microcontrollers/general-purpose-mcus/lpc1700-cortex-m3/512kb-flash-64kb-sram-ethernet-usb-lqfp100-package:LPC1769FBD100>>. [accessed October 2019].
- [88] KEIL, *MCB1700 Evaluation Board User's Guide*, 2019. [online]. Available at: <[http://www.keil.com/support/man/docs/mcb1700/mcb1700\\_intro.htm](http://www.keil.com/support/man/docs/mcb1700/mcb1700_intro.htm)>. [accessed October 2019].
- [89] Blue Arrow, *Blue Arrow Sub-Micro Servo S03610*, 2019. [online]. Available at: <<https://servodatabase.com/servo/blue-arrow/s03610>>. [accessed October 2019].
- [90] BOSCH BNO055, *Bosch SensorTec BNO055: Intelligent 9-axis absolute orientation sensor Datasheet*, 2016. [PDF]. Available at: <<https://www.bosch-sensortec.com/media/boschsensortec/downloads/datasheets/bst-bno055-ds000.pdf>>. [accessed October 2019].
- [91] BOSCH BME280, *Bosch BME280: Combined temperature, humidity and pressure sensor Datasheet*, 2018. [PDF]. Available at: <<https://www.bosch-sensortec.com/media/boschsensortec/downloads/datasheets/bst-bme280-ds002.pdf>>. [accessed October 2019].
- [92] ST VL6180X, *Proximity and Ambient Light Sensing (ALS) module Datasheet*, 2016. [PDF]. Available at: <<https://www.st.com/resource/en/datasheet/vl6180x.pdf>>. [accessed October 2019].
- [93] TI ADC128S102, *Texas Instruments Analog to Digital Converter ADC128S102 Datasheet*, 2015. [PDF]. Available at: <<http://www.ti.com/lit/ds/symlink/adc128s102.pdf>>. [accessed October 2019].
- [94] Allegro ACS70331, *Allegro Hall-effect sensor ACS70331 Datasheet*, 2019. [PDF]. Available at: <<https://www.allegromicro.com/en/Products/Sense/Current-Sensor-ICs/Zero-To-Fifty-Amp-Integrated-Conductor-Sensor-ICs/ACS70331>>. [accessed October 2019].
- [95] Weiner, P., Starke, J., Hundhausen, F., Beil, J., and Asfour, T., *The KIT Prosthetic Hand: Design and Control*, 2018. In: IEEE/RSJ International Conference on Intelligent Robots and Systems (IROS). IEEE, 2018. [PDF]. Available at: <<https://h2t.anthropomatik.kit.edu/pdf/Weiner2018a.pdf>>. [accessed November 2019].
- [96] Smith Metal, *Acetal (POM-C & POM-H) Technical Datasheet*, 2018. [PDF]. Available at: <<https://www.smithmetal.com/pdf/plastics/acetal.pdf>>. [accessed December 2019].
- [97] NASA, *NASA Docking System (NDS) Interface Definitions Document (IDD)*, 2013. Internal Document NASA Johnson Space Center, JSC65795. [PDF]. Available at: <<https://ntrs.nasa.gov/archive/nasa/casi.ntrs.nasa.gov/20150014481.pdf>>. [accessed January 2020].

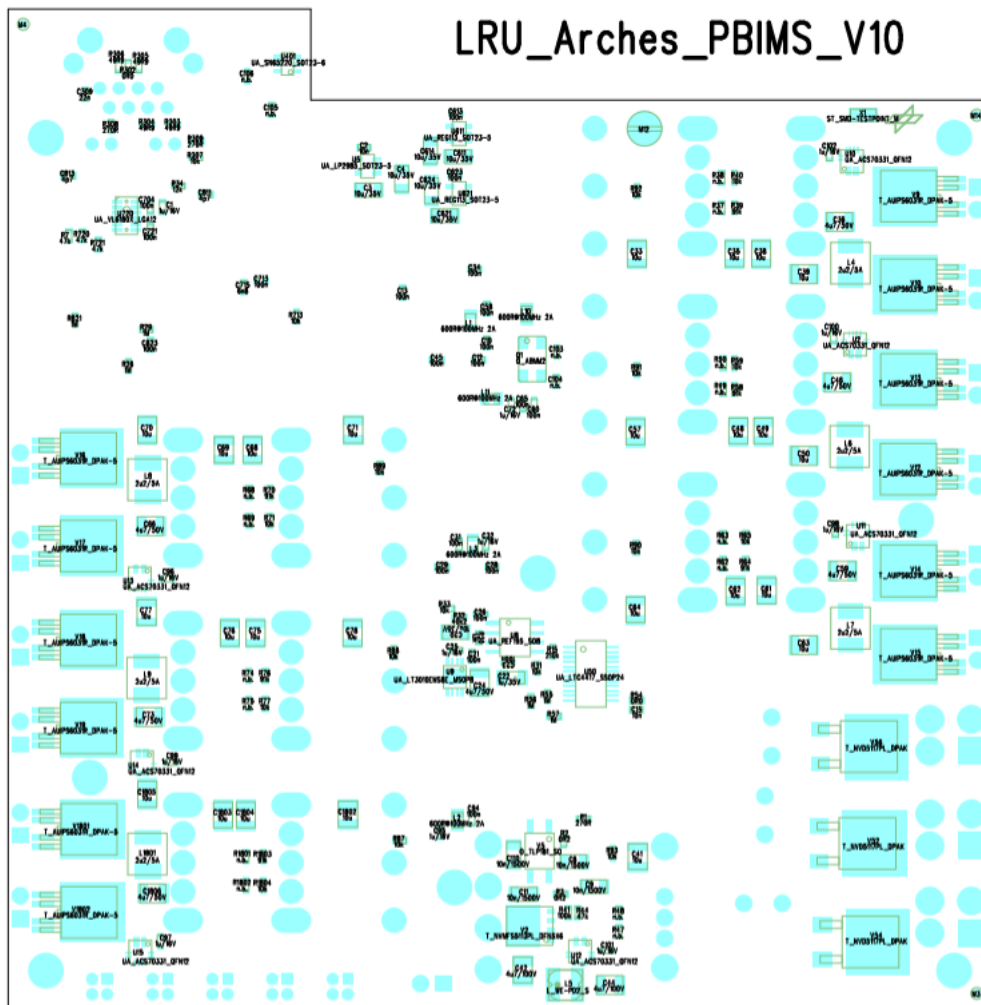
## Appendices

## Appendix A – PBIMS Layout

Top part of PBIMS



Bottom part of PBIMS



## Appendix B – Modularity Qualitative Assessment

### Mechatronics infrastructure Modularity Qualitative Assessment

		ATHLETE	SCARAB	REMRIS	ATRON	CEBOT	ARCHES
Standardization	Standard Interfaces	4	2	5	5	4	4
	Standard Modules	3	1	5	5	4	5
	Plug and Play	1	3	3	2	2	5
		2.66	2	4.33	4	3.3	4.66
Versatility	Multi-function	3	1	2	1	1	5
	reconfigurable	4	1	4	3	2	4
	upgradable	3	1	3	2	2	5
	scalable	4	0	5	5	4	5
	Multi-level	1	1	3	1	1	5
		3	0.8	3.4	2.4	2	4.8
Maintainability	serviceable	4	3	4	3	3	5
	Repairable	4	3	5	3	3	5
		4	3	4.5	3	3	5
Integration	with external systems (HW)	3	1	5	1	1	5
	with sub-systems (HW)	4	4	5	4	4	5
	with external systems (SW)	1	1	2	1	1	4
	with sub-systems (SW)	1	1	3	3	1	5
		2.25	1.75	3.75	2.25	1.75	4.75
Manipulability	docking process	3	1	3	4	3	5
	payload portability	4	2	5	1	1	5
		3.5	1.5	4	2.5	2	5
Operationality	capability of payloads operate independently	1	1	5	1	1	5
		1	1	5	1	1	5
Total		2.73	1.67	4.16	2.52	2.18	4.8

# Power Management and Data Handling Board Modularity Qualitative Assessment

		SCARAB (RESOLVE)	REMRIS	ARCHES	ATRON
Standardization	standard interfaces	1	5	5	5
	standard modules	1	4	5	4
	plug and play	1	3	5	3
		1	4	5	4
Versatility	multi-function	1	2	5	1
	multi-level	1	2	5	1
	upgradable	2	2	4	2
	scalable	1	2	4	1
	reconfigurable	1	1	2	1
		1.2	1.8	4	1.2
Maintainability	serviceable	1	1	3	1
	repairable	5	5	5	5
		3	3	4	3
Total		1.73	2.93	4.33	2.73